THE PLUMBING SYSTEMS AND PARENTAL MAGMA COMPOSITIONS OF SHIELD VOLCANOES IN THE CENTRAL OREGON HIGH CASCADES AS INFERRED FROM MELT INCLUSION DATA

by

STANLEY PAUL MORDENSKY II

A THESIS

Presented to the Department of Geological Sciences
and the Graduate School of the University of Oregon
in partial fulfillment of the requirements
for the degree of
Master of Science

September 2012

THESIS APPROVAL PAGE

Student: Stanley Paul Mordensky II

Title: The Plumbing Systems and Parental Magma Compositions of Shield Volcanoes in the Central Oregon High Cascades as Inferred from Melt Inclusion Data

This thesis has been accepted and approved in partial fulfillment of the requirements for the Master of Science degree in the Department of Geological Sciences by:

Dr. Paul Wallace	Chair
Dr. Ilya Bindeman	Member
Dr. Katharine Cashman	Member
Dr. Dana Johnston	Member

and

Kimberly Andrews Espy	Vice President for Research & Innovation/Dean of the Graduate School

Original approval signatures are on file with the University of Oregon Graduate School.

Degree awarded September 2012

THESIS ABSTRACT

Stanley Paul Mordensky II

Master of Science

Department of Geological Sciences

September 2012

Title: The Plumbing Systems and Parental Magma Compositions of Shield Volcanoes in the Central Oregon High Cascades as Inferred from Melt Inclusion Data

Long-lived and short-lived volcanic vents often form in close proximity to one another. However, the processes that distinguish between these volcano types remain unknown. Here, I investigate the differences of long-lived (shield volcano) and short-lived (cinder cone) magmatic systems using two approaches. In the first, I use melt inclusion volatile contents for shield volcanoes and compare them to published data for cinder cones to investigate how shallow magma storage conditions differ between the two vent types in the Oregon Cascades. In the second, I model the primitive magmas that fed shield volcanoes and compare these compositions to those of nearby cinder cones to determine if the volcanoes are drawing magma from the same sources.

The volatile concentrations suggest that long-lived and short-lived magmatic plumbing systems are distinct. Modeling of parental magmas and differentiation processes further suggest that long-lived and short-lived volcanoes have erupted lava from the same mantle magma source.

CURRICULUM VITAE

NAME OF AUTHOR: Stanley Paul Mordensky II

GRADUATE AND UNDERGRADUATE SCHOOLS ATTENDED:

University of Oregon, Eugene, Oregon

The George Washington University, Washington, DC

DEGREES AWARDED:

Master of Science in Geological Sciences, 2012, University of Oregon

Bachelor of Arts in Geological Sciences, 2009, The George Washington University

Bachelor of Science in Economics, 2009, The George Washington University

AREAS OF SPECIAL INTEREST:

Volcanology

Shallow Crustal Magmatic Processes

Igneous Petrology

PROFESSIONAL EXPERIENCE:

Graduate Teaching/Research Fellow, University of Oregon, 2010-2012

Geologist (USGS/NAGT Intern), US Geological Survey, 2010

Substitute Teacher, Montgomery Country Schools, 2010

Teaching Assistant, The George Washington University, 2009

Field Assistant, US Geological Survey, 2009

Field/Lab Assistant, Department of Marine and Wildlife Resources, 2008

Intern, Joint Program in Survey Methodology, 2007

Intern, New Economy Strategies, 2007

Lab Intern, Science Applications International Corporation, 2004-2005

GRANTS, AWARDS, AND HONORS:

Honors Program Graduate, The George Washington University Honors Program, 2009

Foshag Award, Razor Ridge Mapping Project, Mineralogical Society of the District of Columbia, 2009

Eagle Scout, Boy Scouts of America, 2004

ACKNOWLEDGMENTS

The initiation, continuation, and finalization of this thesis would not have been possible without the wide array of supportive individuals who helped me along this path. My family has always stood by me. They were continually supportive of my decision to go to graduate school and move to Oregon. More importantly, they always reminded me to keep a balanced life even when my studies and research were at full force.

Dr. Paul Wallace, my advisor, deserves my sincerest thanks for direction and guidance during the countless times I entered his office with new ideas, new data, or just a general concern regarding my research. His open-door advising policy is admirable for a man of his position and speaks to the nature of his professional and personal character. I always enjoyed working in the field with him – whether it was collecting samples or teaching field camp. Although Dr. Katharine Cashman left for sabbatical in Bristol, England a year before the completion of this research, she remained resolute in offering sincere and helpful guidance. This project would have been incomplete without her efforts and I wish to express a great deal of thanks. Without the use of Dr. Wallace's and Dr. Cashman's National Science Foundation grant, this project would have been impossible. I would also like to thank Dr. Ilya Bindeman and Dr. Dana Johnston for finding time in their busy schedules to meet with me and provide different perspectives and fresh ideas about the roles and possibilities of my research and the potential implications of my data. Additionally, I extend my thanks to John Donovan for helping me use the microprobe and scanning electron microscope to collect my data.

I doubt I would have been permitted to continue my geologic studies into graduate school without the opportunities provided by Professor Richard Tollo, my

undergraduate advisor at The George Washington University. The unparalleled dedication he gives to his students is unique and laudable. He extended every opportunity I could imagine to me, a senior just entering the world of geology. Under his guidance, I learned petrology and developed my love for volcanology. The long and extensive conversations I held with Professor Tollo gave me a perspective on not just my future in geology but what is important in life. After sharing all those long hours spent in the abyss of the GWU petrology lab and traversing about out in the field, I thank Paul Shakotko for being able to call him a trusted colleague and, now, an old friend.

As for all the friends I have made in Oregon, thank you for sharing this experience with me. Some individuals require personal mention. To Ryan Seward – without you and your garage, my only means of transit would have died a long time ago. To Scott "Meet the Mets" Maguffin – we did it, man. We met the Mets. To Katie Marks, Win McLaughlin, and Nick Famoso – thank you for helping me to remember what it is like to live strong. To Lucy Walsh – for that too often necessary infectious laugh. To Mike Darin – for always expecting me to see with the blast shield down. To the many I have not mentioned, thank you for being there in whatever way you were. My graduate studies would have been lacking something without all of you.

In the memory of Professor George Stephens

The field has never known a more thorough man or kinder soul.

TABLE OF CONTENTS

Chapter Page

Chapter Page

LIST OF FIGURES

Figure Page

Figure Page

LIST OF TABLES

Table Page

CHAPTER I

INTRODUCTION

1.0. Background

Cinder cones and shield volcanoes often form in the same volcanic fields. Despite their proximity, cinder cones typically erupt as monogenetic events, whereas shield volcanoes tend to be polygenetic in that they involve many eruptive events (Connor and Conway, 2000). Why some vents erupt once for a relatively short period of time (months to years) but others nearby remain active long enough to build shields (hundreds or thousands of years) remains ambiguous. This study investigates and contrasts the nature of polygenetic magmatic plumbing complexes against those of monogenetic systems in the central Oregon Cascades. Identifying the distinctions of polygenetic and monogenetic magma systems will help lead to a better understanding of how these plumbing systems evolve from smaller, immature volcanoes to larger, longer-lived volcanoes as well as lend insight to the geology shaping the region in which the cinder cones and shield volcanoes reside (*e.g.* Schmidt and Grunder, 2009; Schmidt and Grunder 2011). While regional tectonic stress fields may exact influence on the mode of eruption (Hildreth, 2007), the present study investigates other factors that may control behavior.

I used two tests to contrast polygenetic magma characteristics to those of monogenetic systems. 1) To constrain differences in shallow magma storage characteristics, I compared the H_2O and CO_2 concentrations in olivine-hosted melt inclusions from tephra deposits of the late-stage eruptions of three mafic, polygenetic shield volcanoes – Belknap, Mount Washington, and North Sister – with published data for nearby monogenetic cinder cones. 2) To determine if monogentic and polygenetic

volcanoes share the same mantle source, I compared the primitive melts that were parental to the basalts erupted from the shield volcanoes to those of nearby cinder cones. As part of the second goal, I modeled fractional crystallization of primitive low-K tholeiite and calc-alkaline basalt and basaltic andesite magmas and compared the results to my melt inclusion compositions and to whole rock data for the three shield volcanoes (Schmidt and Grunder, 2009; Conrey, unpublished). To model the melt compositions over a range of temperatures and pressures, I used MELTS and pMELTS, which are thermodynamic models that compute equilibrium conditions between melts and their accompanying solid phases over a range of temperatures, pressures, and oxygen fugacities (Ghiorso and Sack, 1995; Asimow and Ghiorso, 1998).

The H_2O and CO_2 concentrations for the melt inclusions suggest that shield volcanoes and cinder cones have differences in their magmatic plumbing systems. Polygenetic volcanoes display evidence of more evolved, more complex magmatic plumbing systems than monogenetic volcanoes. The modeling of parental magma fractional crystallization trends shows that cinder cone and shield volcanoes erupt lavas of similar mantle origin. Therefore, the cause of monogenetic or polygenetic behavior of volcanoes is determined somewhere between the upper crust and the upper mantle. Magma supply rate, overall magma volume, and magma buoyancy may all play a role as deciding factors in a vent's life-span.

1.1. Regional Geology

Belknap, Mount Washington, and North Sister, three calk-alkaline basaltic andesite shield-like volcanic vents, are located in the central Oregon Cascades (Fig. 1). This region is part of the larger Cascade volcanic range that spans over 1250 km from

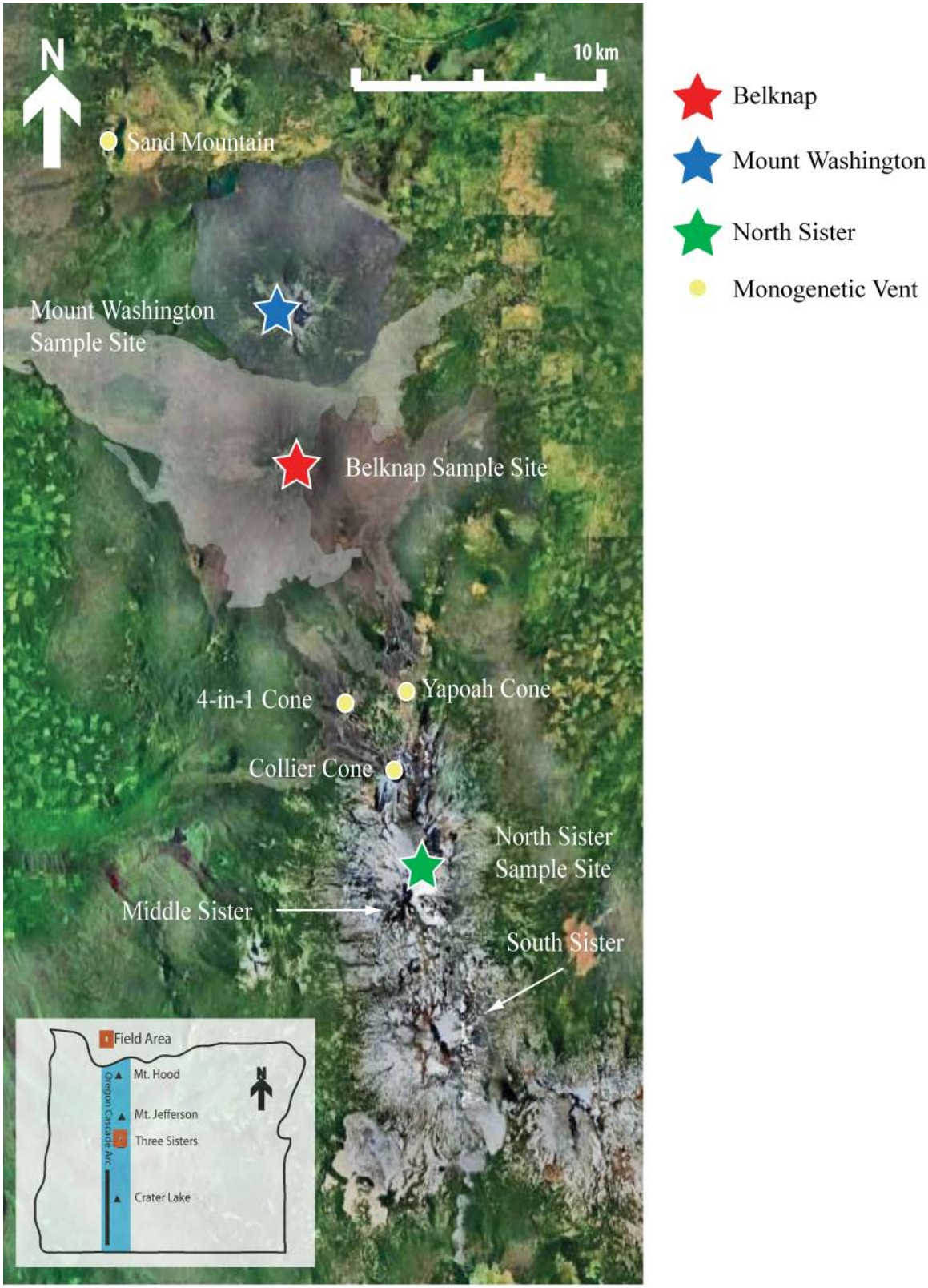

Figure 1: Belknap, Mount Washington, North Sister Volcanic Area

northern California to southwestern British Columbia. The Cascade Range contains over 2300 Quaternary vents that are a product of Juan de Fuca plate subduction beneath the North American continent. The young, hot Juan de Fuca plate is ~8-9 Ma at the trench with a 10-15° dip beneath the forearc and 60-80° dip beneath the arc (Weaver and Baker, 1988; Wilson, 2002). At ~40 Ma, the orthogonal convergence rate of the Juan de Fuca and North American plates began to decrease; however, the obliquity of convergence increased, leading to the clockwise rotation of the Siletz Terrane at a rate of 9-12 ± 1 mm/year with an Euler pole located in eastern Washington (Priest, 1990; Taylor, 1990; Wells et al., 1998) The clockwise rotation of the Siletz Terrane initiated E-W extension along the central Oregon High Cascade crest at 8 Ma and created the central Oregon High Cascade graben (Priest, 1990; Taylor, 1990; Wells, 1990; Conrey et al., 2000; Conrey, 2002). The High Cascade graben faults strike just west of north on the western boundary, just east of north on the eastern boundary, and are intersected by the northwest trending Brothers Fault Zone, a hypothesized extension of the Basin and Range system, in the Three Sisters region (Taylor, 1981; Bacon, 1983; Lawrence, 1976; Wood and Kienle, 1990). Belknap, Mount Washington, and North Sister are located in the High Cascade graben.

Extension in the High Cascade graben region allowed magmas of basaltic to rhyolitic composition to erupt by exploiting regional tensile weaknesses in the crust, leading to formation of the mafic platform of the region between 5-8 Ma (Hughes and Taylor, 1986; Conrey, 2004). Primitive magmas, which originated from varying sources, were products of fluid-flux melting and/or mantle upwelling (Bacon et al., 1997; Conrey et al., 1997; Ruscitto et al., 2010). MORB-like low-K tholeiites were common in the

Cascades between the Miocene and the Pliocene (Conrey, 2002). Conrey (2002) cites the extensional environment leading to decompression melting as the origin of the low-K tholeiites. The extension is interpreted to have initiated near the Three Sisters, where the High Cascade graben is widest and the density of vents the greatest (Conrey, 2002). The graben continues to widen at 1 mm/yr (Wells et al., 1998).

Much of the Quaternary volcanism in the Oregon segment of the Cascades, ~1054 vents varying from cinder cones, shields, and fissures to stratovolcanoes over a 9500 km^2 area, lies in the High Cascade graben (Hughes and Taylor, 1986; Hildreth, 2007). The smaller volume (< 1 km^3), more mafic volcanism of the cinder cones and shields is often found in volcanic fields containing up to 100s of vents (Connor and Conway, 2000). Basalt constitutes ~85% of the volcanic rocks of the High Cascades, with the silicic centers distributed intermittently along the arc (McBirney and White, 1982). The silicic centers that define the high topography did not develop until the Quaternary (Priest and Vogt, 1983; Taylor, 1989).

1.2.0. Terminology

1.2.1. Melt Inclusions

Volatiles exsolve substantially from melt both before and during subaerial eruptions. Melt inclusions, which form from irregular crystal growth, provide a means to quantify magmatic volatile concentrations before eruption (Métrich and Wallace, 2008). Melt inclusions are defined as small volumes of melt trapped in phenocrysts during crystallization. When these melt inclusions form, the magma compositions at entrapment are isolated and preserved, though some post-entrapment modification does occur (e.g. Wallace, 2005; Ruscitto et al., 2010).

1.2.2. Calc-alkaline and Low-K Tholeiite Magmas

There are several potential mantle sources identified for magmas erupted in the Oregon Cascades. The differing geochemical characteristics of magmas from different mantle sources can be used to identify from which particular mantle source a magma originates. If there was evidence for different mantle sources between shields and cinder cones, then this would suggest that shield and cinder cones draw magma from different mantle sources, which could provide an explanation for the disparate eruptive life-spans.

In this study, I focus on the two more common types of mantle magmas, calc-alkaline and low-K tholeiitic magmas. Calc-alkaline basalts and basaltic andesites contain olivine and spinel phenocrysts. Plagioclase phenocrysts, if present, are present in low modal abundances because the presence of H_2O up to several wt. %, common in calc-alkaline magmas, suppresses plagioclase crystallization (Sisson and Grove, 1993) and reduces the enrichment of FeO in the melt (Fig. 2). Calc-alkaline magmas are often associated with the fluid-flux environment of a subducting slab (Bacon et al., 1997; Conrey et al., 1997; Ruscitto et al., 2010).

Low-K tholeiitic basalts and basaltic andesites, also known as high aluminum olivine tholeiites (HAOT), contain relatively lower H_2O (< 1 wt. % [Ruscitto et al., 2010], < 1.3 wt. % [Rasmussen, 2012], and < 1.7 wt. % [Shaw, 2011]), resulting in higher temperature plagioclase crystallization, which enriches the melt in FeO (Fig. 2). Low-K tholeiites are defined by relatively low K_2O (< 0.5 wt. %) and SiO_2 (~48 wt. %) and high Al_2O_3 (~17-18 wt. %). Whereas the origin of low-K tholeiites as products of decompression melting versus slab fluid-flux melting is debated by Borg et al. (1997),

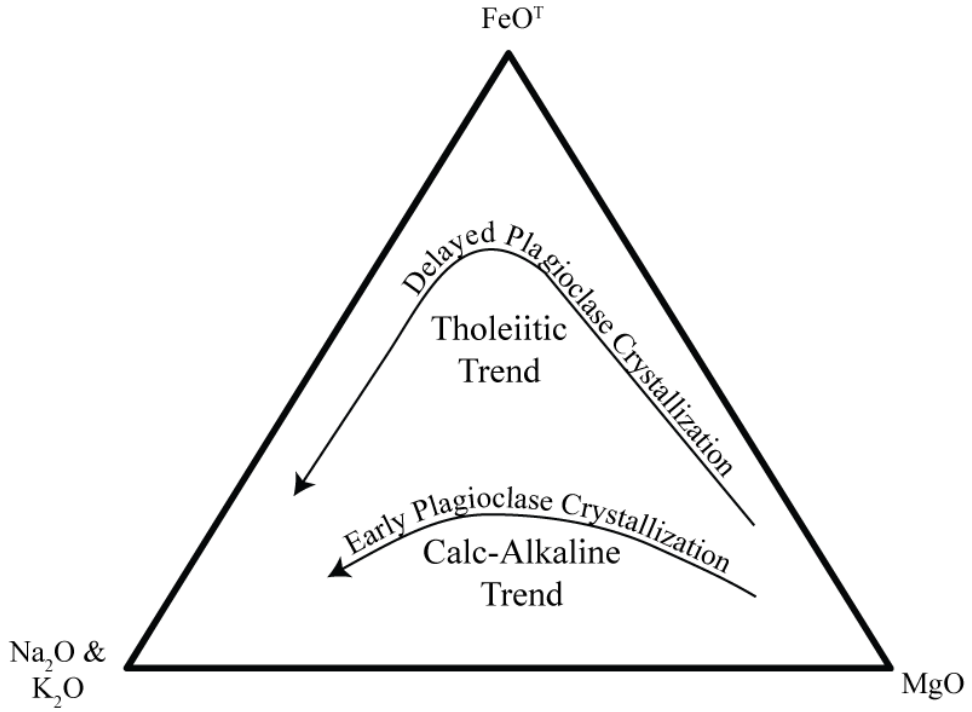

Figure 2: Ternary Diagram of Calc-alkaline and Low-K Tholeiite Magmas
The Calc-alkaline-Tholeiitic distinction from Irvine and Baragar (1971). The higher H_2O content of CAB magmas suppresses early higher temperature plagioclase crystallization, causing melts to retain low FeO relative to LKT magmas, which lack the H_2O of the CAB magmas. As a result, earlier higher temperature plagioclase crystallization enriches the LKT in FeO.

Grove et al. (2002), Leeman et al. (2005), Ruscitto et al. (2010), and Rasmussen (2012), their geochemical distinction from calc-alkaline magmas is well defined.

1.2.3. Vent Classification

The terms used to classify volcanic vents are often misused in the scientific literature. Conrey (2003) refers to North Sister as a shield volcano, whereas other sources, like the Cascade Volcano Observatory, label North Sister as a stratovolcano. North Sister, by strict definition, is a composite shield volcano with characteristics of both a shield and a composite volcano (Sigurdsson, 2000; Hildreth, 2007).

Sigurdsson (2000) provides the classifications (Fig. 3) for each vent construct as follows. Cinder cones are hill-sized deposits produced by the buildup of ash or other

Cinder Cone

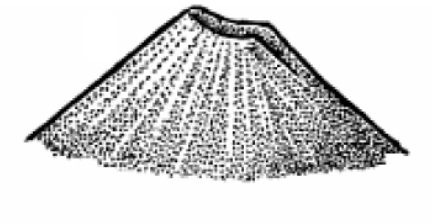

Cinder cones are not classified by their slope relief like other vent construct types. Instead, cinder cones are characterized by the hill-sized deposit formed by tephra around the vent.

Shield Volcano

Shield volcanoes are characterized by low slope relief (slopes with less than 5°)

Composite-Shield

Composite-shield volcanoes are loosely defined as having slopes (10°) twice that of shield volcanoes.

Stratovolcano

Stratovolcanoes are characterized by high slope relief up to the angle of repose (35°)

Figure 3: Vent Constructs
Images provided by the Merrian-Webster Dictionary (http://www.merriam-webster.com/)

pyroclastic fragments around a central volcanic vent. Shield volcanoes are broad, low relief volcanic constructs made up of fluid lava flows with slopes of ≤ 5°. Hasenaka (1994) adds that loose tephra is often associated with shield eruptions, but the tephra is limited to the vent area. The term composite shield is used to describe volcanoes with vent constructs intermediate between shields and composite volcanoes. Composite volcanoes are defined as having slopes roughly twice as steep as shields and are relatively large, long-lived edifices comprised of lava and volcaniclastics erupted from one or more vents. Composite volcano and stratovolcano are used interchangeably to refer to volcanoes constructed of alternating layers of lava flows and pyroclastic rocks with slopes reaching up to 35° (Sigurdsson, 2000).

Although the three volcanoes that are the focus of this study range from a true shield volcano (Belknap) to a composite shield (North Sister), these classifications are becoming inadequate as labels and often create confusion due to their misuse. The slope morphology of Belknap defines the vent as a shield volcano, but this site, the most shield-like of any vents in the nearby area, is capped by a cinder cone (Sherrod et al., 2004). In the Cascades, the Sigurdsson (2000) classifications of cinder cones, shields, composite shields, and stratovolcanoes more accurately define points on a volcanic vent spectrum rather than provide clear and precise vent descriptions. For purposes of this study, the three polygenetic vents are referred to as shield volcanoes because each site has behaved as a shield volcano with multiple effusive lava flows at some point in their respective eruptive histories. Belknap, Mount Washington, and North Sister are representative of central Oregon High Cascade polygenetic activity and therefore, they are ideal magmatic systems to compare to the nearby monogentic volcanoes.

1.3.0. Geochemical Characteristics of the Volcanoes in this Study

Hughes and Taylor (1986) classified the calc-alkaline basaltic andesites of the central Oregon High Cascades into two groups. The North Sister (NS) type basaltic andesite is characterized by low levels of incompatible elements and high FeO^T/MgO ratios. The Mount Washington (MW) type basaltic andesite contains higher incompatible element concentrations with relatively lower FeO^T/MgO ratios. Although the causes of the compositional differences between MW-type and NS-type magmas is not exactly known, Hughes and Taylor (1986) postulate that there are 2-3 potential mantle sources for basaltic andesites in the central Oregon Cascades responsible for the varying calc-alkaline compositions. Schmidt (2005) postulates that vent position along the arc is correlated to the basaltic andesite type produced at the vent. NS-type compositions are found along the crest of the arc. Conversely, MW-type basaltic andesites are found to the west of the crest, suggesting that volatile induced melting from the subducting Juan de Fuca slab plays a significant role in providing incompatible elements to the MW-type basaltic andesites. In this interpretation, the NS-type basaltic andesites immediately to the east do not receive the same fluid input because the rapidly sinking plate has already been significantly dehydrated before the arc crest. Through melt inclusion H_2O and trace element analysis, Walker et al. (2003) found dehydration-driven, flux-melting to persist across the Central American arc, with decompression melting significantly affecting melt compositions in the back-arc region across the Central American subduction zone. However, Ruscitto et al. (2010) did not find strong evidence favoring magma source variation across the Cascade arc in Central Oregon, making the interpretation of Walker et al. (2003) and the postulation of Schmidt (2005) an unlikely explanation for the

production of MW-type and NS-type basaltic andesites. Belknap and Mount Washington are classified as MW-type shields, whereas North Sister is classified as an NS-type shield.

1.3.1. Belknap

Belknap is a shield volcano that stands ~450 m above the surrounding topography of the central Oregon High Cascades with a basal diameter of ~6.6 km. Assuming the volcano to be a perfect cone, Belknap's volume is ~21 km^3. The edifice grew through repeated lava flow eruptions from ~2.6 to 1.5 ^{14}C ka and is capped by a cinder cone (Sherrod et al., 2004). Earlier ^{14}C dating reported rock as young as 1775 ± 400 B.P., though ^{3}He dating by Liccardi (1999) reported a minimum age of 2000 yr B.P., suggesting the older ^{14}C age is more accurate (Taylor, 1990).

The top of the cinder cone capping the shield contains two craters. Immediately east of Belknap is Little Belknap, which is compositionally distinct (54.8-56.9 wt. % SiO_2) from the basaltic andesite lavas of Belknap (49.8-53.6 wt. % SiO_2). C^{14} dating overlaps early Belknap activity with late-stage Little Belknap eruptive events. However, field relations suggest Little Belknap flows to be younger than those of Belknap (Sherrod et al., 2004).

1.3.2. Mount Washington

Mount Washington, located ~5 km to the north of Belknap (Fig. 1), is a relatively unstudied, glacially-eroded composite shield volcano standing ~850 m above the surrounding terrain with a basal diameter of ~7.3 km and a volume of ~48 km^3 assuming the volcano was originally a perfect cone. An absolute age is not known for Mount Washington, but Sherrod et al. (2004) estimate the volcano to be ~300 ka. Unlike

Belknap, Mount Washington has experienced at least one glaciation, which has left glaciated flanks with exposed volcanic layers and glacial till (Scott, 1990; Sherrod et al., 2004).

1.3.3. North Sister

North Sister, located approximately 15 km to the south-southeast of Belknap, is a composite shield volcano that stands ~1430 m above the local topography with a base ~11.9 km in diameter and a volume of 214 km^3 assuming the volcano was originally a perfect cone. Schmidt and Grunder (2009) dated North Sister to ~400 ka. North Sister has withstood the Penultimate (400-390 ka) and Wisconsin (80-18 ka) glaciation events (Scott, 1977; Scott, 1990). During the last glacial maximum, glaciers covered the central Oregon High Cascades from Mount Jefferson in the north to Mount McLaughlin in the south. Like at Mount Washington, this glaciation exposed the flanks of North Sister, dissecting the volcano and removing the original slope morphology (Schmidt and Grunder, 2009).

Schmidt and Grunder (2009) found four general eruptive sequences at North Sister. The first (~400 ka) constructed the lower shield. The second (182-99 ka) erupted material sub-glacially. The third (~80 ka) constructed the upper shield. The fourth stage (70-55 ka) produced abundant pyroclastic material with no significant change observed in SiO_2 concentrations.

Although olivine and plagioclase are common phenocrysts at North Sister, Schmidt and Grunder (2011) used whole rock Ni concentrations to conclude that olivine fractionation did not play a role in magmatic evolution at North Sister. Mercer and Johnston (2008) found North Sister magmas to have last equilibrated with an augite-rich

gabbro at the base of the crust (~12 kbar). Schmidt and Grunder (2009) describe the 40 km^3 of North Sister basaltic andesites as compositionally monotonous in their major element compositions and argue that North Sister compositions were produced by sustained recharge of mantle-derived low-K tholeiitic magma that slightly assimilated an Al-rich crustal source. Over time, the highly incompatible elements of the crust became depleted by the partial melting of this continual magmatic interaction. Therefore, later eruptions became less enriched in highly incompatible elements as the crustal source became increasingly refractory. The magma evolved to its basaltic andesite composition at ~35-40 km depth through pyroxene and plagioclase fractionation (Schmidt and Grunder, 2009; Schmidt and Grunder, 2011). Schmidt and Grunder (2011) postulate that low-K tholeiitic basaltic andesites underplate a 200 km segment of the Cascade arc, where extension was at its greatest, including beneath Belknap and Mount Washington.

CHAPTER II

METHODS

2.0. Sample Collection

Tephra was collected from the top several cm of exposed deposits using a steel bladed trenching tool. I attempted to find the most recent tephra deposits at the three field sites. At Belknap, sampling from the youngest eruptive unit was possible; however, glaciation may have removed the youngest tephra units at Mount Washington and North Sister. The tephra collected at these two sites instead comes from the youngest exposed tephra units. I avoided sampling from oxidized tephra deposits, which are characterized by a red color compared to non-oxidized deposits.

Dr. Paul Wallace collected the initial set of the Belknap samples in 2009 from the flanks of the summit crater. I conducted my own sampling in 2011 from the same location (10 T 592376 4904173) (Fig. 1). The deposit I collected from was a gray color of unknown thickness that appeared to be the predominantly exposed unit on the summit with tephra size varying from ash to blocks and bombs. Both sets of samples displayed similar physical characteristics and similar compositional values.

I used Sherrod et al. (2004) to find a Mount Washington palagonite tuff deposit exposed during glaciation on the western flank of the shield (10 T 592229 4909515). The palagonite tuff deposit was a yellow-tan color of unknown thickness with tephra size varying from ash to blocks and bombs in a predominantly poorly indurated deposit, though some sections of the deposit varied to well indurated. Although younger lava flows followed the eruption of the palagonite tuff, the palagonite tuff is a later-stage eruptive event in the overall eruptive history of Mount Washington. The melt inclusions

from this tuff represent magma younger than that of the oldest eruptive event, as the palagonite tuff is underlain by a considerable but unknown volume of Mount Washington lavas.

Schmidt and Grunder (2009) group North Sister volcanic units into seven ages, but provide no further age resolution. Volcanic material from a single unit may vary by several tens of thousands of years. The youngest unit, the North Sister basaltic andesite scoria deposit (PC), erupted between 70 to 55 ka and represents the final eruptive period for North Sister. The PC unit has been mostly removed by glaciation with only limited exposures remaining. I collected North Sister tephra from the PC exposure found on the volcano's southern face where the southeastern and southwestern ridges bifurcate (10 T 598002 4890559) (Fig. 1). There was no visible stratigraphy of the deposit, which was colored red-gray to gray. The thickness of the PC unit is unconstrained. Tephra grain size varied from ash to blocks and bombs.

2.1. Sample Preparation

Samples were hand washed, dried, and sieved at the University of Oregon. Olivine grains were handpicked with a LEICA MZ9s binocular microscope and then placed in 1.657 refractive index immersion oil to identify melt inclusions. The olivine crystals were not bathed in HBF_4 or HF because matrix glass was minimal and did not inhibit inclusion inspection. Target olivine crystals hosting fully enclosed melt inclusions were ground and polished into wafers hosting doubly intersected glass melt inclusions using 600 and 400 grit paper and 6 µm, 1 µm, and 0.25 µm diamond pastes. Water was used as lubrication on the 600 and 400 grit paper. Olive oil was used as lubrication with the diamond pastes. Wafer thicknesses ranged from ~10-100 µm. Before grinding and

polishing the second side of the wafer, photos of the inclusions were taken using a LEICA DFC 320 camera interfaced with a LEICA DMLP petrographic microscope.

2.2. FTIR

The olivine-melt inclusion wafers were analyzed for H_2O and CO_2 concentrations with a Thermo-Nicolet Nexus 670 Fourier Transform Infrared (FTIR) spectrometer interfaced with a Continuum IR microscope at the University of Oregon using methods similar to Johnson et al. (2009) and Ruscitto (2010). I used the Beer-Lambert law to calculate H_2O and CO_2 concentrations:

$$c = \frac{ma}{\rho d \varepsilon} \quad (1)$$

in which c is the weight percent of the absorbing species, m is the molecular weight of the absorbing species, a is an absorbance intensity of the band of interest, ρ is the density of the glass, d is the sample thickness, and ε is the molar absorptivity. A digital micrometer provided the thickness of the melt inclusion and hosting olivine wafers. I used the interference fringe method from Wysoczanksi and Tani (2006) to provide another means of measuring thickness, which allowed me to double check the micrometer thicknesses. Figure 4 provides examples of absorbance spectra produced during FTIR analysis. I measured H_2O concentrations from the 3550 cm^{-1} fundamental OH stretching vibration. Other H_2O peaks were too near or below the background noise of the spectra to be utilized. I used the carbonate doublet at 1515-1430 cm^{-1} to determine the CO_2 concentrations. I calculated glass densities using oxide molar volumes from Luhr (2001) and determined the densities of the hydrous inclusions by iteration. I used VolatileCalc (Newman and Lowenstern, 2002) to model entrapment pressures using the H_2O and CO_2 concentrations. Gaussian error propagation was used to compute analytical uncertainties

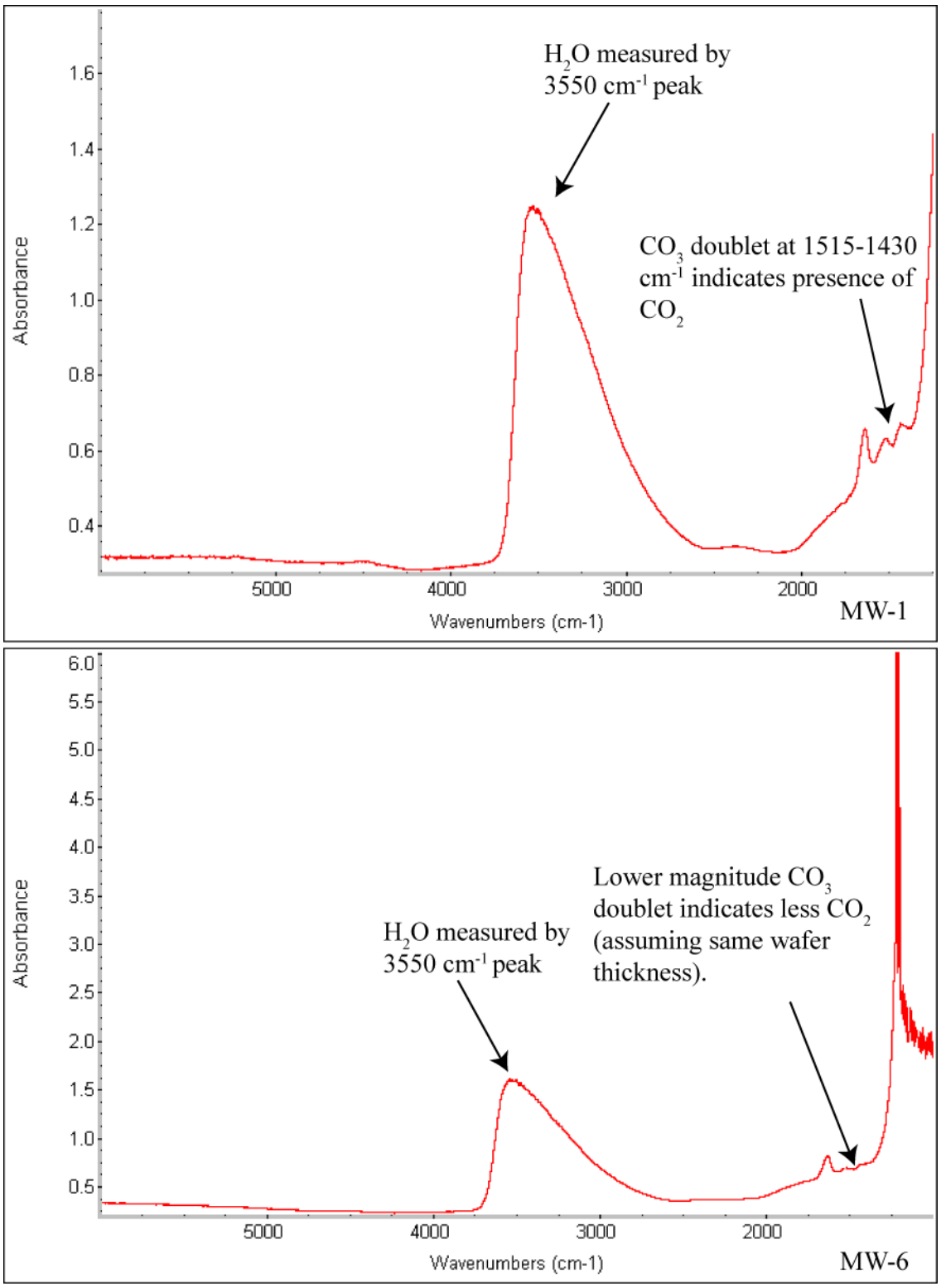

Figure 4: Fourier Transform Infrared Spectroscopy Spectra
These absorance spectra from two Mount Washington melt inclusions display similar concentrations of H_2O (assuming similar wafer thicknesses). MW-1 displays a CO_2 doublet while the lower magnitude CO_2 doublet in MW-6 indiciatees less CO_2.

for H_2O, CO_2, and the major elements. A form of the Gaussian error propagation equation specific for multiplication and/or division functions is:

$$\frac{S\bar{z}}{\bar{z}} = \sqrt{\left(\frac{S\bar{x}}{\bar{x}}\right)^2 + \left(\frac{S\bar{y}}{\bar{y}}\right)^2 + \cdots} \qquad (2)$$

in which $\bar{x}$ and $\bar{y}$ are the averages of the uncorrelated x and y variables, $S\bar{x}$ and $S\bar{y}$ are the standard deviations of the averages of the uncorrelated x and y variables, $\bar{z}$ is the computed average, and $S\bar{z}$ is the standard deviation of the computed average (Bevington, 1969).

Sometimes the melt inclusions were not perfectly intersected and olivine remained on one of the two sides of the inclusion. To correct for this, the absorbance of the olivine crystal was measured and the peak of the Si-O bands in the region 1850-1580 cm^{-1} was measured. The ratio of the peak heights in this region for the olivine-only spectrum and the melt inclusion plus olivine spectrum provided the ratio of olivine thickness overlying the melt inclusion. The olivine thickness was subtracted from the measured wafer thickness to give the true melt inclusion thickness.

After inclusion entrapment, the trapped melt may start to crystallize olivine and thereby change the trapped melt composition (Wallace, 2005). I used a correction similar to Ruscitto et al. (2010) to account for post-entrapment crystallization (PEC). Olivine in equilibrium with the melt composition was added in 0.1 wt. % intervals to the melt composition until the restored melt composition was in equilibrium with the Fo content of the host crystal. The K_D value for the olivine addition procedure was calculated using the method of Toplis (2005). K_2O and H_2O are similarly incompatible in olivine, so the two components should behave similarly during olivine crystallization. Therefore, the

$K_2O_{corrected}$ /$K_2O_{uncorrected}$ ratio serves as a means to calculate the original H_2O, CO_2, S, and Cl wt. %, which would have become enriched during PEC. The samples were checked for Fe loss as described in Danyushevsky (2000), but no additional correction was necessary.

2.3. EPMA

I mounted the wafers in EPOFIX epoxy for host crystal and glass analysis with the University of Oregon Cameca SX-100 electron microprobe (EPMA). For operating conditions, I used 10 nA and a 10 μm diameter beam with 15 kV accelerating voltage for Si, Mg, Al, Fe, Ca, Na, K, and Mn. For Ti, S, Cl, P, and F, I used 50 nA and a 10 μm diameter beam with 15 kV accelerating voltage. I analyzed 3-5 spots per inclusion to measure glass compositions. Time dependent intensity corrections were applied for Si, Al, Na, and K.

Using MELTS, I modeled the crystallization paths of the more primitive inclusions to see if predicted compositional trends accurately estimated the range of inclusion and whole rock compositions. Initial temperatures were set above the liquidus with $\Delta T = -10°$ C. Initial pressure was set to maximum observed pressure in the melt inclusions (~3 kbar) with $\Delta P = -15$ bar.

2.4. SEM

I mounted 2-4 mm tephra grains with EPOFIX epoxy and then ground and polished the tephra to intersect phenocrysts and microlites in the sample. I acquired high magnification imagery of tephra samples with an FEI Quanta 200 Scanning Electron Microscope (SEM) at the University of Oregon. Images from samples from all three sites

were taken at 150x, 500x, 1000x, 1500x, and 10000x magnification to observe phenocrysts and microlite characteristics.

2.5. Modeling Primary Shield Magmas

Volcanoes across and along the Cascade arc draw magmas from varying sources, which were identified by Ruscitto et al. (2010). Ruscitto et al. (2010) modeled the primitive cinder cone magmas of the central Oregon Cascades to range from primitive basalts to primitive basaltic andesites. After using several models to restore the observed Belknap, Mount Washington, and North Sister lava compositions to primitive compositions (in equilibrium with mantle olivine Fo_{90} or mantle clinopyroxene Mg# 92), I can compare the magma sources of shield volcanoes and cinder cones to ascertain if the primitive magmas are the same. To restore the shield lavas to primary magma compositions, I used four methods.

For the first, I employed a method from Ruscitto et al. (2010) in which 0.1 wt. % equilibrium olivine was added incrementally until the new composition was in equilibrium with Fo_{90}. In the second, I used the Danyushevsky (2001) approach, which calculates the equilibrium compositions of olivine, plagioclase, and clinopyroxene and adds the equilibrium components to the melt by 0.1 wt. % increments until Fo_{90} or clinopyroxene Mg# 92 is achieved. The Danyushevsky (2001) model modifies the model of Danyushevsky (1996), which compared many model estimates (*e.g.* Ford et al., 1983; Ariskin et al., 1988; Roeder and Emslie, 1970; Weaver and Langmuir, 1990; Nielsen and Dungan, 1983) for olivine, plagioclase and/or clinopyroxene fractionation from melts over a range of pressures, temperatures, and oxygen fugacities. Danyushevsky (1996) uses the three models (see Appendix A) that best estimate the fractionation of three the

phases from the 393+ compositions that were used for testing and calibration. Ford et al. (1983) best described olivine fractionation, Weaver and Langmuir (1990) best modeled plagioclase fractionation, and Ariskin et al. (1988) best modeled clinopyroxene fractionation.

For the third and fourth methods, I used MELTS and pMELTS to compute the liquidus phase(s) at 1 kb and 8 kb, respectively, and added the phase(s) in 1 wt. % increments to the composition until the compositions were in equilibrium with Fo_{90} or clinopyroxene Mg# 92.

2.6. Modeling Primitive Low-K Tholeiites

In addition to modeling the primary magmas of the shield volcanoes to compare to the primary magmas of the cinder cones, I used the modeled primary calc-alkaline and low-K tholeiite compositions to run forward fractional crystallization models using MELTS. The goal of this was to determine if the lavas observed at the surface are consistent with the calculated parental magmas and to distinguish whether the calc-alkaline or low-K tholeiite primitive compositions provide the best match.

Ruscitto et al. (2010) calculated primitive calc-alkaline compositions for several cinder cones in the central Oregon Cascades by adding 0.1 wt. % increments of equilibrium olivine to the melt compositions until they were in equilibrium with Fo_{91}, the composition of refactory mantle-equilibrated olivine. I chose the Ruscitto et al. (2010) primitive Collier Cone composition (labeled as CABa in all figures and tables) as this study's representative calc-alkaline parent magma due to Collier's proximity to North Sister and similar K_2O content.

I modeled primitive central Oregon Cascade low-K tholeiite compositions using two methods. In the first, I used the same methods as Ruscitto et al. (2010) with a low-K tholeiite (FLR-03-1) from Rowe et al. (2009), found ~20 km west of North Sister. The whole rock composition is labeled LKT1 and the melt inclusion composition LKT2 in all figures and tables. In the second, I used the Danyushevsky (2001) model to restore LKT1 and LKT2 to be in equilibrium with Fo_{90} or clinopyroxene Mg# 92.

I then used the calculated primitive CABa and LKT compositions as starting points for fractional crystallization models using MELTS. Using a range of temperatures and pressures (1-8 kbar) for each composition, I used MELTS to crystallize the primitive compositions until they resembled the melt inclusion compositions. For Collier Cone, Ruscitto et al. (2010) found an f_{O2} of NNO + 0.25, which I used for my CABa MELTS analysis. For the FLR-03-1 low-K tholeiite, Rowe et al. (2009) found an f_{O2} of QFM + 0.09, which I used for my LKT MELTS analysis. I then compared major element crystallization trends to find which parent melt, the CABa or LKT, generated the closest match to the shield compositions.

CHAPTER III

DATA

3.0. Volatile Data

Melt inclusions from all three volcanoes display a wide range in H_2O contents (Fig. 5, Table 1). Some melt inclusions contained vapor bubbles (Table 2, see Appendix B). Belknap's maximum H_2O content (2.4 ± 0.2 [1 s.d.] wt. % H_2O) was within error of Mount Washington's maximum H_2O concentration (2.3 ± 0.1 wt. % H_2O). North Sister inclusions contained the highest H_2O concentrations (2.8 ± 0.2 wt. % H_2O). Low values of < 1 wt. % at were found at all three volcanoes. These low values are part of a continuous range of H_2O content much like H_2O values from long-lived cinder cone melt inclusions (*e.g.* Cerro Negro [Roggensack et al., 1997], Jorullo [Johnson et al., 2008], Paricutin [Pioli et al., 2008], and Sand Mountain [Ruscitto, 2010]). However, the high frequency of melt inclusions with < 1 wt. % H_2O is not typically observed in melt inclusions from cinder cones in the Oregon and Northern California Cascades (*e.g.* Ruscitto, 2010; Walowski et al., 2011).

Melt inclusions from the three shield volcanoes also display a wide range in CO_2 concentrations (Fig. 5, Table 1). Belknap inclusions are the least CO_2 rich and contain a CO_2 maximum of 765 ± 50 ppm. Mount Washington's maximum CO_2 (865 ± 56 ppm CO_2) is similar to that of North Sister's. North Sister exhibits the maximum CO_2 (977 ± 16 ppm CO_2) of the three volcanoes. Several Mount Washington and North Sister melt inclusions and many of the Belknap inclusions display CO_2 below detection limits, but these inclusions seem to form a continuous range of values with the rest of the data set,

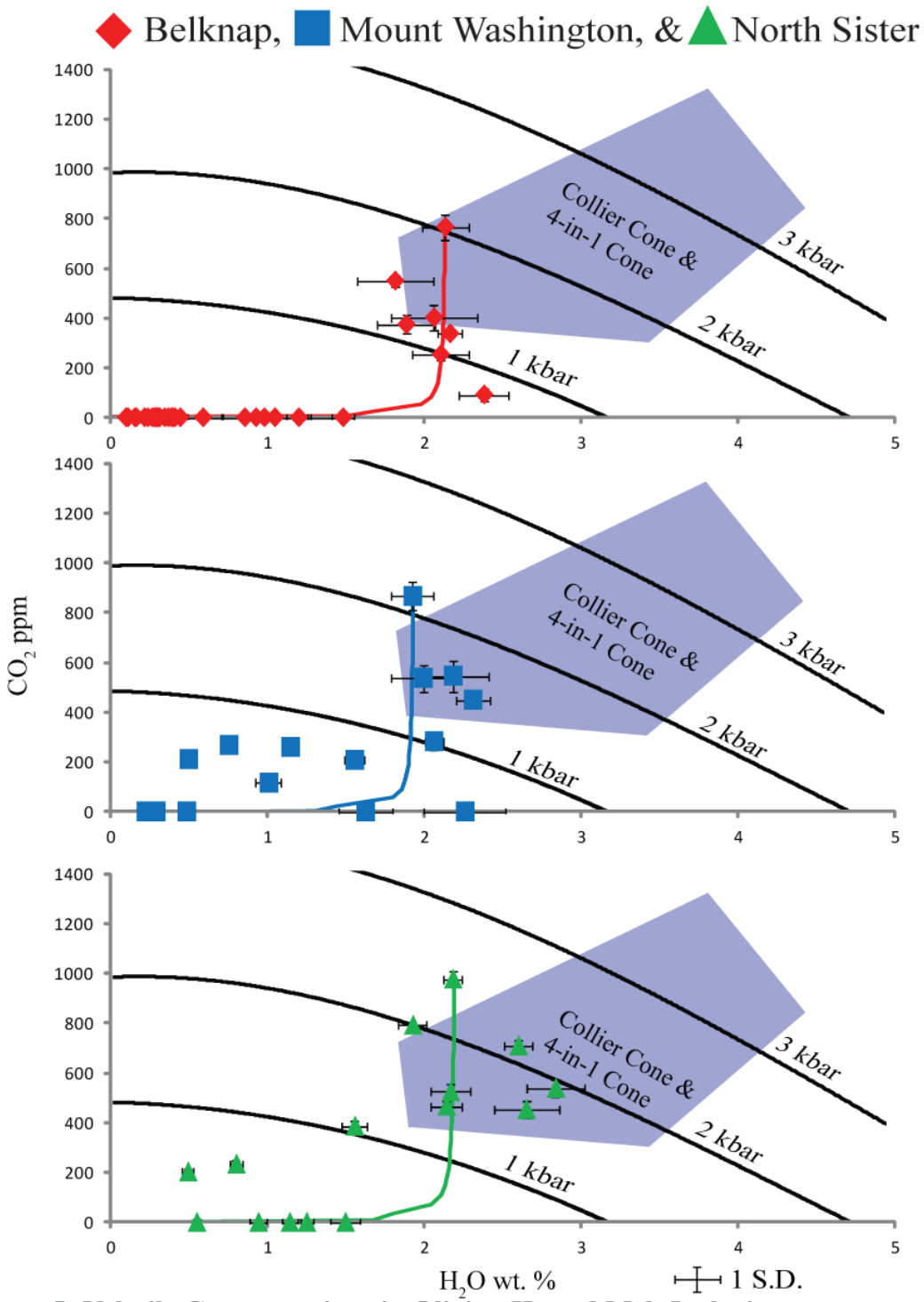

Figure 5: Volatile Concentrations in Olivine-Hosted Melt Inclusions
Collier Cone and 4-in-1 Cone data provided by Ruscitto (2010). VolatileCalc (Newman and Lowenstern, 2002) modeled isobars for a composition of 49% SiO_2. Closed degassing paths, which were also modeled from Newman and Lowenstern (2002), are based on highest observed CO_2 concentration at each volcano.

Belknap	H_2O (wt. %)	Std. Dev.	CO_2 (ppm)	Std. Dev.	Entrap. Press. (bars)
B1	0.85	0.15	BDL	0	17
B4	0.41	0.05	BDL	0	141
B6	1.20	0.08	BDL	0	80
B7	0.92	0.07	BDL	0	1
B8	0.10	0.01	BDL	0	14
B11	0.36	0.03	BDL	0	92
B12	0.98	0.49	BDL	0	5
B13	0.21	0.02	BDL	0	1
B14	0.11	0.03	BDL	0	6
B20	0.23	0.02	BDL	0	10
B21	0.31	0.03	BDL	0	362
B23	1.88	0.18	373	37	34
B24	0.59	0.13	BDL	0	1194
B25	2.16	0.08	337	9	9
B26	0.29	0.05	BDL	0	8
B28	0.27	0.01	BDL	0	104
B30	1.04	0.21	BDL	0	218
B31	1.48	0.07	BDL	0	9
B32	0.29	0.01	BDL	0	7
B33	0.26	0.01	BDL	0	10
B34	0.31	0.01	BDL	0	10
B35	0.39	0.04	BDL	0	16
B37	0.30	0.01	BDL	0	10
B38	0.38	0.04	BDL	0	15
B39	0.15	0.01	BDL	0	3
B50	2.06	0.28	402	50	1287
B51	1.81	0.24	549	23	1488
B52	0.16	0.02	BDL	0	3
B53	2.10	0.18	253	20	991
B54	2.13	0.15	765	50	2040
B55	2.38	0.16	92	27	767
B56	0.34	0.04	BDL	0	12
B57	0.44	0.03	BDL	0	20

Mount Washington	H_2O (wt. %)	Std. Dev.	CO_2 ppm	Std. Dev.	Entrap. Press. (bars)
MW1	1.92	0.14	865	56	2145
MW2	1.62	0.17	BDL	0	262
MW3	0.49	0.05	210	16	477
MW4	2.06	0.06	281	35	1034
MW5	1.14	0.04	259	11	682
MW6	2.26	0.26	BDL	0	509
MW7	1.55	0.06	206	4	686
MW8	2.31	0.11	449	20	1490
MW9	1.01	0.08	116	10	348
MW10	0.75	0.05	267	16	623
MW11	1.99	0.20	536	54	1531
MW12	0.29	0.03	BDL	0	9
MW13	2.18	0.23	546	62	1629
MW14	0.48	0.05	BDL	0	23
MW17	0.22	0.02	BDL	0	5
MW18	2.11	0.06	459	52	1425
North Sister					
PC1-1	1.92	0.09	792	13	2006
PC1-2	0.94	0.06	BDL	0	84
PC1-3	0.49	0.03	202	14	460
PC1-4	1.49	0.10	BDL	0	221
PC1-6	0.80	0.04	234	12	563
PC1-8	2.14	0.10	466	22	1452
PC1-9	2.65	0.21	453	36	1663
PC1-10	1.25	0.04	BDL	0	154
PC1-11	1.14	0.05	BDL	0	127
PC1-13	2.60	0.09	709	23	2148
PC1-14	2.16	0.13	524	30	1578
PC1-15	0.55	0.02	BDL	0	30
PC1-16	1.55	0.08	387	21	1067
PC1-17	2.84	0.18	539	35	1934
PC1-18	2.18	0.06	977.00	31	2461

Table 1: Uncorrected Volatile Concentrations

BDL - Below Detectable Limits

Inclusion ID	Inclusion Height (um)	Inclusion Width (um)	Inclusion Depth (um)	Inclusion Volume (um^3)	Vapor Bubble Height (um)	Vapor Bubble Width (um)	Vapor Bubble Depth (um)	Vapor Bubble Volume (um^3)	Bubble Percent Volume of Inclusion
B 11	80	60	70	3.36E+05	31	20	26	1.62E+04	4.82
B 12	80	60	70	3.36E+05	25	16	21	8.63E+03	2.57
B 13	80	80	80	5.12E+05	27	18	23	1.13E+04	2.20
B 21	100	60	80	4.80E+05	36	25	30	2.70E+04	5.63
B 24	120	80	100	9.60E+05	35	24	29	2.44E+04	2.54
B 30	120	80	100	9.60E+05	54	41	48	1.06E+05	10.99
B 39	120	110	115	1.52E+06	48	33	41	6.58E+04	4.33
MW 1	100	80	90	7.20E+05	37	20	29	2.17E+04	3.01
MW 3	200	200	200	8.00E+06	91	60	76	4.14E+05	5.18
MW 4	110	80	95	8.36E+05	42	28	35	4.23E+04	5.06
MW 5	100	40	70	2.80E+05	34	21	28	2.00E+04	7.15
MW 7	200	200	200	8.00E+06	83	60	72	3.60E+05	4.50
MW 8	140	100	120	1.68E+06	50	33	42	6.94E+04	4.13
MW 9	160	80	120	1.54E+06	58	39	49	1.10E+05	7.17
MW 11	160	60	110	1.06E+06	72	42	57	1.73E+05	16.43
MW 12	40	30	35	4.20E+04	18	13	16	3.74E+03	8.90
MW 13	310	100	205	6.36E+06	77	55	66	2.77E+05	4.35
MW 18	120	60	90	6.48E+05	29	20	25	1.47E+04	2.26
PC 1	60	40	50	1.20E+05	20	13	17	4.33E+03	3.61
PC 2	40	40	40	6.40E+04	10	7	8	5.56E+02	0.87
PC 4	140	100	120	1.68E+06	61	41	51	1.26E+05	7.49
PC 6	200	100	150	3.00E+06	88	59	74	3.84E+05	12.80
PC 8	60	60	60	2.16E+05	20	14	17	4.34E+03	2.01
PC 10	60	60	60	2.16E+05	23	16	19	6.79E+03	3.15
PC 11	60	60	60	2.16E+05	26	17	21	9.45E+03	4.37
PC 14	100	100	100	1.00E+06	33	21	27	1.89E+04	1.89
PC 17	100	60	80	4.80E+05	34	21	28	1.99E+04	4.14

Table 2: Vapor Bubble Volume

unlike Ruscitto (2010), in which the few data points with below detection CO_2 concentrations are clearly outliers to the majority of volatile data.

Using VolatileCalc (Newman and Lowenstern, 2002), I calculated the crystallization pressures for the olivine host crystals using the H_2O and CO_2 data. The distribution of olivine crystallization pressures varies (Fig. 6). The modal trapping pressure of Belknap (~20 bar) is the lowest of the three sites. Mount Washington's modal trapping pressure (~500 bar) is significantly higher. North Sister trapping pressures do not display a distinct mode like at Belknap and Mount Washington. While the three sites display a wide range in trapping pressures, Belknap, Mount Washington, and North Sister maximum trapping pressures are similar (2461, 2145, and 2040 bars, respectively). Minimum trapping pressures also display a narrow range between sites (30, 5, and 1 bar(s), respectively). The distribution of trapping pressures appears mostly evenly distributed, except at Belknap, where melt inclusions trapped at very low pressure conditions are most common (Fig. 6).

The maximum H_2O values are not from the same inclusions as the maximum CO_2 values, suggesting slightly different degassing paths for different batches of magma. Variations between open and closed systems or closed systems with slightly varying contents of exsolved gas would alter the degassing profile. (*e.g.* Johnson et al., 2008). Some volcanoes degas steadily whereas other volcanoes appear to store gas over prolonged periods of time (Delmelle and Stix, 2000). Systems that degas steadily are referred to as open systems. In an open system, CO_2 exsolves and loses interaction with the magma. As a result, additional CO_2 exsolves and CO_2 quickly depletes itself in the magma with little change in H_2O (Fig. 7). Volcanoes that retain gas over a long period of

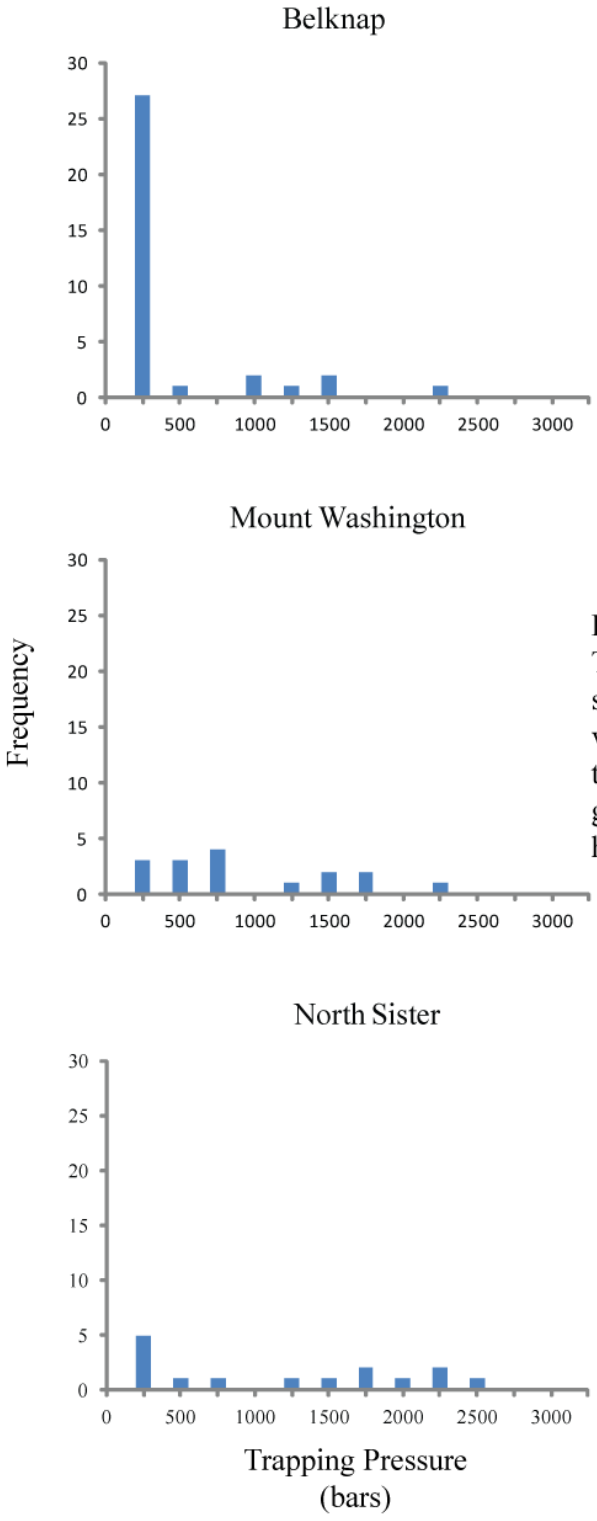

Figure 6: Trapping Pressures
The trapping pressure distribution at all three sites suggests continuous crystallization at varying pressures except at Belknap, where the trapping pressure frequency is much greater at low pressures (~250 bars) than at higher pressures.

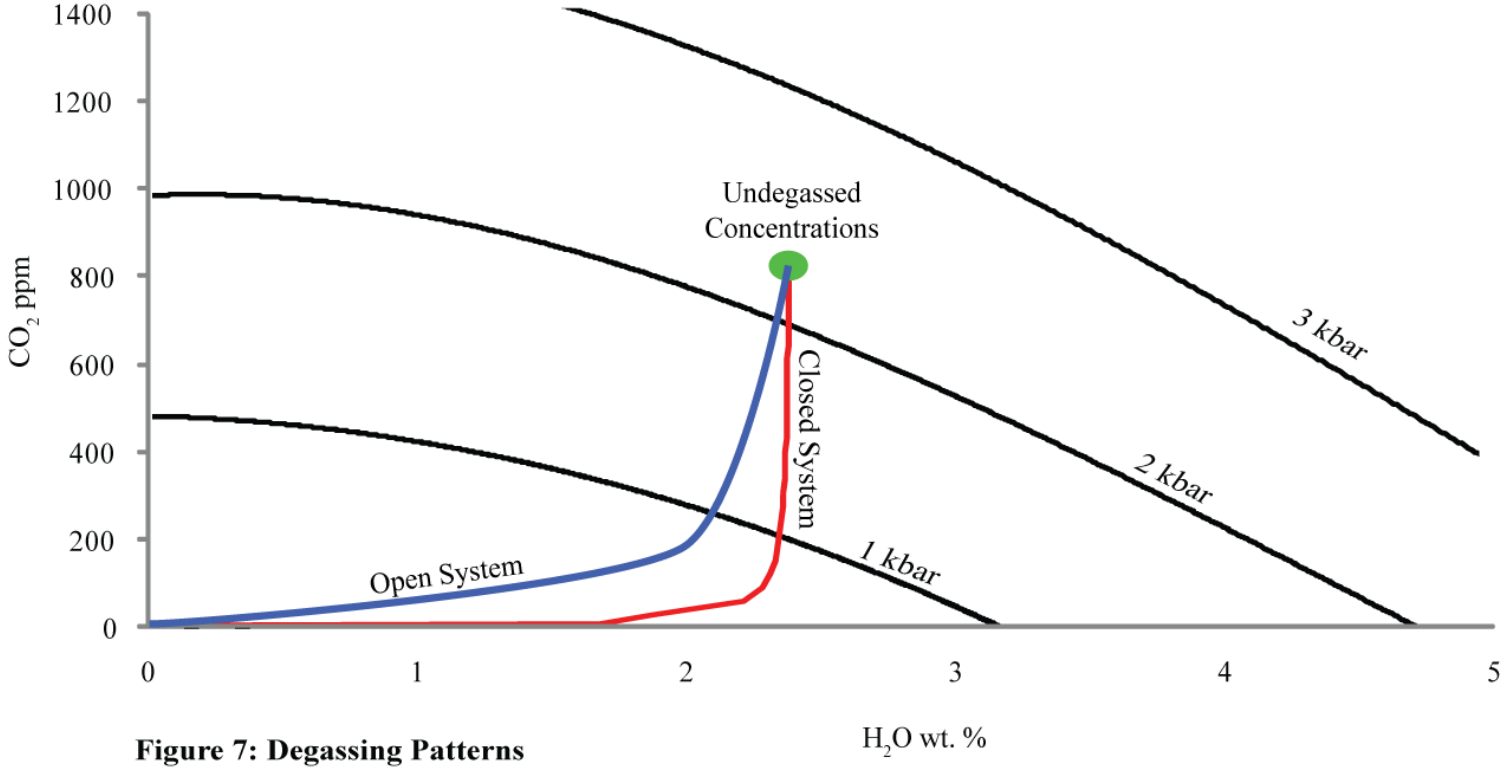

Figure 7: Degassing Patterns
Open systems exsolve CO_2 more quickly relative to H_2O than closed systems. Before significant H_2O loss occurs in an open system, CO_2 is nearly completely degassed. Under closed system conditions, exsolved CO_2 inhibits additional CO_2 from exsolving from the magma.

time are labeled as closed systems. In a closed system, the exsolved CO_2 remains in contact with the magma and additional CO_2 does not degas as readily, causing CO_2 contents to remain higher than in open system conditions over the same pressures (Fig. 7).

Additionally, the presence of vapor bubbles in several of these inclusions suggests that some of the volatiles dissolved in the melt inclusions at the time of trapping were lost from the melt to the vapor phase post-entrapment (see Section 4.1 for a discussion on the the origin of the vapor bubbles and an estimate of CO_2 lost). CO_2 was likely the most affected by this process, meaning that CO_2 values and trapping pressures reported here are likely lower than the original trapping pressure (Anderson and Brown, 1993). Johnson et al. (2010) calculate CO_2 partitioning into the vapor phase in melt inclusions and show that it can cause underestimates of up to 1 kbar. Although several inclusions contained vapor bubbles, vapor bubbles are not present in all inclusions. Belknap, Mount Washington, and North Sister each contain inclusions with < 1 wt. % H_2O that remain vapor bubble free, indicating shallow late-stage crystallization.

3.1. Major Element Geochemistry

The major element compositions of the melt inclusions (Fig. 8, Fig. 9, Table 3) are subalkaline and similar to calc-alkaline lavas from the Cascades (Conrey, unpublished; Mitchener, 1998; Schmidt, 2005; Mercer, 2009; Schmidt and Grunder, 2009; Schmidt and Grunder, 2011). The North Sister whole rock data (Conrey, unpublished; Schmidt and Grunder, 2009; Schmidt and Grunder, 2011) are limited in their range of major element compositions. However, Mercer (2009) analyzed melt inclusions from the second North Sister eruptive unit, NSba2. These melt inclusion

◆Belknap, ■ Mount Washington, ▲North Sister, & ● Whole Rock

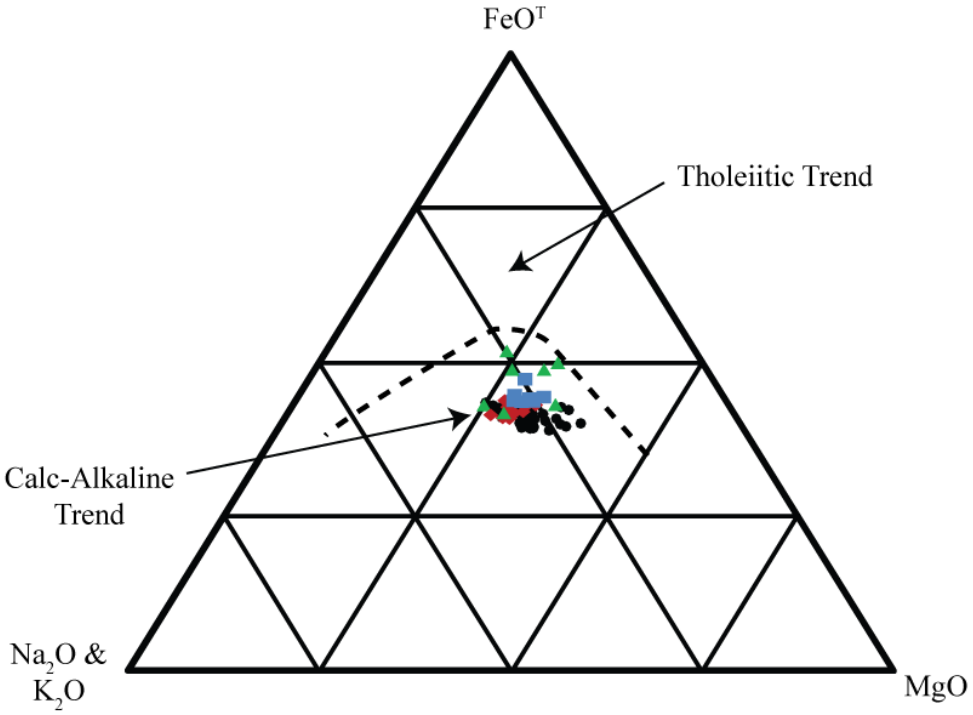

Figure 8: Ternary Diagram of Melt Inclusion & Whole Rock Compositions
Belknap, Mount Washington, and North Sister melt inclusion and whole rock data plot distinctly as calc-alkaline in origin.

Components are in wt. %.

Tholeiitic-Calc-alkaline distinction from Irvine and from Irvine and Baragar (1971).

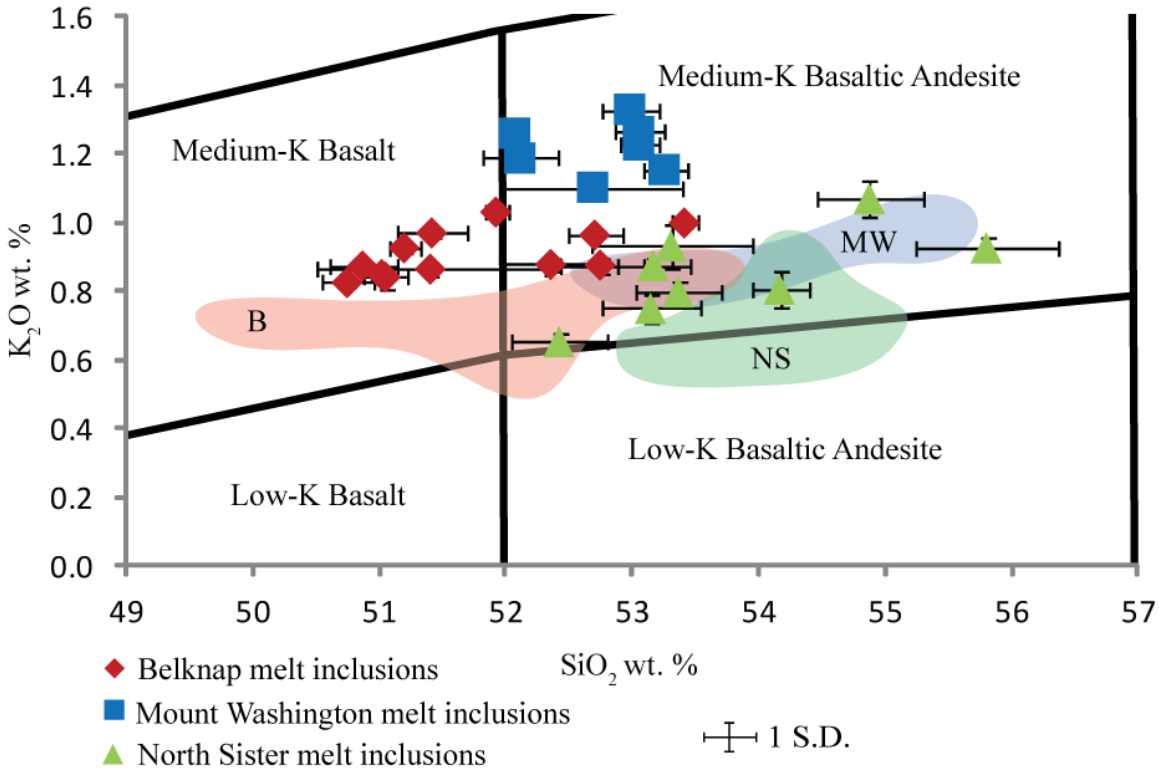

The shaded regions represent whole rock data from other studies.

Figure 9: Gills (1981) Calc-alkaline - Low-K Tholeiite Classification
According to the andesite series established from Gill (1981), from which this figure is modified, most of the shield compositions are classified as calc-alkaline basaltic andesites. Some Belknap melt inclusion and whole rock compositions have low enough SiO_2 to be classified as basalts. Some North Sister whole rock compositions contain low enough K_2O to be classified as low-K tholeiite basaltic andesites.

Belknap Mean Wt. %	B3-12	B3-13	B3-14	B3-22	B3-23	B3-30	B3-31	B3-32	B3-34	B3-37	B3-38	B3-39
SiO_2	52.36	51.03	51.93	51.41	52.75	51.05	53.42	51.42	51.20	52.71	50.75	50.87
Al_2O_3	18.29	19.63	18.47	19.97	19.46	18.67	16.81	18.75	17.74	18.58	19.58	18.70
Fe_2O_3	1.58	1.40	1.50	1.38	1.25	1.54	1.66	1.54	1.58	1.38	1.42	1.53
FeO	6.48	6.06	6.52	5.83	5.79	6.77	7.05	6.87	7.46	6.09	6.31	6.83
MgO	5.23	5.14	5.15	5.04	4.40	5.95	5.28	5.15	6.26	5.04	5.48	5.71
CaO	8.70	9.59	8.86	9.06	8.96	9.05	7.90	8.78	8.22	8.70	9.29	9.09
Na_2O	4.36	4.15	4.29	4.26	4.42	3.91	4.62	4.17	4.45	4.48	4.10	4.22
K_2O	0.88	0.85	1.03	0.86	0.88	0.84	1.00	0.97	0.93	0.96	0.82	0.87
TiO_2	1.31	1.28	1.42	1.37	1.24	1.32	1.40	1.44	1.36	1.31	1.29	1.31
MnO	0.13	0.12	0.11	0.12	0.11	0.13	0.16	0.13	0.12	0.10	0.10	0.13
P_2O_5	0.47	0.47	0.49	0.41	0.46	0.48	0.47	0.50	0.47	0.46	0.52	0.47
FeO (total)	7.90	7.32	7.87	7.07	6.91	8.15	8.55	8.26	8.89	7.32	7.59	8.20
S	0.07	0.07	0.06	0.06	0.07	0.08	0.06	0.09	0.07	0.06	0.07	0.08
Cl	0.11	0.10	0.09	0.08	0.10	0.09	0.12	0.11	0.11	0.10	0.11	0.08
F	0.02	0.12	0.09	0.14	0.12	0.12	0.06	0.09	0.02	0.03	0.13	0.10
Wt. % Ol added	0.0	1.8	2.0	1.0	3.7	2.7	1.2	2.8	5.4	2.5	2.9	3.2
Std. Dev.												
SiO_2	0.41	0.08	0.09	0.90	0.33	0.18	0.10	0.28	0.13	0.22	0.20	0.26
Al_2O_3	0.50	0.18	0.11	0.15	0.27	0.03	0.16	0.10	0.12	0.16	0.41	0.11
FeO	0.41	0.15	0.17	0.43	0.17	0.15	0.07	0.17	0.23	0.21	0.35	0.16
MgO	0.47	0.03	0.03	0.09	0.06	0.05	0.05	0.04	0.08	0.04	0.05	0.07
CaO	0.05	0.04	0.05	0.04	0.04	0.50	0.59	0.04	0.06	0.05	0.48	0.60
Na_2O	0.33	0.13	0.20	0.19	0.20	0.11	0.11	0.17	0.24	0.10	0.14	0.15
K_2O	0.02	0.02	0.01	0.02	0.02	0.03	0.01	0.01	0.02	0.02	0.01	0.01
TiO_2	0.02	0.02	0.01	0.04	0.03	0.01	0.02	0.02	0.01	0.02	0.04	0.02
MnO	0.00	0.00	0.01	0.01	0.01	0.01	0.03	0.01	0.01	0.02	0.02	0.01
P_2O_5	0.01	0.01	0.01	0.02	0.01	0.01	0.01	0.01	0.00	0.01	0.01	0.01
S	0.00	0.00	0.00	0.00	0.00	0.00	0.00	0.00	0.00	0.00	0.00	0.00
Cl	0.00	0.01	0.00	0.00	0.00	0.00	0.00	0.01	0.00	0.00	0.00	0.00
F	0.04	0.12	0.13	0.15	0.17	0.19	0.01	0.16	0.02	0.04	0.15	0.10

Table 3: Major Elements

Mount Washington Mean Wt. %	MW1	MW3	MW6a	MW8	MW9	MW10	MW12
SiO_2	53.06	53.06	53.26	52.69	52.99	52.12	52.08
Al_2O_3	18.66	18.91	18.12	17.70	16.87	17.50	19.55
Fe_2O_3	1.56	1.47	1.58	1.63	1.79	1.63	1.48
FeO	6.39	6.21	6.49	7.22	7.95	7.21	6.22
MgO	5.50	4.71	5.33	6.24	5.66	5.93	4.88
CaO	8.35	9.00	8.52	8.08	7.63	8.61	8.84
Na_2O	3.57	3.60	3.93	3.71	3.90	3.97	3.78
K_2O	0.91	0.97	0.91	0.88	1.05	1.01	0.98
TiO_2	1.26	1.23	1.15	1.10	1.33	1.19	1.26
MnO	0.14	0.14	0.12	0.13	0.15	0.13	0.12
P_2O_5	0.31	0.42	0.38	0.41	0.44	0.36	0.42
FeO (total)	7.79	7.53	7.92	8.69	9.56	8.67	7.55
S	0.08	0.06	0.07	0.07	0.07	0.08	0.08
Cl	0.06	0.07	0.06	0.08	0.07	0.06	0.07
F	0.14	0.15	0.08	0.06	0.11	0.21	0.23
Wt. % Ol added	0.0	1.0	0.0	3.0	2.9	3.0	0.7
Std. Dev.							
SiO_2	0.19	0.15	0.17	0.71	0.23	0.30	0.01
Al_2O_3	0.32	0.20	0.23	0.42	0.05	0.09	0.04
FeO	0.05	0.19	0.21	0.08	0.20	0.11	0.06
MgO	0.23	0.06	0.07	0.03	0.03	0.01	0.03
CaO	0.05	0.06	0.07	0.79	0.04	0.60	0.00
Na_2O	0.21	0.08	0.09	0.14	0.29	0.14	0.09
K_2O	0.04	0.02	0.02	0.03	0.01	0.01	0.02
TiO_2	0.02	0.03	0.04	0.03	0.03	0.03	0.01
MnO	0.01	0.02	0.02	0.01	0.01	0.01	0.02
P_2O_5	0.01	0.00	0.01	0.01	0.00	0.01	0.00
S	0.00	0.00	0.00	0.00	0.00	0.00	0.00
Cl	0.00	0.00	0.00	0.01	0.00	0.00	0.01
F	0.14	0.12	0.14	0.08	0.15	0.19	0.14

Table 3: Major Elements (continued)

North Sister Mean Wt. %	PC2	PC3	PC4	PC6	PC9	PC13	PC16	PC18
SiO_2	53.31	53.17	53.37	54.88	53.15	54.17	52.43	55.80
Al_2O_3	14.31	15.65	17.13	17.14	16.98	16.47	17.46	16.40
Fe_2O_3	2.27	2.03	1.65	1.48	1.73	1.90	1.85	1.44
FeO	9.30	8.88	6.77	6.47	7.08	7.87	8.04	6.34
MgO	7.03	4.82	5.57	4.48	6.80	5.01	5.91	5.10
CaO	6.87	8.14	8.13	7.32	7.89	7.67	8.41	7.42
Na_2O	3.34	4.19	4.83	4.70	3.75	4.16	3.56	4.54
K_2O	0.93	0.87	0.80	1.07	0.75	0.81	0.65	0.93
TiO_2	1.79	1.48	1.17	1.67	1.10	1.21	1.06	1.41
MnO	0.19	0.16	0.14	0.13	0.13	0.15	0.15	0.12
P_2O_5	0.38	0.37	0.30	0.44	0.32	0.29	0.26	0.34
FeO (total)	11.34	10.71	8.25	7.80	8.64	9.58	9.71	7.63
S	0.08	0.04	0.04	0.06	0.05	0.07	0.08	0.06
Cl	0.10	0.08	0.09	0.10	0.09	0.08	0.08	0.08
F	0.10	0.10	0.03	0.06	0.17	0.13	0.07	0.02
Wt. % Ol added	0.0	2.3	0.1	1.9	0.0	2.3	2.3	2.2
Std. Dev.								
SiO_2	0.63	0.29	0.34	0.43	0.39	0.22	0.38	0.57
Al_2O_3	0.19	0.13	0.13	0.20	0.11	0.19	0.18	0.16
FeO	0.10	0.18	0.13	0.11	0.12	0.23	0.01	0.14
MgO	0.04	0.29	0.04	0.02	0.46	0.02	0.14	0.09
CaO	0.29	0.16	0.05	0.30	0.08	0.21	0.04	0.16
Na_2O	0.22	0.23	0.07	0.12	0.07	0.14	0.31	0.35
K_2O	0.06	0.02	0.03	0.06	0.04	0.05	0.02	0.03
TiO_2	0.10	0.01	0.04	0.12	0.04	0.05	0.02	0.04
MnO	0.02	0.01	0.01	0.01	0.01	0.01	0.03	0.02
P_2O_5	0.02	0.01	0.00	0.02	0.01	0.00	0.00	0.01
S	0.01	0.00	0.00	0.00	0.00	0.00	0.00	0.00
Cl	0.01	0.00	0.01	0.01	0.01	0.01	0.00	0.01
F	0.12	0.14	0.02	0.14	0.10	0.15	0.03	0.04

Table 3: Major Elements (continued)

compositions represent the only previously analyzed melt inclusions at North Sister. The NSba2 inclusions display a much greater degree of variation in FeO^T and TiO_2 than the whole rock compositions, but are similar to my North Sister inclusion compositions. The FeO^T and TiO_2 contents of the Mercer (2009) NSba2 and my PC melt inclusions span a similar range of values several wt. % higher in FeO^T and nearly 1 wt. % higher in TiO_2 than in the lava compositions.

The largest compositional differences between the shield melt inclusion compositions are observed with SiO_2, K_2O, P_2O_5, TiO_2, and FeO^T (Fig. 10, Fig. 11). Belknap, Mount Washington, and North Sister melt inclusion SiO_2 range from 50.8-53.4, 52.1-53.3, and 52.4-55.8 wt. %, respectively (Fig. 10). Belknap melt inclusions contain the highest concentrations of P_2O_5 (Fig. 10a) and Al_2O_3 (Fig. 10b) followed by Mount Washington with North Sister with the lowest concentrations of these oxides. North Sister TiO_2 contents display the highest variability, with the highest and lowest values of the three sample sites similar to Mercer's (2009) melt inclusion analyses from the North Sister second eruptive unit. Belknap's average TiO_2 contents are higher than Mount Washington's (Fig. 11a). K_2O and SiO_2 are positively correlated, with Mount Washington inclusions containing the highest K_2O values, followed by Belknap, and then North Sister (Fig. 10d).

FeO^T and MgO concentrations are negatively correlated at Belknap and Mount Washington (Fig. 11a). North Sister FeO^T displays the greatest variability of the three sites, with no distinct relationship with MgO. North Sister FeO^T appears to decrease with increasing SiO_2 also like Mercer's (2009) analyses (Fig. 10c, Fig. 11c). Melt inclusion

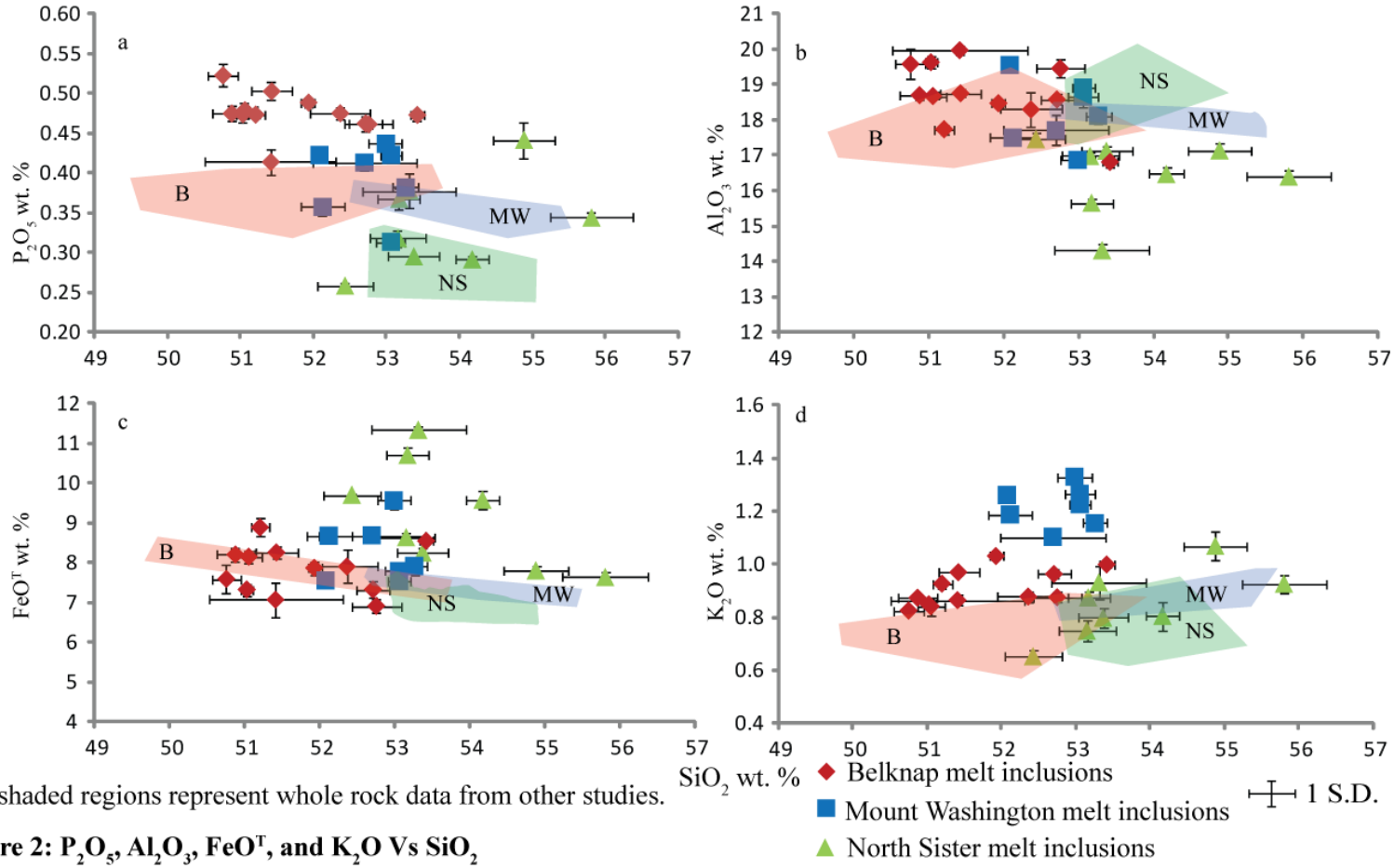

The shaded regions represent whole rock data from other studies.

Figure 2: P_2O_5, Al_2O_3, FeO^T, and K_2O Vs SiO_2

(a) Belknap inclusions often have the highest concentration of incompatible components. (b) Al_2O_3 concentrations do not vary greatly between volcanoes, though Belknap displays Al_2O_3 wt. % greater than Mount Washington and Mount Washington displays Al_2O_3 wt. % greater greater than North Sister. (c) Belknap and Mount Washington display similar levels of FeO^T, but North Sister FeO^T concentrations display large variability. (d) Belknap does not always display the highest concentations of incompatible elements. Mount Washington has higher K_2O contents than Belknap.

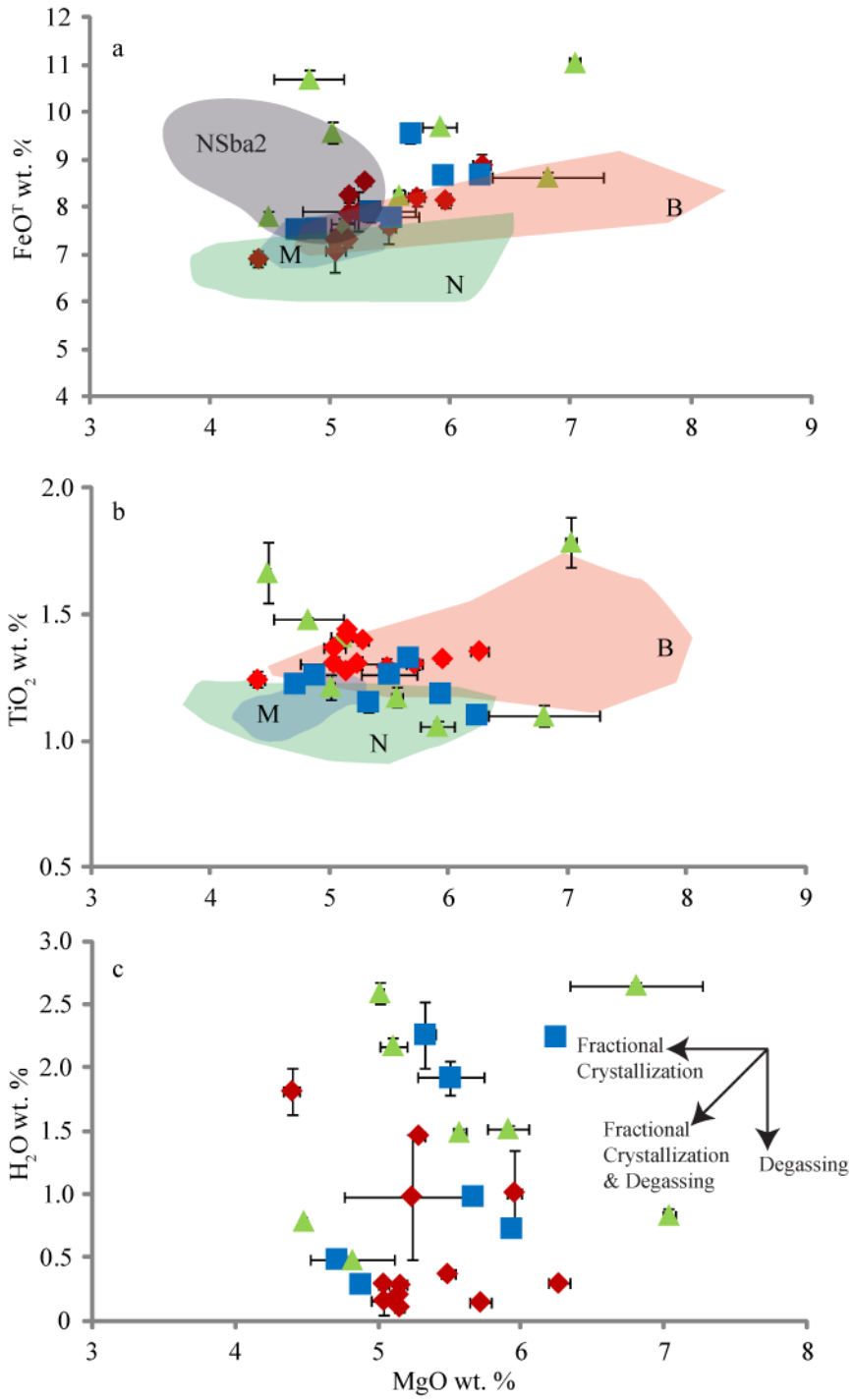

Figure 11: Distinct Major Oxides Vs MgO

(a,b) Belknap and Mount Washington contain similar FeO^T and TiO_2 values, while North Sister FeO^T and TiO_2 contents vary greatly. (c) H_2O and MgO do not appear correlated.

H_2O contents do not show any systematic variation with MgO in any of the shield suites (Fig. 11b).

In the Lassen region of the southern Cascades, Borg (1995) found that olivine crystals from larger, more complex magmatic systems often displayed lower Fo contents than crystals from smaller systems. The olivine host crystals from the shield volcanoes (Belknap $Fo_{79.7}$ to $Fo_{82.6}$; Mount Washington $Fo_{78.9}$ to $Fo_{81.6}$; North Sister $Fo_{74.0}$ to $Fo_{81.2}$) show a similar pattern, with lower forsterite contents than those of nearby cinder cones (~Fo_{84}) (Ruscitto, 2010), suggesting shield volcano magmas experience greater extents of differentiation prior to entrapment (Fig. 12). The observed North Sister olivine host crystal Fo contents were similar to the Fo contents of North Sister olivine crystals analyzed by Mercer (2009).

3.2.0. Modeled Primary Magmas

To determine from which mantle sources the volcanoes drew their magmas, I used several models to try to restore observed primitive (high MgO) melt inclusion compositions to their original, mantle-like primary compositions. Using more than one restoration method allowed me compare results and observe if one restoration method was anomalous to the others. However, no single method stood out from the others and produced modeled-primary compositions drastically different from the other methods (Fig. 13). I then used these modeled-primary shield compositions and compared them to those of cinder cones by Ruscitto et al. (2010) to determine if the shields and cinder cones shared the same mantle source.

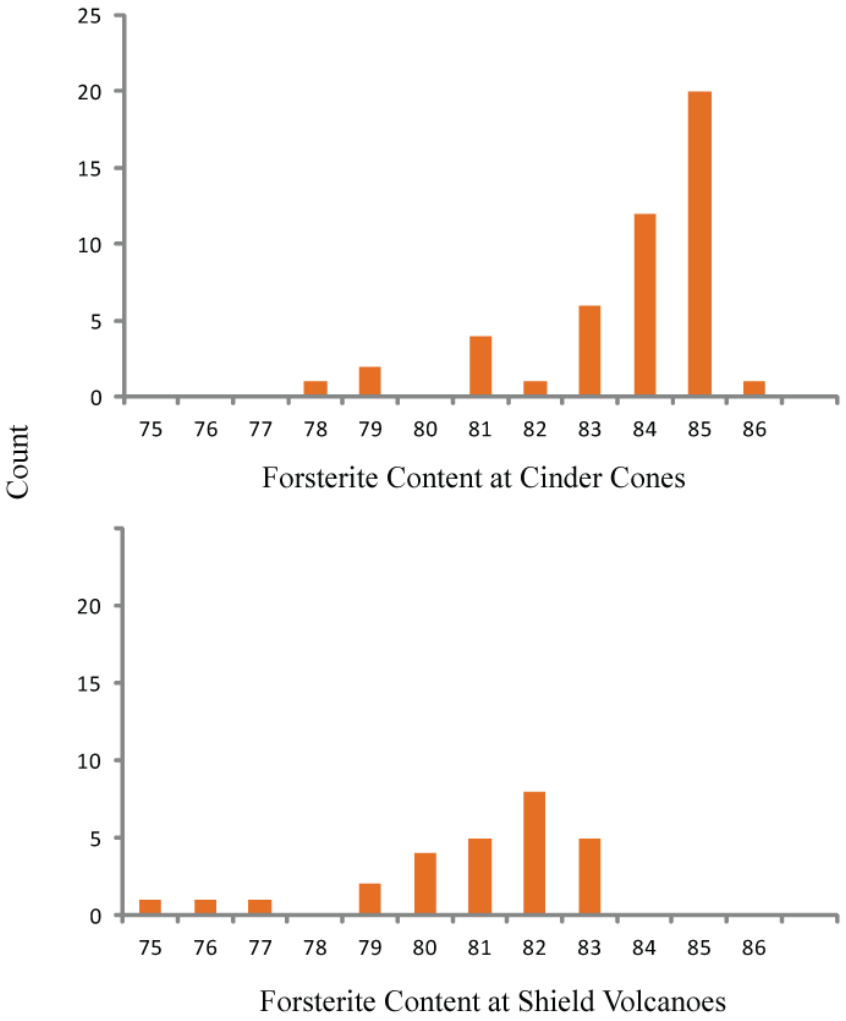

Figure 12: $Fo_{\#}$ of Central Oregon Cinder Cones and Shields
Olivine crystals from shield volcanoes display lower Fo content than that of nearby cinder cones. Cinder cone data provided by Ruscitto (2010). Bin values indicate minimum $Fo_{\#}$. More primitive, less evolved compositions produce higher olivine crystals. Olivine crystals from Cascade shields have a lower $Fo_{\#}$ than Cascade cinder cones, a trend that is consistent between these two vent types from other arcs (Borg, 1995).

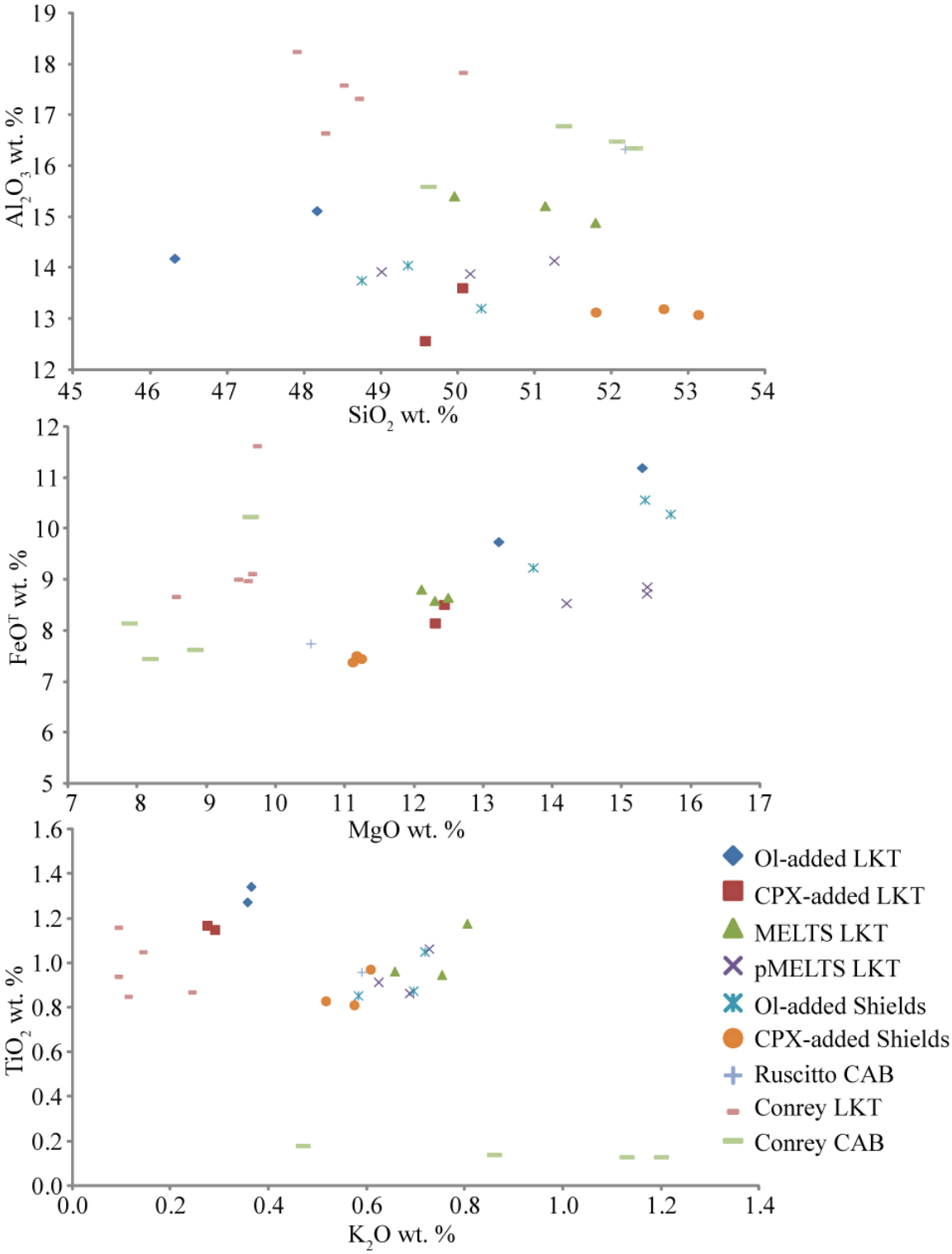

Figure 13: Restored Magma Compositions
Conrey compostions are from Conrey et al. (1997).
Ruscitto composition is from Ruscitto et al. (2010).

3.2.1. Restoring Primitive Shield Compositions

The mass of solid phases added to the melt to return the composition to that of a primary magma varied by the method used. Olivine addition typically required less olivine added than clinopyroxene during clinopyroxene addition. Using the method of adding 0.1 wt. % equilibrium olivine, Belknap required addition of 28.9 wt. % olivine to return the melt to equilibrium with Fo_{90} (Table 4). Mount Washington required 22.5 wt. % olivine addition and North Sister required 28.5 wt. %. Although the model from Danyushevsky (2001) was to add both olivine and clinopyroxene when the phases were in equilibrium with the melt composition, only clinopyroxene was added because the model never found the melt compositions to be in equilibrium with olivine. Restoring primitive compositions by adding clinopyroxene only until the compositions were in equilibrium with clinopyroxene Mg# 92 required a higher wt. % addition than when adding olivine. Belknap required 34.4 wt. % clinopyroxene addition, Mount Washington required 34.1 wt. %, and North Sister required 30.1 wt. %.

Though olivine, clinopyroxene, plagioclase and spinel crystallization may potentially all have been involved, MELTS and pMELTS only found olivine to be an equilibrium liquidus phase. Thus, the results from the MELTS and pMELTS models are inconsistent with those of the Danyushevsky (2001) model. When using MELTS at 1 kb to add 1 wt. % of the liquidus phase, Belknap required 14 wt. % olivine addition, Mount Washington required 15 wt. % olivine addition, and North Sister required 13 wt. % olivine addition. When using pMELTS at 8 kb to add 1 wt. % of the liquidus phase, Belknap required 24 wt. % olivine addition, Mount Washington required 24 wt. % olivine addition, and North Sister required 7 wt. % olivine addition.

	SiO_2	Al_2O_3	Fe_2O_3	FeO	MgO	CaO	Na_2O	K_2O	TiO_2	MnO	P_2O_5	FeO^T	Wt. % Ol/CPX added
Primitive CAB													
CAB	52.2	16.5	1.6	6.3	10.5	7.7	3.6	0.6	1.0	0.1	0.2	7.8	16.41
Olivine Restored LKT													
LKT1	48.2	15.1	1.4	8.5	13.2	8.8	2.7	0.4	1.3	0.2	0.3	9.7	12.00
LKT2	46.3	14.2	1.5	9.9	15.3	8.5	2.1	0.4	1.4	0.1	0.3	11.2	23.40
CPX Restored LKT													
LKT1	50.1	13.6	0.8	7.4	12.3	11.6	2.3	0.3	1.2	0.2	0.2	8.1	27.26
LKT2	49.6	12.6	1.0	7.7	12.4	13.4	1.6	0.3	1.2	0.2	0.2	8.5	38.94
Olivine Restored Shields													
Belknap	48.8	13.8	1.5	9.2	15.3	6.4	3.5	0.7	1.1	0.1	0.4	10.6	28.90
Mount Washington	49.4	14.1	1.4	8.0	13.7	6.4	2.9	0.7	0.9	0.1	0.3	9.2	22.50
North Sister	50.3	13.2	1.5	8.9	15.7	6.1	2.9	0.6	0.9	0.1	0.2	10.3	28.50
CPX Restored Shields													
Belknap	51.8	13.1	0.9	6.7	11.2	11.3	3.0	0.6	1.0	0.1	0.3	7.5	34.40
Mount Washington	52.7	13.3	0.8	6.7	11.1	11.1	2.5	0.6	0.8	0.1	0.3	7.4	34.06
North Sister	53.1	13.2	0.8	6.8	11.2	10.5	2.6	0.5	0.8	0.1	0.2	7.5	30.72
Olivine-added with MELTS 1kb													
Belknap	50.0	15.4	1.4	7.6	12.1	7.2	3.9	0.8	1.2	0.1	0.4	8.8	14
Mount Washington	51.1	15.2	1.4	7.4	12.5	7.0	3.2	0.8	0.9	0.1	0.4	8.7	15
North Sister	51.8	14.9	1.5	7.2	12.3	6.9	3.3	0.7	1.0	0.1	0.3	8.6	13
Olivine-added with pMELTS 8kb													
Belknap	49.0	13.9	1.2	7.7	15.4	6.5	3.5	0.7	1.1	0.5	0.4	8.9	24
Mount Washington	50.2	13.9	1.3	7.6	15.4	6.4	2.9	0.7	0.9	0.5	0.3	8.7	24
North Sister	51.3	14.1	1.4	7.2	14.2	6.6	3.1	0.6	0.9	0.2	0.3	8.5	7

Table 4: Primitive Compositions

CAB: Primitive Collier Cone from Ruscitto et al. (2010)

LKT1: FLR-03-1 Whole rock from Rowe et al. (2009)

LKT2: FLR-03-1 Melt inclusion from Rowe et al. (2009)

Primitive compositions calculated by olivine addition contained higher H_2O than by clinopyroxene addition because more clinopyroxene was required, resulting in more dilution of the H_2O. Olivine-added primitive shield compositions displayed greater variability in MgO, K_2O, and FeO^T than clinopyroxene-added compositions. SiO_2 after olivine addition ranged from 48.8-51.8 wt. %, whereas SiO_2 after clinopyroxene addition ranged from 51.8-53.1 wt. % (Fig. 13).

3.2.2. Restoring the Primitive Low-K Tholeiite

As another means for determining the origins of the magmas feeding the volcanoes, I used MELTS to model the liquid line of descent for a primary calc-alkaline magma from Ruscitto et al. (2010) as well as a primary low-K tholeiite magma described in Section 2.6. The results for modeling the primary the LKT magma compositions are described in this section.

The low-K tholeiite (FLR-03-1) from Rowe et al. (2009) required 12.0 (whole rock) to 23.4 (melt inclusion) wt. % olivine addition to return to mantle conditions (Table 4). Returning FLR-03-1 to a composition in equilibrium with the mantle using clinopyroxene addition required 27.3 (whole rock) to 38.9 (melt inclusion) wt. % addition. By means of comparison, Ruscitto et al. (2010) added 14.9 wt. % olivine to return a Collier Cone melt inclusion from a calc-alkaline basaltic andesite to a composition in equilibrium with mantle olivine.

In general, the olivine-added primitive compositions have SiO_2, MgO, and FeO^T contents that cover a wider range in concentrations than in the clinopyroxene-added primitive compositions (Fig. 13, Table 4). Both the olivine-added primitive low-K tholeiite and clinopyroxene-added low-K tholeiite contain lower SiO_2 than the restored

calc-alkaline basaltic andesite from Ruscitto et al. (2010). The primitive low-K tholeiite compositions from both restoration methods also displayed considerably higher MgO, FeO^T, and TiO_2 than the Ruscitto et al. (2010) calc-alkaline basaltic andesite, though the low-K tholeiite restored by clinopyroxene addition had values more similar to the Ruscitto et al. (2010) calc-alkaline basaltic andesite than the olivine addition low-K tholeiite (Fig. 13, Table 4).

All primary restoration models yielded Al_2O_3 contents lower than observed in regional LKTs and CABs (Fig. 13). This is likely because plagioclase plays some role during fractionation, but none of the models used calculated plagioclase to be a liquidus phase. The absence of plagioclase addition to the compositions being modeled reduced the Al_2O_3 concentrations in the final modeled compositions. Inaccuracies in estimating f_{O2}, H_2O content, or pressure for model inputs could explain the erroneous absence of plagioclase from the modeled system.

In summary, the Danyushevsky (2001) model required more wt. % clinopyroxene added than the Ruscitto et al. (2010) olivine addition method required olivine added to return the compositions to mantle equilibrium conditions. The clinopyroxene-added composition contains lower MgO contents than those of the olivine-added method. Also, the clinopyroxene-added compositions display less variation in major elements than the olivine-added compositions.

CHAPTER IV

DISCUSSION

4.0. Overview

This discussion section addresses several aspects of the data. Section 4.1 covers the vapor bubble correction employed to find the original volatile contents of the melt inclusions at the time of trapping, which are not very different than the measured values. Section 4.2 addresses the evidence for shallow degassing inferred from the volatile data. Section 4.3 analyzes the geochemical trends of the major element compositions of the melt inclusions. Section 4.4 continues the ongoing discussion regarding the origin of parental shield magmas. Section 4.5 reviews the results of the modeling of primary magma compositions and finds that shields and cinder cones can share the same mantle magma source. Section 4.6 discusses upper crustal structure and its relation to long-lived and short-lived vents. Finally, Section 4.7 addresses the hazards implications of shallow degassing and the forecasting of future eruptions.

4.1. Vapor Bubble Correction

Although the majority of melt inclusions in this study do not contain vapor bubbles, several melt inclusions have vapor bubbles and require a correction to accurately determine the initial pressures of entrapment. Vapor bubble frequency appears to favor inclusions formed under low pressures at Belknap and North Sister, while Mount Washington vapor bubbles display no correlation with entrapment pressure (Table 5).

Most vapor bubbles in melt inclusions are interpreted to be a product of melt shrinkage during cooling (Anderson and Brown, 1993). Riker (2005) used Ryan and Sammis (1981) to determine the shrinkage volume as a function of change in temperature

Sample	Mol fraction CO_2	Press. (bars)	Pre-eruptive bubble volume (um)	Molar Volume CO_2 at 1200° C (um^3/mol)	CO_2 in bubble (mol)	Mol. weight CO_2 (g/mol)	CO_2 in bubble (g)	Glass mass (g)	Shrinkage bubble CO_2 conc. (ppm)	H_2O glass (wt %)	CO_2 conc. in glass (ppm)	Original CO_2 (ppm)
B 11	88.78	14	2.69E+05	9.06E+18	2.63E-12	44.01	1.16E-10	8.73E-07	1.33	0.36	BDL	BDL
B 12	88.78	92	1.68E+04	1.33E+18	1.12E-12	44.01	4.93E-11	8.90E-07	0.55	0.98	BDL	BDL
B 13	88.78	5	2.56E+04	2.46E+19	9.22E-14	44.01	4.06E-12	1.36E-06	0.03	0.21	BDL	BDL
B 21	88.78	10	3.84E+05	1.20E+19	2.85E-12	44.01	1.25E-10	1.35E-06	0.93	0.31	BDL	BDL
B 24	88.78	34	4.80E+04	3.61E+18	1.18E-12	44.01	5.19E-11	2.74E-06	0.19	0.59	BDL	BDL
B 30	88.78	104	4.80E+04	1.17E+18	3.63E-12	44.01	1.60E-10	2.49E-06	0.64	1.04	BDL	BDL
B 39	88.78	3	1.21E+06	4.60E+19	2.34E-12	44.01	1.03E-10	4.11E-06	0.25	0.15	BDL	BDL
MW 1	80.08	2146	3.60E+04	5.71E+16	5.05E-11	44.01	2.22E-09	1.87E-06	11.90	1.92	865.40	877
MW 3	94.71	477	6.40E+06	2.57E+17	2.36E-09	44.01	1.04E-07	2.08E-05	49.97	0.49	210.36	260
MW 4	56.44	1034	6.69E+05	1.18E+17	3.19E-10	44.01	1.40E-08	2.16E-06	64.94	2.06	281.24	346
MW 5	80.34	683	2.24E+05	1.79E+17	1.00E-10	44.01	4.42E-09	7.08E-07	62.41	1.14	258.74	321
MW 7	63.46	687	6.40E+06	1.78E+17	2.28E-09	44.01	1.00E-07	2.29E-05	43.90	1.55	206.49	250
MW 8	61.19	1492	1.34E+06	8.21E+16	1.00E-09	44.01	4.41E-08	4.33E-06	101.88	2.31	448.77	551
MW 9	71.10	349	1.23E+06	3.51E+17	2.49E-10	44.01	1.10E-08	3.99E-06	27.49	1.01	115.61	143
MW 11	71.31	1532	5.28E+04	7.99E+16	4.71E-11	44.01	2.07E-09	3.12E-06	6.64	1.99	536.26	543
MW 12	80.34	9	2.10E+03	1.35E+19	1.25E-14	44.01	5.48E-13	1.15E-07	0.05	0.29	BDL	BDL
MW 13	67.77	1630	3.18E+05	7.51E+16	2.87E-10	44.01	1.26E-08	1.76E-05	7.16	2.18	545.58	553
MW 18	65.84	1425	3.24E+04	8.59E+16	2.48E-11	44.01	1.09E-09	1.74E-06	6.28	2.11	459.16	465
PC 1	78.88	792	6.00E+03	6.10E+16	7.75E-12	44.01	3.41E-10	3.14E-07	10.87	1.92	791.86	803
PC 2	88.78	0	3.20E+03	1.45E+18	1.95E-13	44.01	8.60E-12	1.74E-07	0.49	0.94	BDL	BDL
PC 4	88.78	0	1.68E+06	5.54E+17	2.69E-10	44.01	1.18E-08	4.38E-06	27.03	1.49	BDL	BDL
PC 6	88.78	234	1.50E+05	2.17E+17	6.13E-11	44.01	2.70E-09	7.50E-06	3.60	0.80	233.61	237
PC 8	65.50	466	1.08E+04	8.44E+16	8.39E-12	44.01	3.69E-10	5.68E-07	6.50	2.14	466.31	473
PC 10	88.78	0	1.08E+04	7.98E+17	1.20E-12	44.01	5.29E-11	5.85E-07	0.90	1.25	BDL	BDL
PC 11	88.78	0	1.73E+05	9.67E+17	1.59E-11	44.01	6.98E-10	5.76E-07	12.12	1.14	BDL	BDL
PC 14	67.40	524	5.00E+04	7.76E+16	4.34E-11	44.01	1.91E-09	2.59E-06	7.38	2.16	524.15	532
PC 17	55.35	539	2.40E+04	6.33E+16	2.10E-11	44.01	9.23E-10	1.31E-06	7.07	2.84	538.92	546

Table 5: Restored CO_2

BDL - Below Detectable Limits

(ΔT) from crystallization to eruption as depicted by Figure 14. Many of the observed vapor bubbles in the melt inclusions from the polygenetic volcanoes are in excess of the volume predicted for a given ΔT, suggesting exsolved vapor bubbles are primary bubbles that were co-entrapped with the melt during crystallization.

Syn-genetic bubbles are bubbles captured with melt during crystallization. Because bubbles larger than 5% inclusion volume were likely syn-genetic bubbles rather than shrinkage bubbles, I did not correct for CO_2 loss in bubbles > 5% of their inclusion volume (Riker, 2005). Riker (2005) provides the following equation (3) to correct for CO_2 partitioning in shrinkage bubbles:

$$original\ incl.CO2 = \frac{(mol\ fraction\ CO2)(pre\ eruptive\ bubble\ vol)(mol\ weight\ CO2)}{(molar\ vol\ CO2\ at\ 1200^\circ C)(glass\ inclmass)} + incl.CO2 \quad (3)$$

Because trapping pressures relative to other inclusion studies (*e.g.* Johnson et al., 2010; Ruscitto, 2010; Walowski et al., 2012) were low (< 2 kbar), only marginal concentrations of CO_2, often < 50 ppm, were lost into the vapor bubble (Table 5). As a result, the corrected trapping pressures were only marginally higher than the uncorrected values. After the correction for CO_2 partitioning is applied to the melt inclusions from the polygenetic volcanoes, the pattern of continuous degassing to shallow pressures, originally shown with uncorrected volatile values in Figure 5, remains and is shown with corrected volatile values in Figure 15.

4.2. Volatile Degassing

The volatile data suggest shallow degassing was important at each volcano. H_2O degassing induces crystallization because H_2O depresses crystallization temperatures (Sisson and Layne, 1993; Sisson and Grove, 1993; Moore and Carmichael, 1998). The continuous range of degassing pressures from > 2 kbar to < 10 bar in Figure 15 indicates

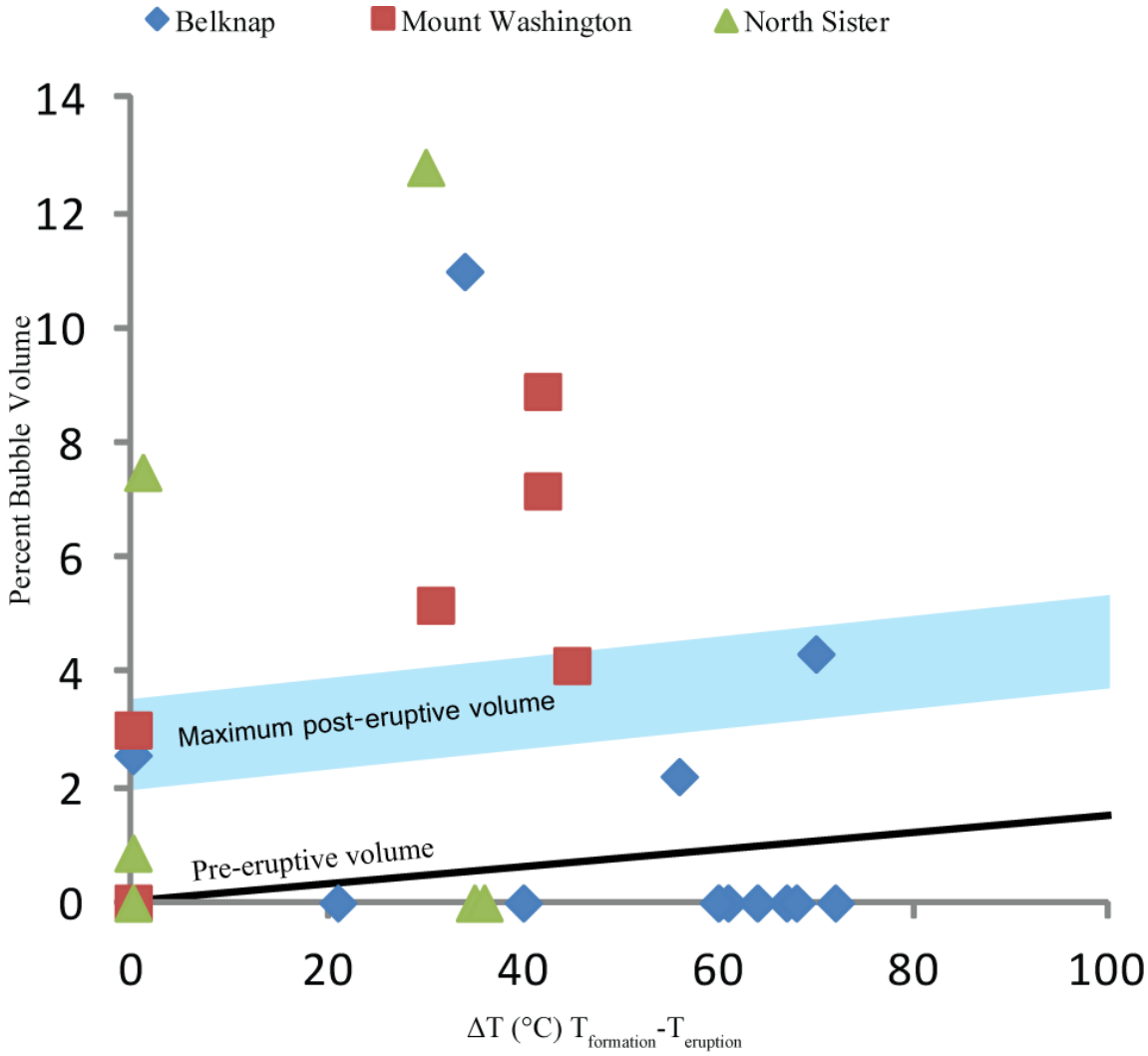

Figure 14: Bubble Volume - Observed and Expected
Maximum post-eruptive volumes are modeled after Riker (2005), which assumed a glass transition temperature of 820° C from Ryan and Sammis (1981) to estimate shrinkage bubble volumes. Bubbles greater than the maximum post-eruptive volume are too large to be shrinkage bubbles and instead are syn-genetic.

This figure is modeled after Riker (2005), in which it was originally used for shrinkage bubbles from Mauna Loa melt inclusions.

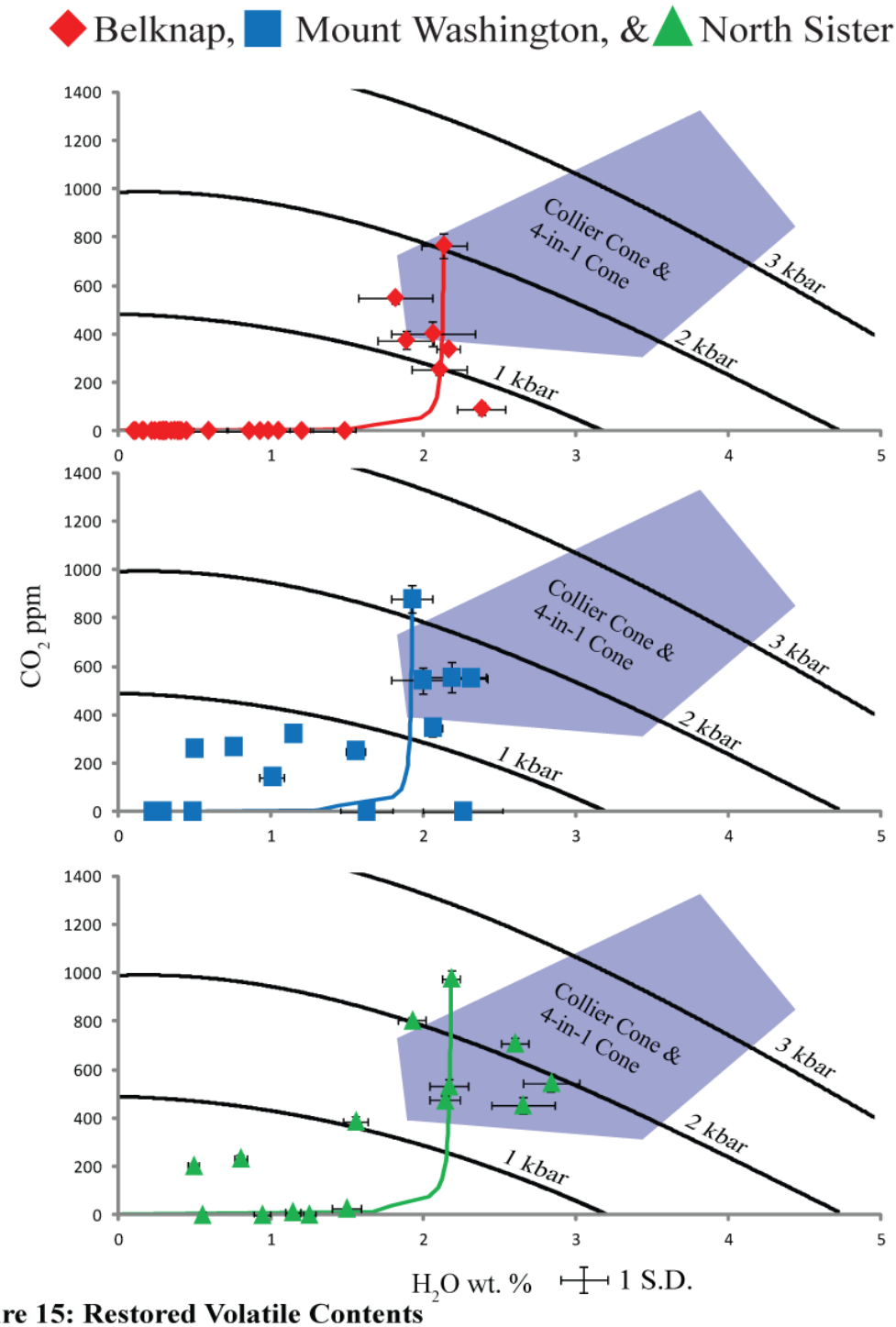

Figure 15: Restored Volatile Contents
Collier Cone and 4-in-1 Cone data provided by Ruscitto (2010). VolatileCalc (Newman and Lowenstern, 2002) calculated isobars for a composition of 49 wt. % SiO_2. Closed degassing paths are based on highest observed CO_2 concentrations at each volcano.

significant degassing from deep to shallow levels. Assuming constant melt inclusion entrapment probability, Figure 6 suggests magmas beneath Belknap and North Sister experienced increased crystallization at lower pressures.

Volatiles are incompatible in the solids crystallizing from the magma, except for S which could potentially enter sulfides. Because K_2O is incompatible in most minerals crystallized from a basaltic or basaltic andesite melt, I have normalized H_2O, S, and Cl by K_2O to account for the affects of crystallization (Fig. 16) (*e.g.* Sadofsky et al., 2008). As the legends on each plot detail, a decrease in H_2O/K_2O, S/K_2O, or Cl/K_2O with no increase in K_2O indicates degassing without crystallization, whereas an increase in K_2O with no change in these ratios indicates crystallization in vapor-undersaturated conditions. Belknap, Mount Washington, and North Sister melt inclusions all display a decrease in H_2O/K_2O, S/K_2O, and Cl/K_2O during an increase in K_2O, which indicates degassing induced crystallization. As the melt is degassing, the decrease in volatiles raises the liquidus temperature, inducing crystallization. This crystallization in turn causes the K_2O of the melt to increase as displayed by the data in Figure 16.

Although K_2O enrichment is a product of early magma fractionation, K_2O can also be significantly affected by assimilation. Schick (1994), Mitchener (1998) and Ruscitto (2010) noted the presence of a K_2O-rich contaminant common in the central Oregon High Cascades. Mitchener (1998) found that trace elements at Mt. Bachelor, a composite shield ~20 km south of North Sister, indicated ~15% crustal assimilation. The assimilation of low volumes (< 5%) of this K_2O-rich contaminant could raise observed K_2O by as much as 20% (Ruscitto, 2010). To avoid the problem of contamination, Ruscitto (2010) uses TiO_2 as the incompatible element to normalize volatiles. A ~5%

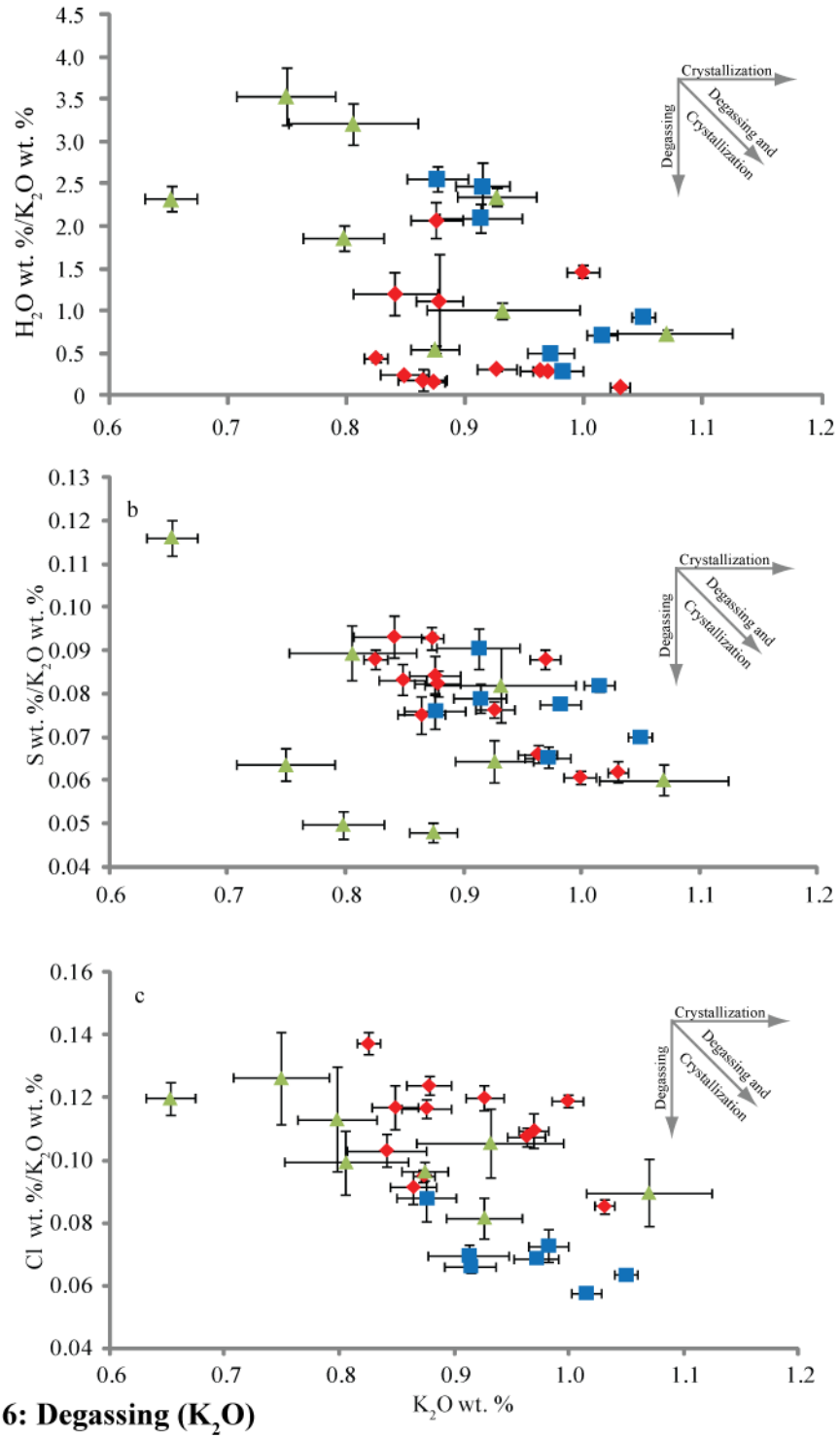

Figure 16: Degassing (K_2O)

(a) All three volcanoes display evidence of dehydration crystallization. (b,c) The distinct trends suggest S and Cl degassed with H_2O as the melt evolved. However, these trends could also be the product of partial assimilation of a K_2O-rich contaminant.

◆ Belknap melt inclusions
■ Mount Washington melt inclusions
▲ North Sister melt inclusions
1 S.D.

assimilation of the potential contamination source would affect TiO_2 concentrations ~3% (Ruscitto, 2010). However, TiO_2 also partitions readily into titanomagnetite, which would decrease observed TiO_2 contents. Figure 17 normalizes H_2O, S, and Cl to TiO_2. The three shields display consistency with their volatile ratios. Belknap displays both the lowest H_2O/K_2O and H_2O/TiO_2 ratios, Mount Washington displays intermediate ratios, and North Sister displays the highest ratios, suggesting titanomagnetite is not significantly affecting TiO_2 contents. H_2O/TiO_2 and S/TiO_2 behave similarly to H_2O/K_2O and S/K_2O, but Belknap and Mount Washington display ambiguous behavior in Figure 17c. Cl/TiO_2 appears to decrease as TiO_2 decreases, suggesting no or little degassing of Cl during the range of crystallization pressures displayed by the melt inclusions.

To check the volatile behavior, I plotted the K_2O normalized volatile values against MgO (Fig. 18), another component affected minimally by contamination. Higher MgO values indicate a more primitive melt, whereas lower MgO values represent a more evolved composition. H_2O and S still display the same trends characteristic of decompression crystallization. The Cl/K_2O vs. MgO trends of the three shields indicate that Cl was not lost to the vapor phase, as is to be expected for Cl contents < 0.2 wt. %, based on Cl solubility of > 1.0 wt. % in magmas of ~50 wt. % SiO_2 (Webster et al., 1999). The SEM images (see Appendix C) also provide strong evidence for degassing induced crystallization. Figure 19, Figure 20, and Figure 21, (Belknap, Mount Washington, and North Sister, respectively) display extensive phenocryst crystallization.

Williams (1976) suggested that shield volcanoes contain a complex series of dikes and sills in the volcanic edifices in which magma can reside prior to eruption. Krauskopf (1948) found that Paricutin's magma exploited crustal weakness and, in one instance, led

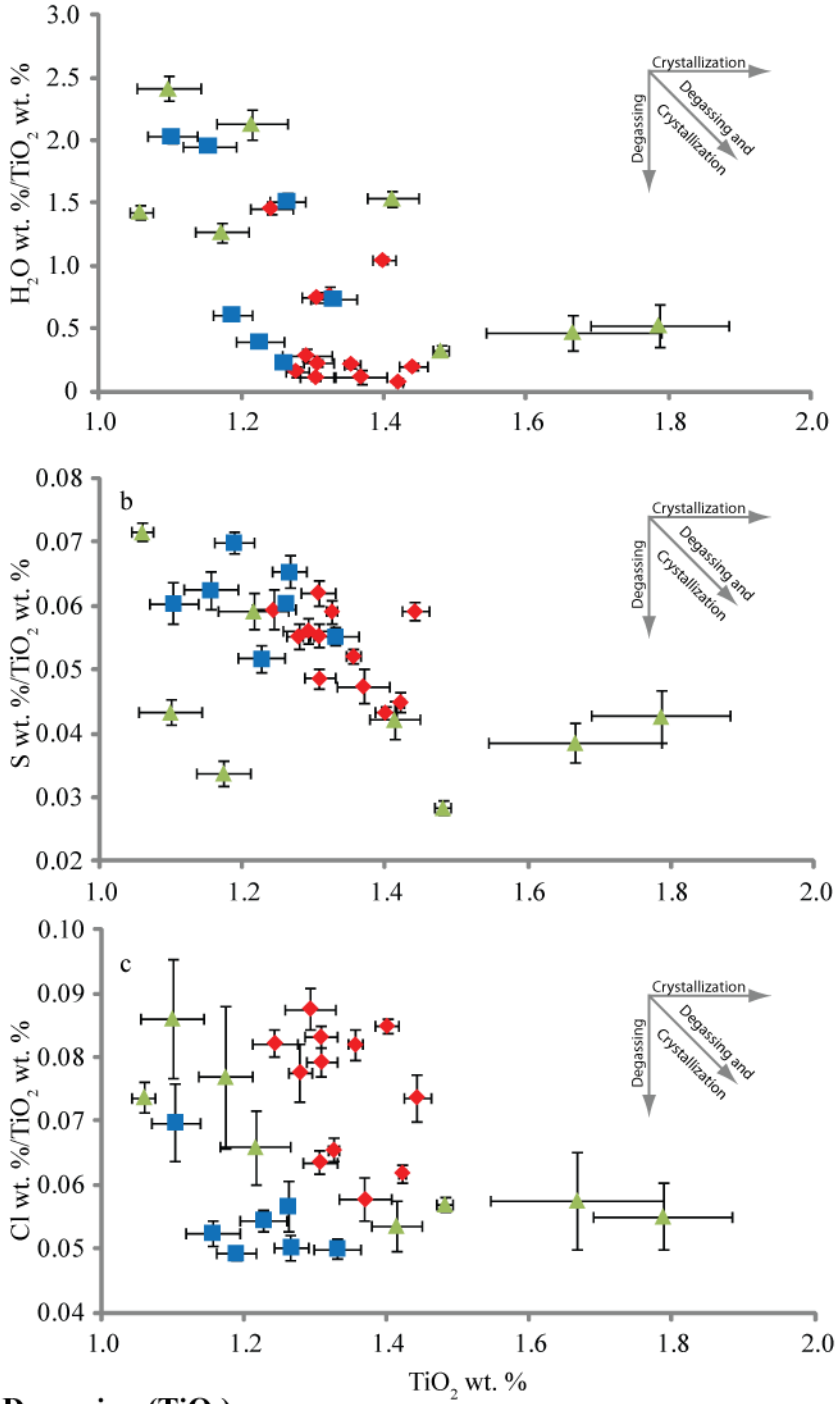

Figure 17: Degassing (TiO_2)

(a,b) Like with the K_2O normalized volatiles, H_2O/TiO_2 and S/TiO_2 indicate that Belknap, Mount Washington, and North Sister degassed H_2O and S. (c) Belknap and Mount Washington do not appear to have degassed Cl.

◆ Belknap melt inclusions
■ Mount Washington melt inclusions
▲ North Sister melt inclusions
1 S.D.

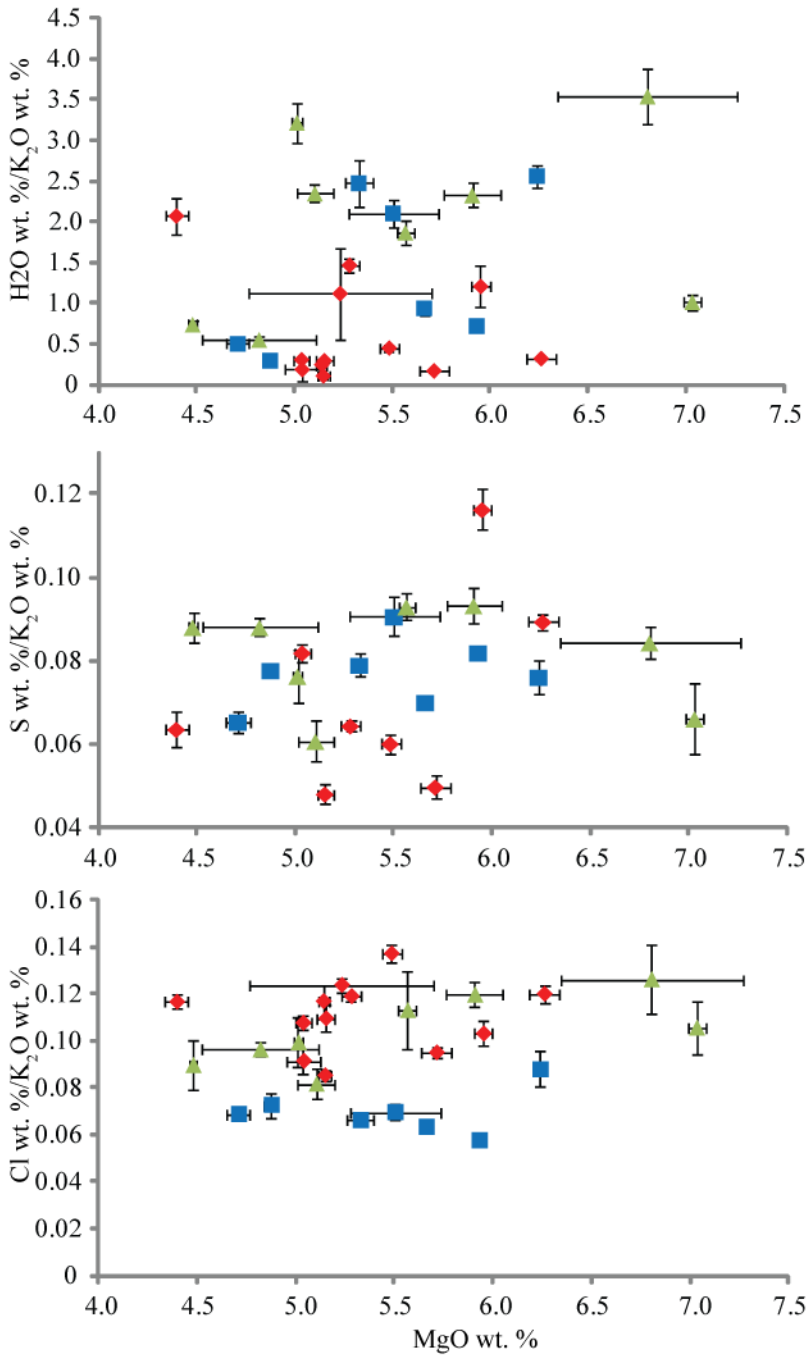

Figure 18: Degassing Behavior
(a) H_2O/K_2O and MgO are positively correlated at each shield, suggesting H_2O degassing induced plagioclase crystallization. (b) The positive correlation between S/K_2O and MgO suggests that S degassed during the crystallization process. (c) There is no clear trend to suggest that the volcanoes degassed Cl.

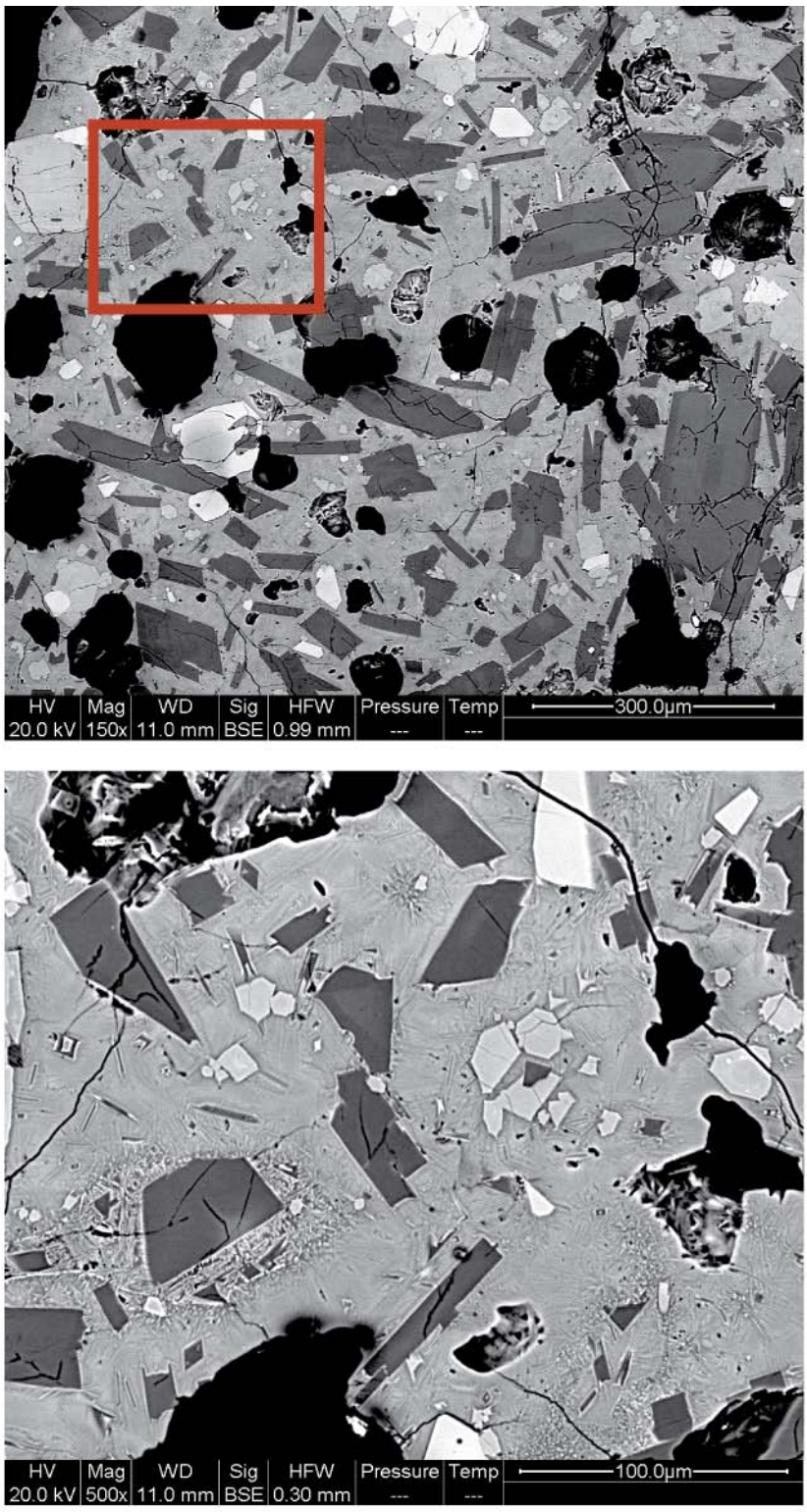

Figure 19: Belknap Tephra Clast

150x & 500x

Location of next higher magnification image

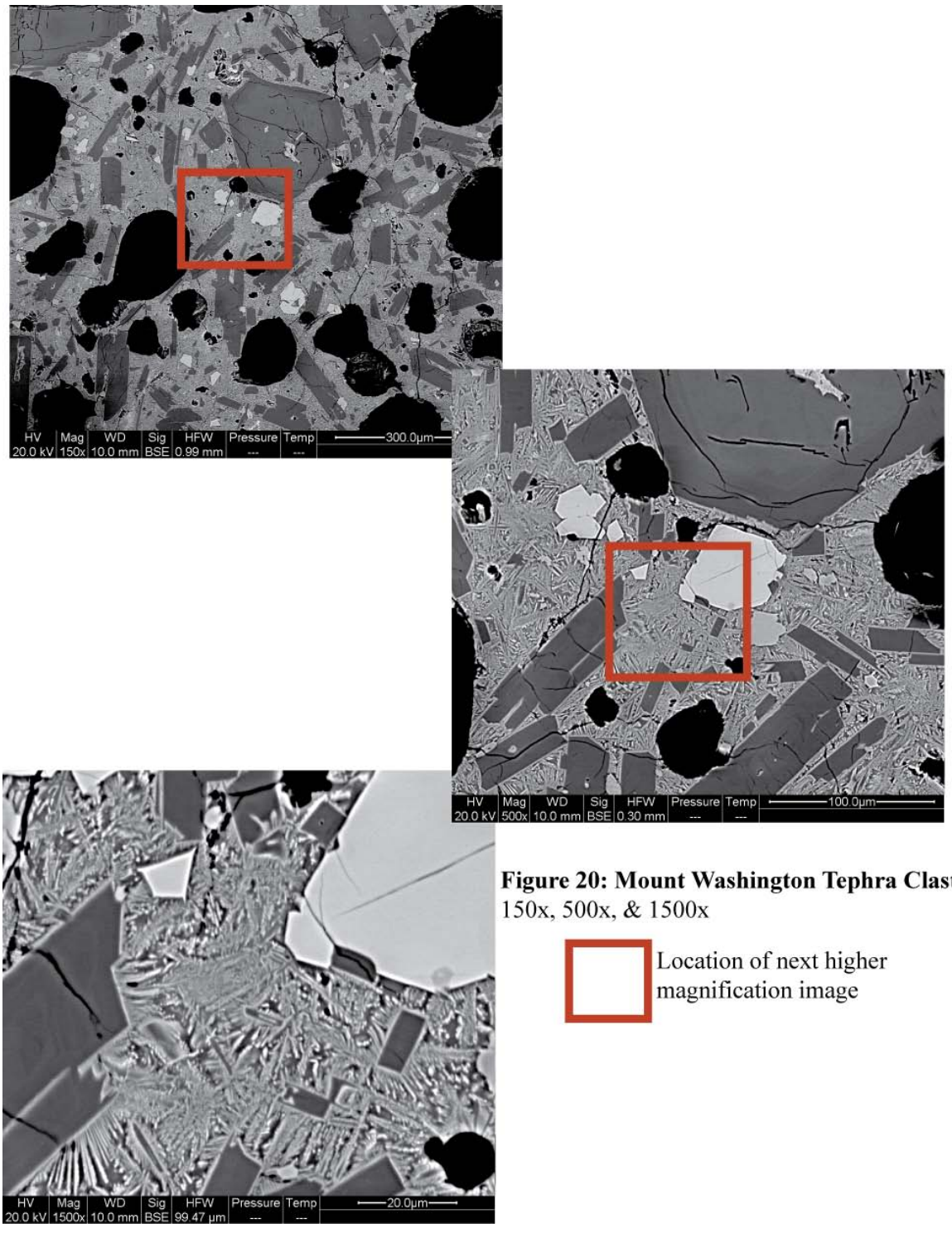

Figure 20: Mount Washington Tephra Clast
150x, 500x, & 1500x

Location of next higher magnification image

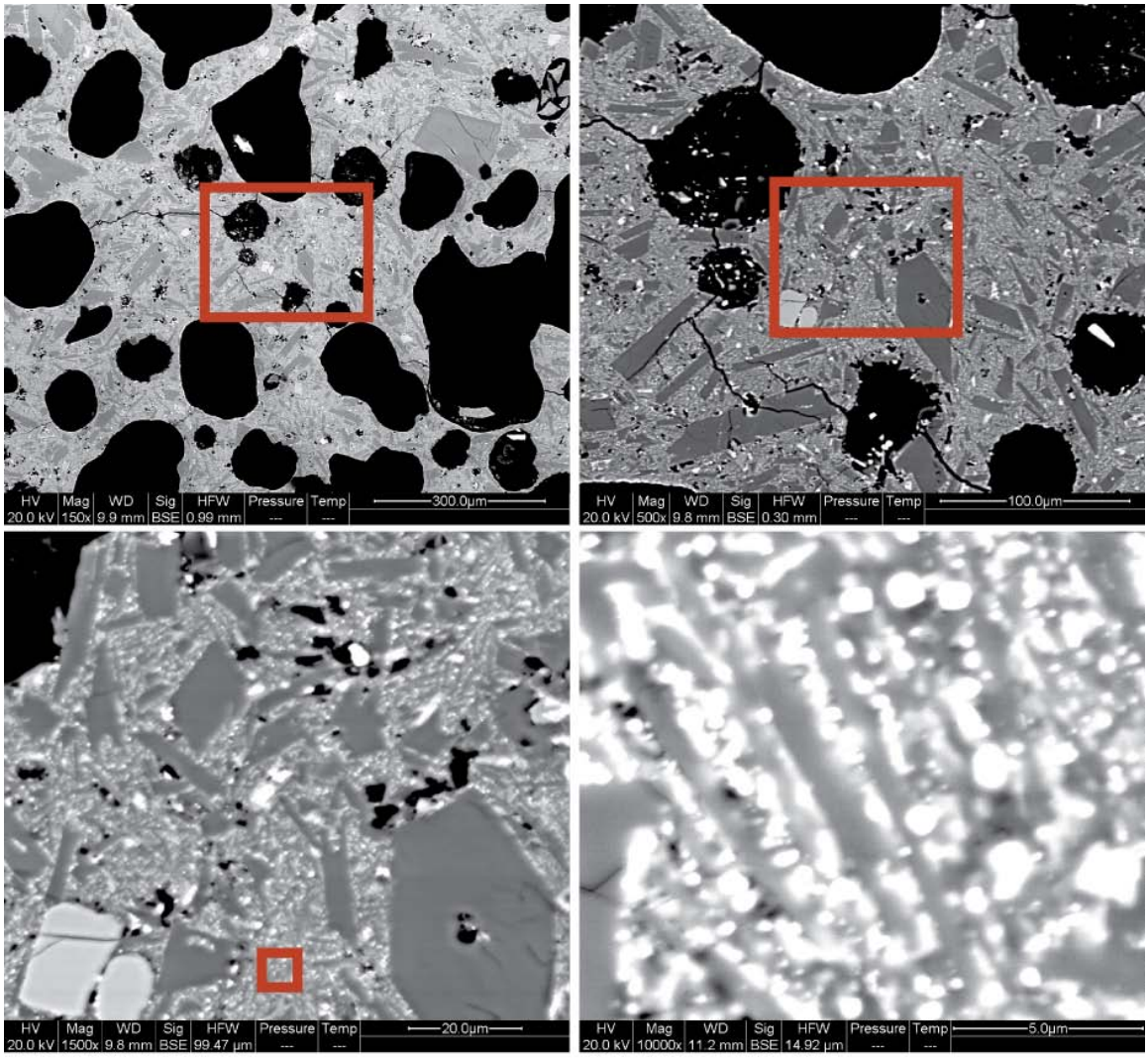

Figure 21: North Sister Tephra Clast
150x, 500x, 1500x, & 10000x

Location of next higher magnification image

to the formation of a satellite vent. The volatile data from Belknap, Mount Washington, and North Sister support the presence of such a shallow storage system. Conversely, cinder cones in the central Oregon Cascades show entrapment depths of > 4 km and little to no evidence for shallow degassing. Because most cinder cones in the central Oregon Cascades are short-lived, their initial eruptions may have no existing plumbing system for the magma to exploit. Instead, the magma must force its way to the surface, allowing little to no time for shallow storage and degassing as depicted by Figure 22. However, not all cinder cones are short-lived. Some continue eruptive activity from several years to 10+ years (*e.g.* Cerro Negro, Jorullo, and Sand Mountain) and display evidence of shallower degassing (Johnson et al., 2010; Ruscitto, 2010). Some have speculated that shield volcanoes are simply cinder cones that have continued their eruptive lives into polygenetic activity with voluminous lava flows from the then established plumbing system (*e.g.* Williams, 1976).

The hypothesis that shields represent cinder cones that have continued on long eruptive lives is not dissimilar from interpretations developed by McBirney and White (1982) regarding the formation of large silicic centers such as composite shields and stratavolcanoes (*e.g.* Mt. Bachelor [Mitchener, 1998] and North Sister [Schmidt and Grunder, 2009; Schmidt and Grunder, 2011]). McBirney and White (1982) observe three stages of growth for these volcanoes. The first stage involves the development of a broad basaltic shield volcano before the initiation of the second stage, explosive basaltic andesite to andesite activity. The final stage is defined by small effusive flows of basalt from satellite vents along the lower flanks of the volcano with compositions similar to

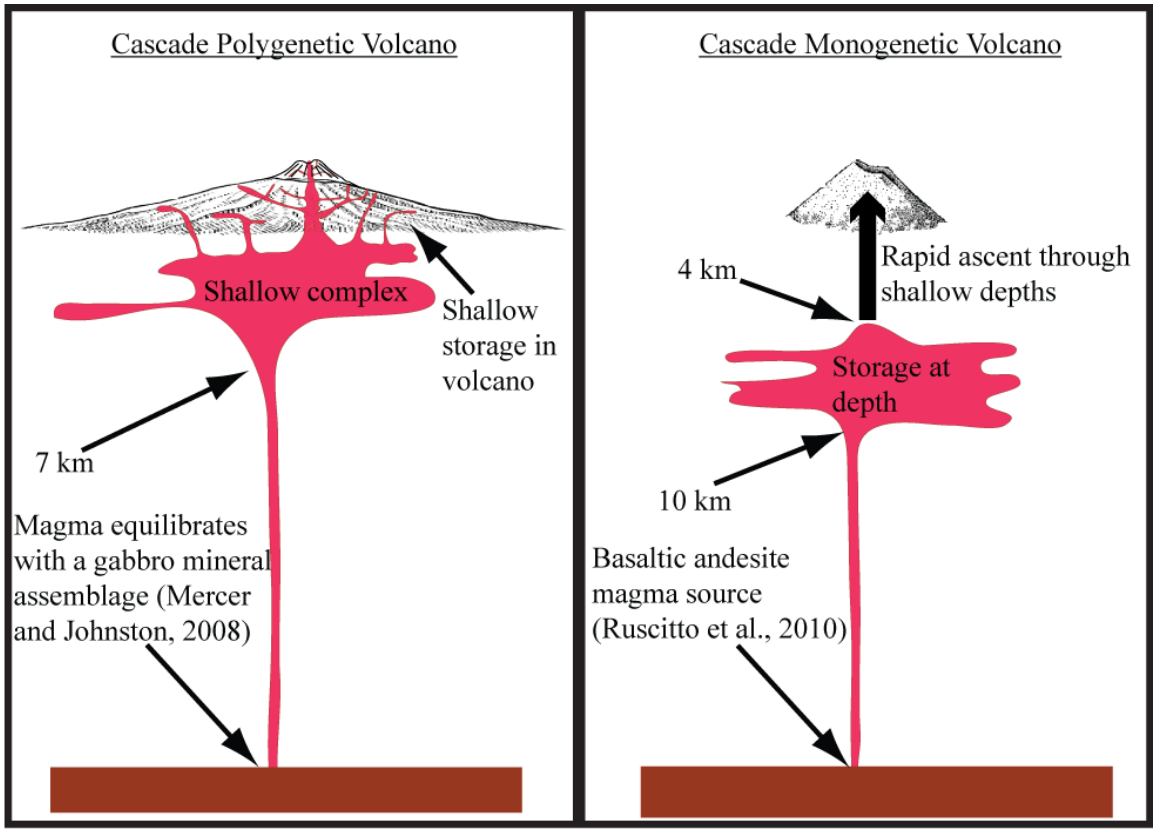

Figure 22: Magma Transport beneath Polygenetic and Monogenetic Volcanoes
The subsurface magma plumbing systems beneath these shield volcanoes and cinder cones are different. H_2O and CO_2 concentrations suggest shield volcanoes degas extensively during olivine crystallization. The wide range in olivine $Fo_{\#}$ and melt inclusion compositions from North Sister suggests some shields are fed by partitioned magma chambers with differing compositions that mix prior to eruption (*e.g.* Clague et al., 1995). Cinder cones are fed by magmas that predominantly crystallized at depths > 4 km (Ruscitto, 2010).

those of the stage one lavas. The subject of cinder cones developing into shields would benefit greatly by a future physical volcanological study of glacially dissected shields.

4.3.0. Major Element Geochemistry

I modeled the crystallization paths of the more MgO-rich melt inclusions using MELTS to see if predicted compositional trends accurately estimated the range of inclusion and whole rock compositions. Initial temperatures were set above the liquidus with $\Delta T = -10°$ C. Initial pressure was set to maximum observed pressure in the melt inclusions (~3 kbar) with $\Delta P = -15$ bar. At Belknap, comparison of the crystallization curves and the melt inclusion data suggest that more H_2O was present in the fractionating magmas than the most MgO-rich melt inclusions indicate. Mount Washington inclusions reflect simple magmatic fractionation, whereas North Sister inclusions display a wide range in compositions compared to the restricted range of whole rock compositions, indicating a more complex magmatic plumbing system feeding North Sister and/or recharge by heterogeneous batches of magma.

4.3.1. Belknap Major Element Geochemistry

During equilibrium and fractional crystallization of a high MgO (6.3 wt. %) melt inclusion from Belknap, MELTS predicts enrichment of FeO^T and TiO_2 (Fig. 23). Instead, the whole rock and melt inclusion compositions appear to trend toward a more evolved composition without the FeO^T and TiO_2 enrichment. Schick (1994) identified Si-rich xenoliths in some of the lavas from Collier Cone. These xenoliths represent a potential contaminant for the basaltic andesites. Assimilation of the SiO_2-rich composition would reduce MgO while increasing SiO_2 values. Figure 24 shows mixing lines between the shield volcano basaltic andesites and the potential SiO_2-rich

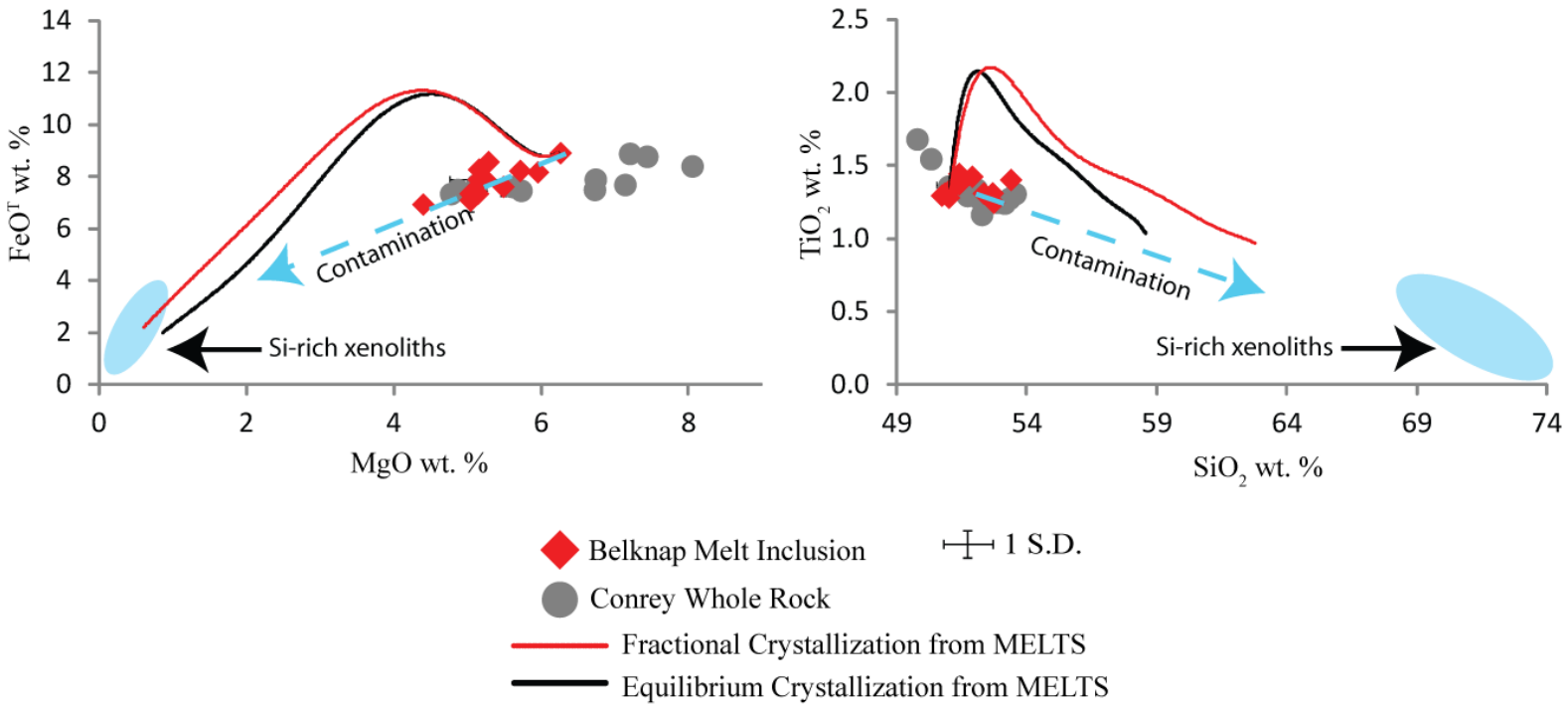

Figure 23: Belknap - Evidence for Partial Assimilation
MELTS predicted high FeO^T enrichment not reflected by the melt inclusion and whole rock data. Instead, the data trend toward a Si-rich xenolith composition, reported by Schick (1994) to be in the vicinity of Belknap, suggesting partial assimilation a Si-rich source.

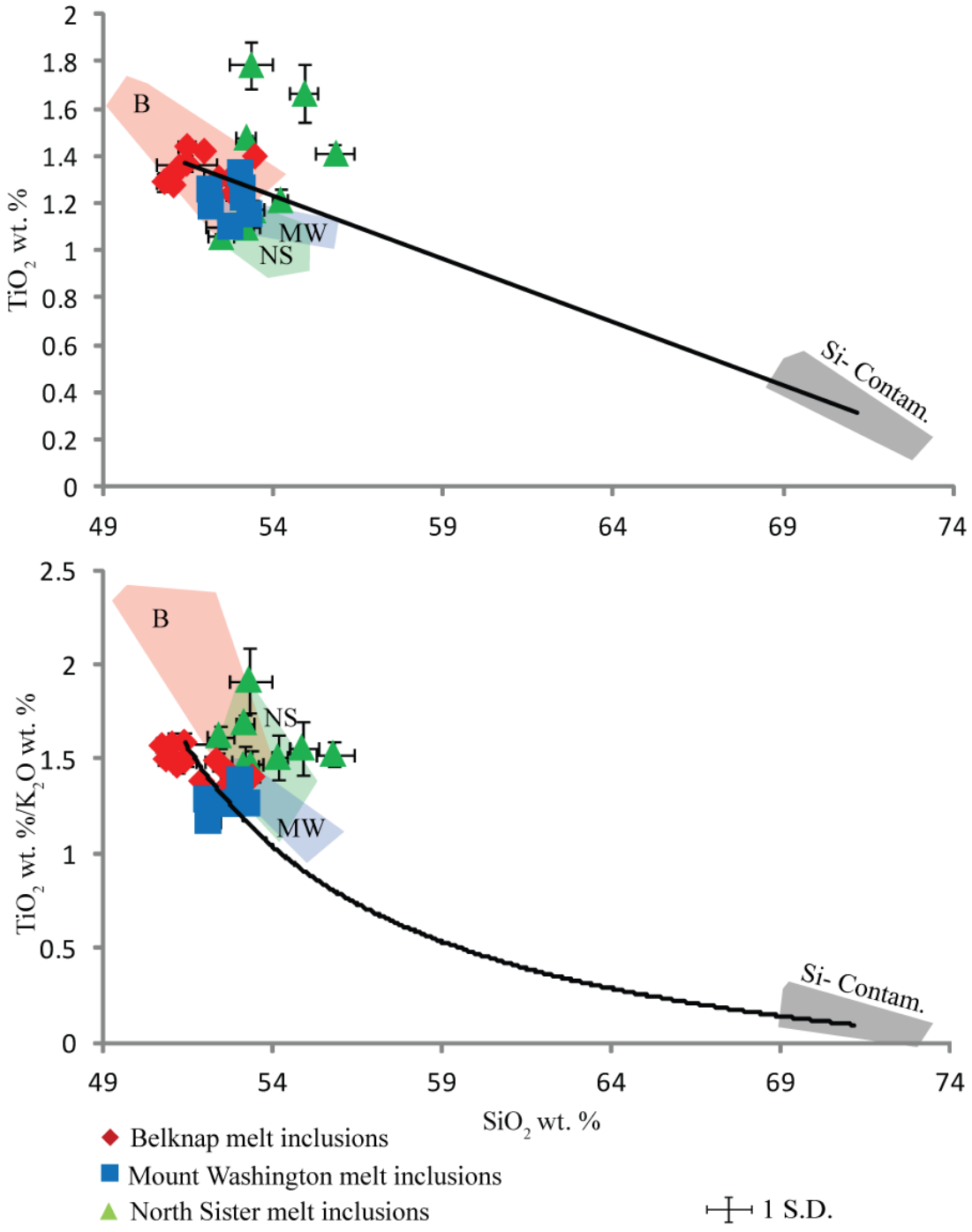

Figure 24: Mixing Trends - Lack of Evidence for Contamination at Belknap
Belknap melt inclusion and whole rock compositions (shaded) do not display evidence of mixing with a Si-rich contaminant, K-rich source (grey shaded).

contaminant. Titanomagnetite crystallization depletes melts of TiO_2 as the melts evolve to higher SiO_2. Mixing with a SiO_2-rich contaminant should produce lower TiO_2 and higher SiO_2 concentrations. K_2O is more incompatible than TiO_2; therefore, early mixing would be signaled by decreasing TiO_2/K_2O values. The TiO_2 vs. SiO_2 and TiO_2/K_2O vs. SiO_2 trends display little evidence of Belknap compositions mixing with any highly evolved Si-rich composition.

The most primitive Belknap melt inclusion contained < 0.3 wt. % H_2O. The low H_2O concentration effectively produces a tholeiitic trend from MELTS. The tholeiitic trend is produced by low H_2O, which results in early plagioclase crystallization. Plagioclase does not incorporate FeO^T and TiO_2 into its crystal structure, causing an enrichment of these two components in the melt (Sisson and Grove, 1993).

Figure 11c displays no trend between H_2O and MgO. The lack of correlation between H_2O and MgO for Belknap, Mount Washington, and North Sister melt inclusions indicates that degassing did not occur simultaneously with olivine crystallization and suggests some more complex process(es). Mitchener (1998) finds stringers, visible elongated bodies of magma that intrude into another visibly contrasting body of magma, in Belknap thin-sections, providing evidence of relatively late-stage magma mixing. The mixing could have been a product of convection or thermal inversion in the shallow magma system (Mitchener, 1998), which would have provided an environment for the variable degassing and MgO content. It is also important to consider that the tephra I sampled at each volcano came from multiple eruptions, and thus the inclusion population of each volcano may be a mixture from several eruptions.

To try to determine the original H_2O content of melts from each volcano, I extrapolated values using the H_2O/K_2O ratios. The highest Belknap H_2O/K_2O was 2.07, which should represent the original Belknap H_2O contents relative to K_2O. Using this ratio, I calculated the minimum value for the initial H_2O content of Belknap magmas to be ~2.1 wt. %. Figure 25 depicts the MELTS run of the most MgO-rich composition for Belknap with 2 wt. % H_2O under the same conditions as the aforementioned MELTS simulations. Under these conditions, plagioclase crystallization is delayed until lower temperatures and the crystallization trend matches the measured melt inclusion values.

4.3.2. Mount Washington Major Element Geochemistry

I used MELTS under the same conditions as with Belknap at Mount Washington to calculate the liquid line of descent for equilibrium and fractional crystallization. Figure 26 plots MgO vs. FeO^T and SiO_2 vs. TiO_2. The equilibrium and fractional crystallization curves are similar. Both crystallization curves fit the Mt. Washington whole rock and melt inclusion compositions well. The whole rock compositions appear more evolved than the melt inclusions, suggesting mixing of the olivine bearing magma with another of a more evolved composition. The high abundance of large olivine crystals (see Appendix B for tephra descriptions) and higher melt inclusion MgO content than that of the whole rock suggest equilibrium crystallization conditions retained crystals until the mixing event, after which the melt inclusion data suggest little to no crystallization followed.

4.3.3. North Sister Major Element Geochemistry

North Sister displays variable melt inclusion compositions and relatively consistent whole rock compositions (Fig. 10, Fig. 11, Fig. 27). Though the PC unit melt inclusions I analyzed initially appear anomalous when compared to the whole rock

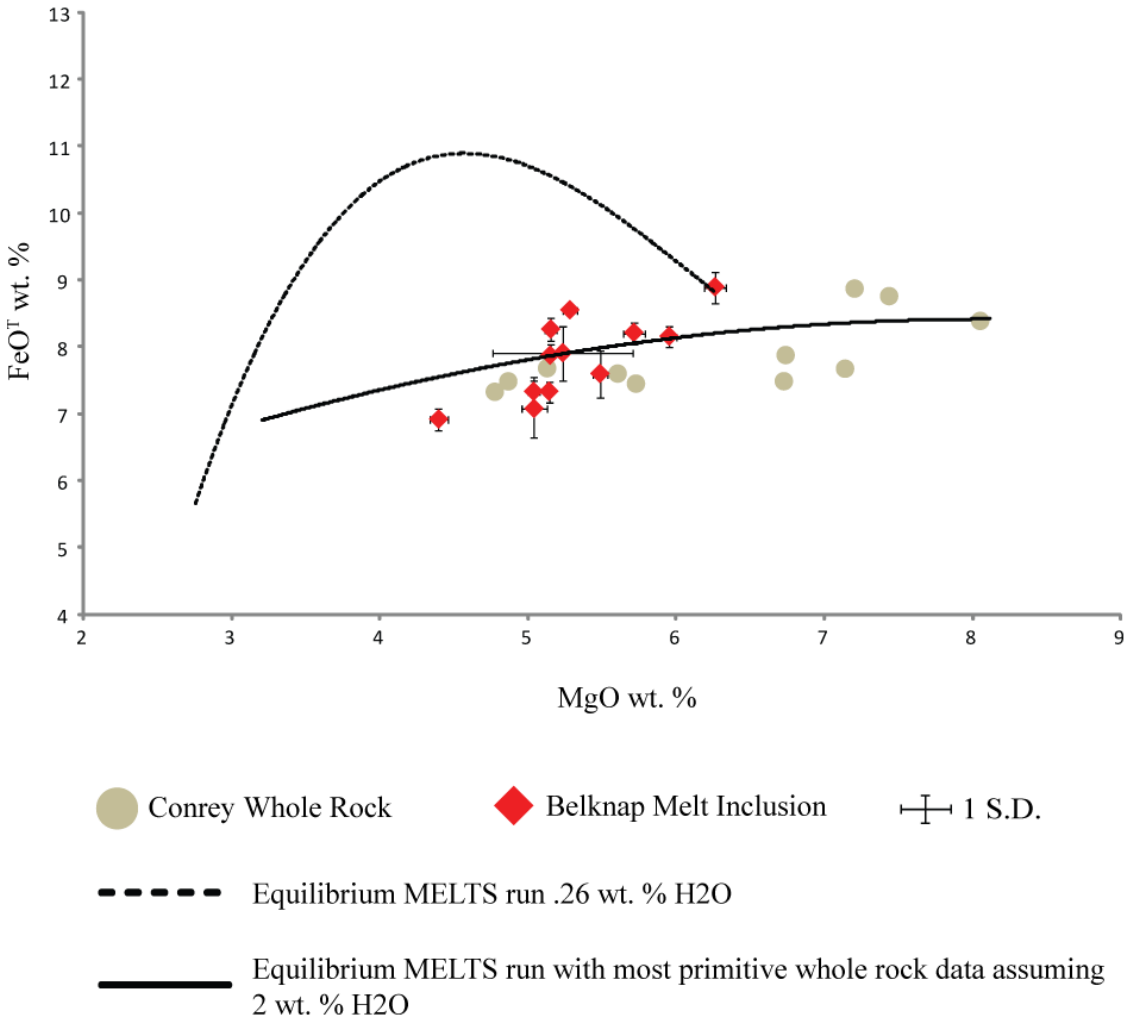

Figure 25: Belknap Lines of Descent - High Vs Low H_2O wt. %
MELTS produced an enriched FeO^T trend from the most primitive melt inclusion composition, which contains .26 wt. % H_2O. The low H_2O trend does not match melt inclusion and whole rock data. However, assuming 2 wt. % H_2O with the most primitive whole rock composition produced a crystallization trend that matches observed melt inclusion and whole rock FeO^T values.

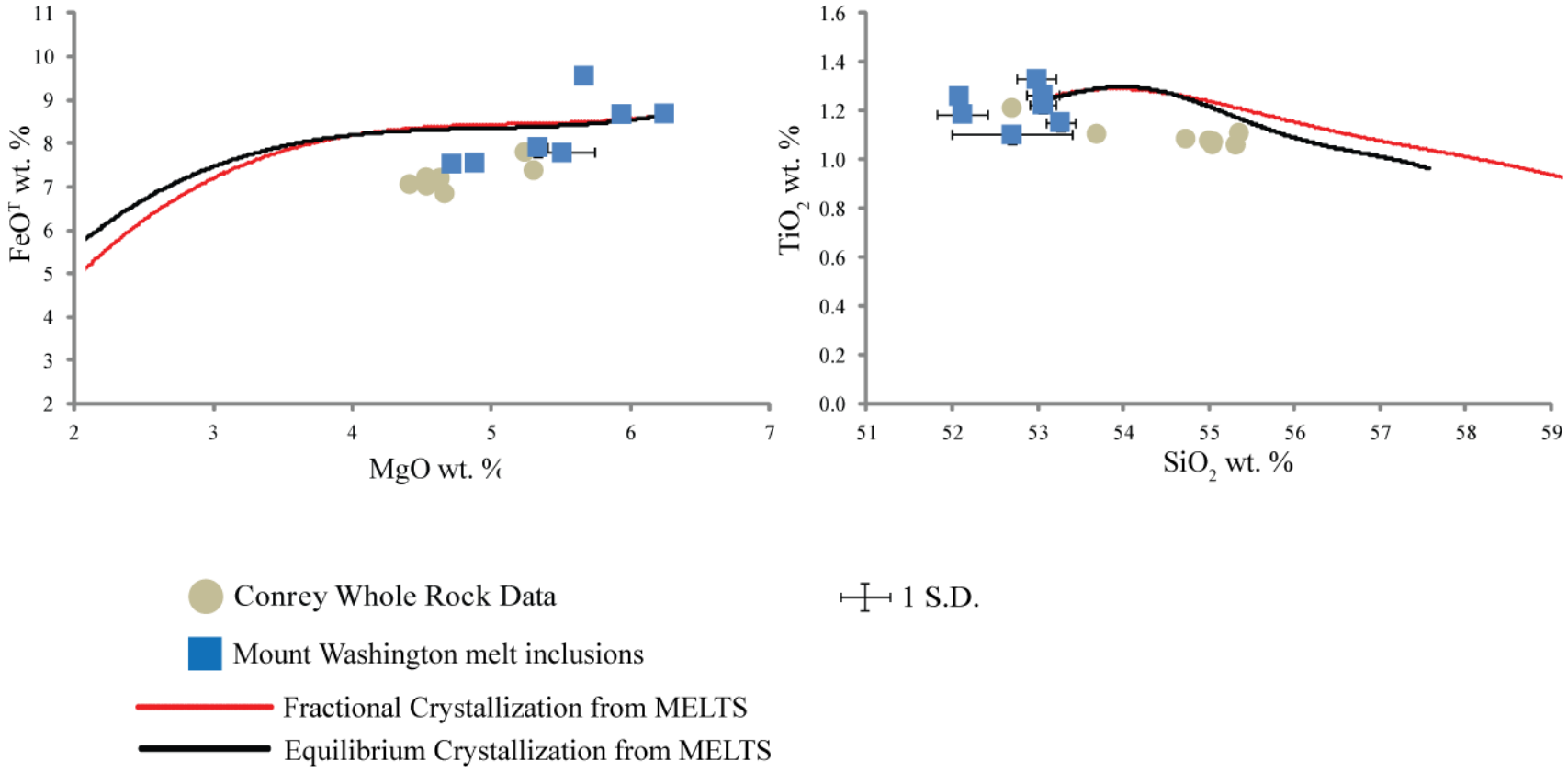

Figure 26: Magma Mixing at Mount Washington
MELTS equilibrium and fractional crystallization trends provide good estimates for more evolved Mount Washington melt inclusion and whole rock compositions. The lower MgO of the whole rock relative to the melt inclusions suggests magma mixing with few to no entrapment events post-mixing.

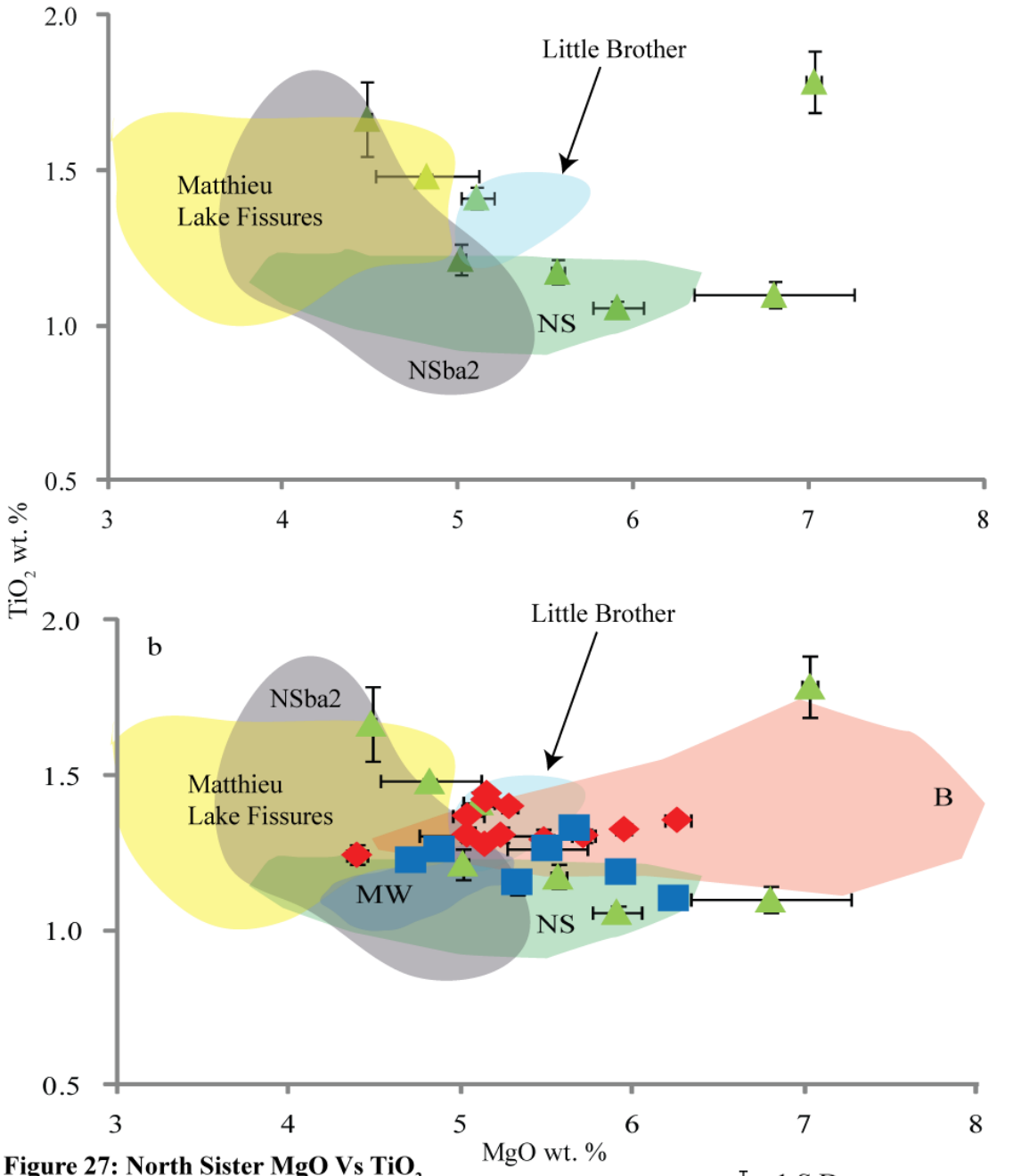

Figure 27: North Sister MgO Vs TiO_2
North Sister melt inclusions display a wide range in compositions relative to North Sister whole rock composition, whereas Belknap and Mount Washington melt inclusions are relatively similar to their respective whole rock values.
All shaded regions represent whole rock data from other studies, except NSba2, which represents melt inclusion analyses for the second oldest North Sister eruptive unit.

analyses, Mercer (2009) found that the North Sister melt inclusions from the NSba2 unit, the second oldest eruptive unit, also contain a wide range in TiO_2 and FeO^T compared to the Schmidt and Grunder (2011) whole rock analyses.

Other studies have found melt inclusions with greater compositional variation than the lavas with which they are erupted. Clague et al. (1995) concluded that melt inclusions from Kilauea's Puna Ridge, Hawaii, were trapped before the crystallizing magma body had a chance to homogenize. The pre-homogenization entrapment produced a range in compositions that was not observed in the whole rock analyses. The significant variation in FeO^T and TiO_2 at North Sister, two components not significantly increased by assimilation, suggests the variation in North Sister melt inclusions compositions reflect isolated magma bodies fractionated and then later homogenized prior to eruption.

The Matthieu Lakes Fissure unit supports this reasoning. Figure 27 shows North Sister melt inclusion data with Little Brother and Matthieu Lakes Fissure, and the Mercer NSba2 inclusion compositions. Little brother is a relatively small MW-type shield < 3 km west of North Sister. Little Brother erupted 150-90 ka. Although initial North Sister eruptions pre-date Little Brother, Little Brother was not as long-lived as North Sister and North Sister's youngest deposits, including those sampled for this study, are younger than Little Brother's final known eruptions (Schmidt and Grunder, 2009; Schmidt and Grunder, 2011). The Matthieu Lake Fissures are a series of dikes that cut across North Sister and erupted in the immediate vicinity of North Sister 75-11 ka (Schmidt and Grunder, 2009). Schmidt and Grunder (2009) interpret the Matthieu Lake Fissures to represent the same magma that fed North Sister but in a more evolved composition.

North Sister melt inclusions overlap with the Little Brother and Matthieu Lake Fissure compositions.

For the melt inclusion compositions found from Puna Ridge, Clague et al. (1995) argued for distinct magma bodies beneath and in the volcano much like the internal structure Williams (1976) observed for dissected Cascade shield volcanoes. With such a geometry, little mixing would have occurred until immediately prior to eruption. As the magma evacuated the partitioned plumbing system, mixing produced the homogenized bulk rock composition. The range of North Sister melt inclusion compositions relative to the monotonous whole rock analyses supports a similar interpretation for processes beneath North Sister. Additionally, a wide range in host olivine Fo contents supports this reasoning. Figure 22 includes the distinct magma bodies from Williams (1976) to produce the variable magma compositions of the melt inclusions.

4.4. Conflicting Evidence for Parental Magmas

The composition of the magmas feeding the volcanoes continues to be debated. The Danyushevsky (2001) model found clinopyroxene to be the predominant mineral crystallized during fractionation of the primitive shield compositions; however, the MELTS and pMELTS methods found olivine to be primary mineral produced during fractionation. Clark (1983) used phase relations and Rayleigh distribution coefficients with South Sister compositions to find that olivine fractionation played an important role in magmatic evolution beneath the Three Sisters. In contrast, Schmidt and Grunder (2011) concluded that olivine crystallization beneath North Sister was only a late-stage event and not a major fractionating phase, as shown in Figure 28, based on high Ni contents found in all North Sister units. Mercer and Johnston (2008) conclude that North

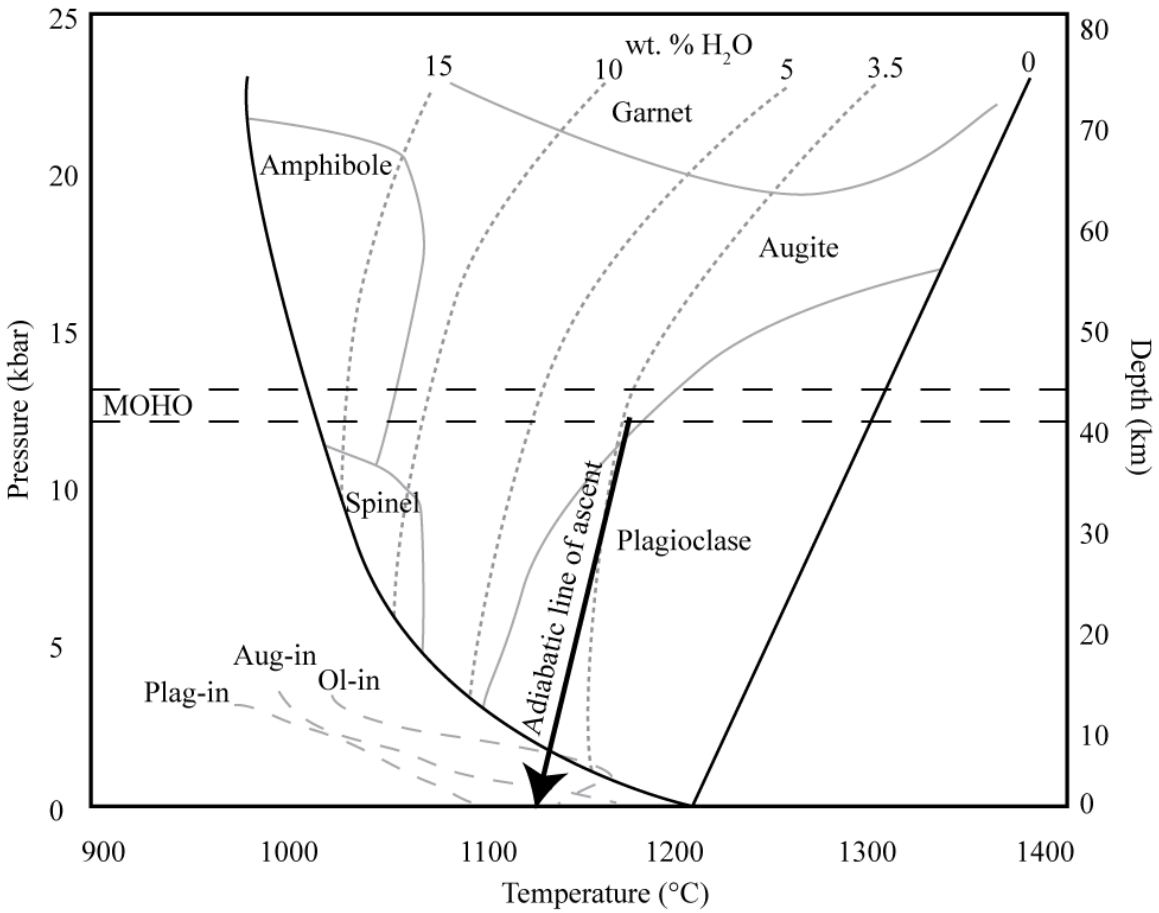

Figure 28: Phase Diagram - Late-Stage Olivine Crystallization
After generation near the MOHO at ~12 kbar with ~3.5 wt. % H_2O, the melt adiabatically ascends from the augite stability field, through the plagioclase stability field, toward lower pressures. Only near the very shallow conditions (< 3 kbar) is olivine able to crystallize and affect melt composition

Figure is taken from Mercer and Johnston (2008).

Sister magmas last equilibrated with an anhydrous augite-rich gabbro at ~12 kbar and ~1175° C before erupting. Figure 29 (see Appendix C for SEM analysis) displays a plagioclase and pyroxene cumulate found in the palagonite tuff from which the Mount Washington samples were collected. The crystallinity of the clast is too great for the clast to be a product of the magma that erupted producing the tuff. Instead, it may be a xenolith from the plagioclase and pyroxene crystallization at depth.

Schmidt and Grunder (2011) attributed mantle-derived low-K tholeiite mixing with an Al-rich source near the base of the crust followed by pyroxene and plagioclase fractionation to explain North Sister compositions, but these exact processes cannot be at play beneath Belknap and Mount Washington because of their relatively higher incompatible element concentrations. Additionally, the H_2O contents of North Sister magmas (3.5-4.0 wt. % [Mercer and Johnston, 2008]) exceed the usually observed maximum H_2O content for a low-K tholeiite (~1.0 wt. % [Ruscitto et al., (2010)] to ~1.7 wt. % [Shaw, 2010]), making a low-K tholeiite parent seem unlikely for even North Sister much less the incompatible element-rich Belknap and Mount Washington magmas. (Ruscitto et al., 2012). Although low-K tholeiite magmas are inferred to underplate the central Oregon Cascades from north of Mount Washington to south of North Sister, neither Belknap nor Mount Washington appear depleted in incompatible elements (*e.g.* K_2O and P_2O_5). The K_2O-rich nature of lavas from Mount Washington and Belknap may be due to their positions closer to the trench. While Walker et al. (2003) concluded that dehydration-driven, flux melting was important across the width of the Central American arc and decompression melting was increasingly important toward the back-arc region, Sadofsky et al. (2008) did not find the same regional trend using melt inclusion volatiles

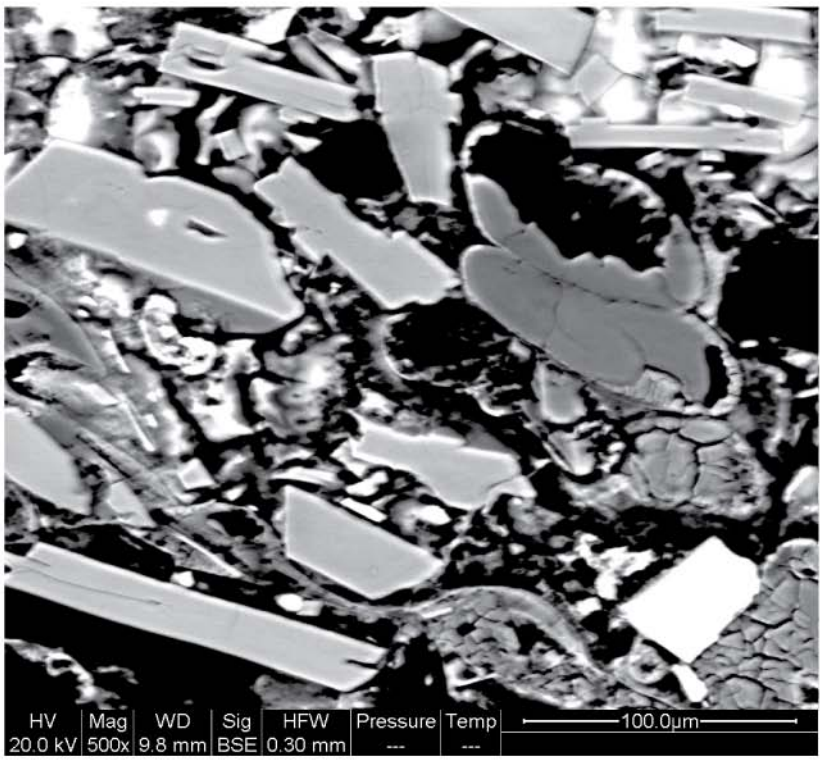

Figure 29: Mount Washington Pyroxene Cumulate

150x & 500x  Location of next higher magnification image

and trace elements. Instead, Sadofsky et al. (2008) concluded that a heterogeneous mantle accounts for the volatile and trace element variability observed from the Central American arc. These conclusions agree with those of Ruscitto et al. (2010) for the central Oregon Cascades, where no trends in volatiles or trace elements are seen consistently across the arc, providing evidence in support of the Hughes and Taylor (1986) postulation that MW-type and NS-type magmas are products of differing mantle sources. Furthermore, the forward crystallization model discussed in Section 4.5 favors a calc-alkaline parent restored by olivine addition rather than a low-K tholeiite parent for not only Belknap and Mount Washington but also North Sister.

4.5. Modeled Primitive Magma Implications

The primary magma compositions for the shield volcanoes modeled using the four methods discussed in Section 3.2 suggest that the compositions observed at Belknap evolved from a calc-alkaline basalt parent, whereas Mount Washington and North Sister evolved from primitive basaltic andesites. The basaltic andesite parents are distinguished by higher SiO_2, lower MgO, and lower incompatible element abundances, including high field strength elements and heavy rare earth elements. The calc-alkaline basalt parent contains similar abundances of large ion lithophile elements (LILEs) as the basaltic andesite parents, but have lower SiO_2 and higher MgO. Sr-rich basalts are similar to basalts in composition, but contain higher alkali and LILE concentrations (Ruscitto et al., 2010). Figure 30 plots the modeled primitive compositions against other modeled primitive source compositions of the central Oregon High Cascades.

Because magma evolution beneath the shield volcanoes likely involved olivine and clinopyroxene fractionation, each shield's primary composition likely falls between

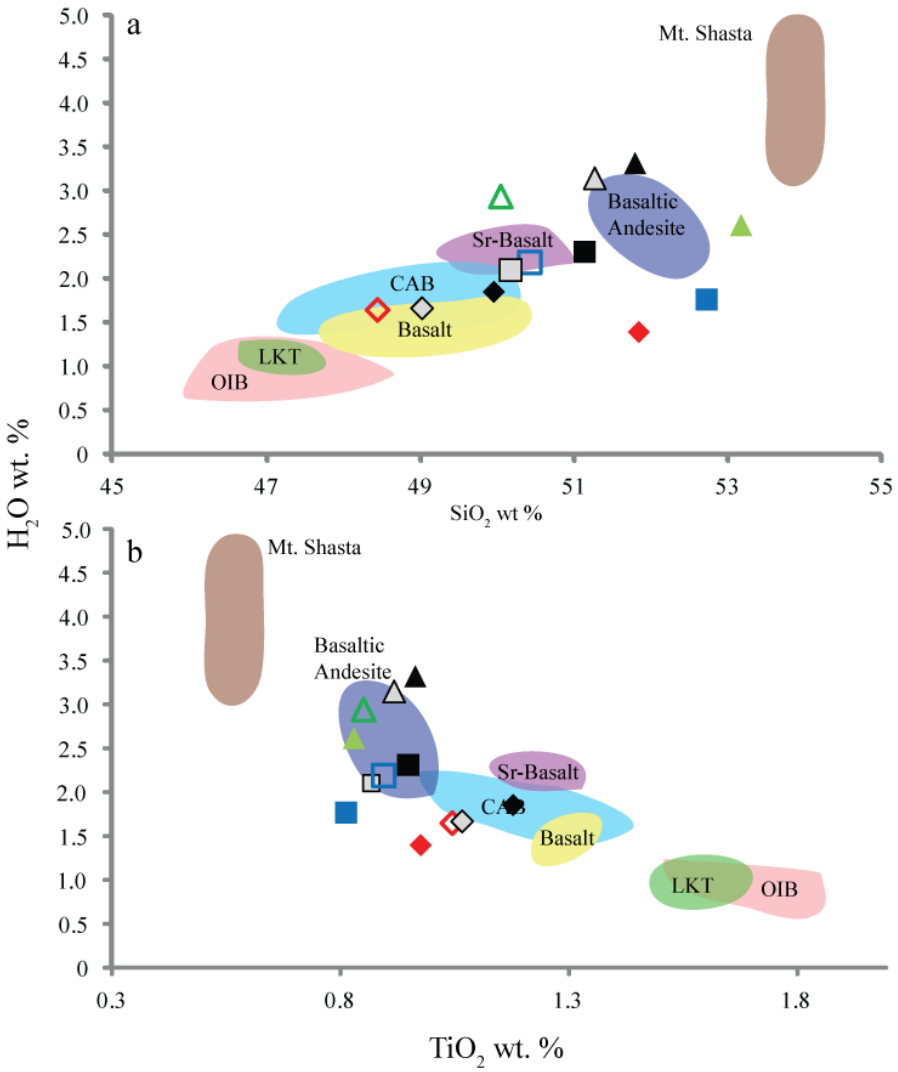

Belknap CPX-added
Mount Washington CPX-added
North Sister CPX-added
Belknap Olivine-added
Mount Washington Olivine-added
North Sister Olivine-added
Belknap MELTS Derived 1 kb
Mount Washington MELTS Derived 1 kb
North Sister Melts Derived 1 kb
Belknap pMELTS Derived 8 kb
Mount Washington pMELTS Derived 8 kb
North Sister pMelts Derived 8 kb

Figure 30: Parental Compositions (a,b) The primary mantle-derived magma modeled for North Sister overlaps with a primary basaltic andesite modeled by Ruscitto et al. (2010) for the Central Oregon Cascades. Belknap and Mount Washington have similar SiO_2 and TiO_2 wt. % as the primary basaltic andesite, but lack similar H_2O wt. %. H_2O wt. % values for the shields are extrapolated from maximum observed H_2O/K_2O ratios. The low H_2O may reflect partial degassing before inclusion entrapment at Belknap and Mount Washington. This figure is modified from Ruscitto et al. (2010).

the respective olivine-added and clinopyroxene-added endmember compositions in Figure 30a,b. The MELTS and pMELTS modeling results produce primary shield compositions either between or near these endmembers. The relative agreement of compositions from the four different models indicates the true primary compositions are reflected somewhere between or near these endmembers. Figure 30a,b suggest that Belknap is a product of a primary calc-alkaline basalt. Mount Washington plots near both the Sr-rich basalt and basaltic andesite in Figure 30a, but appears only similar to basaltic andesite in Figure 30b. Like Mount Washington, North Sister displays characteristics similar to Sr-rich basalt and basaltic andesite with respect to SiO_2, but has TiO_2 concentrations of a primitive basaltic andesite rather than a Sr-rich basalt.

H_2O was extrapolated using the maximum H_2O/K_2O values observed. Ruscitto et al. (2010), Shaw (2011), and Rasmussen (2012) found that original low-K tholeiitic magmas had H_2O contents that were relatively low (< 1 wt. %, < 1.7 wt. %, and < 1.3 wt. %, respectively). Although the relatively low Belknap and Mount Washington H_2O values (1.4 and 1.8 wt. %, respectively) are similar to low-K tholeiites, the K_2O wt. % of Belknap and Mount Washington melt inclusion and whole rock data preclude the likelihood of a low-K tholeiite parent. Furthermore, the SiO_2 and TiO_2 contents for the modeled Belknap and Mount Washington magmas make a low-K tholeiite parent for these shields appear improbable.

The MELTS analyses (see Appendix D) agree with Figure 30 that the shield compositions are derived from basalt to basaltic andesite sources and suggest the primary compositions feeding the shields were calc-alkaline. Figure 31 plots MgO vs. other oxides from primitive CABa and LKT equilibrium fractional crystallization paths. The

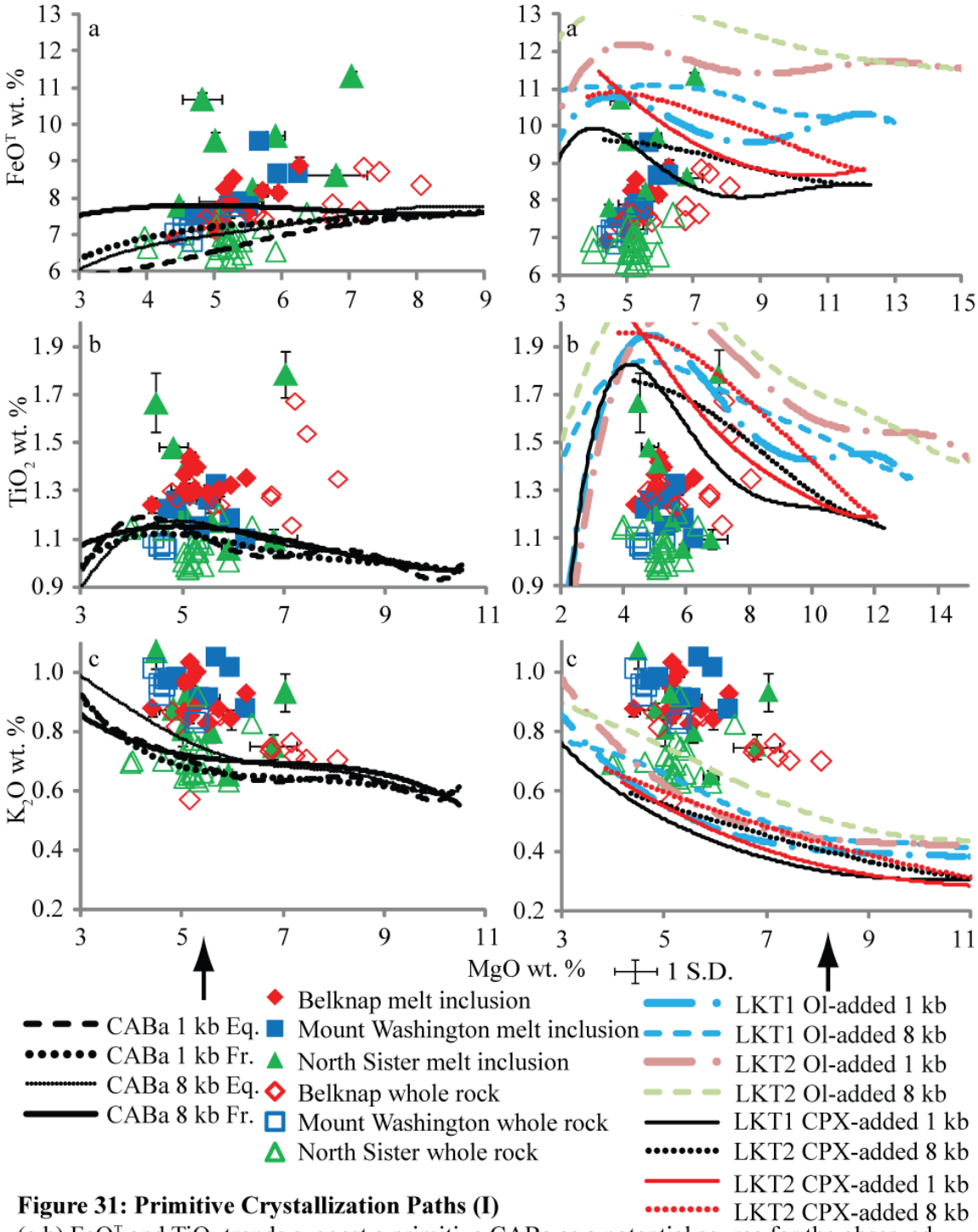

Figure 31: Primitive Crystallization Paths (I)
(a,b) FeO^T and TiO$_2$ trends suggest a primitive CABa as a potential source for the observed shield whole rock and melt inclusion compositions. (c) Though both CABa and LKT parents can produce K$_2$O compositions, the CABa produces higher K$_2$O melts more consistent with MW-type shields.

primitive CABa source produces FeO^T (Fig. 31a) and TiO_2 (Fig. 31b) consistent with observed shield values. While Al_2O_3 (Fig. 32a) and CaO/Al_2O_3 (Fig. 32b) are ambiguous regarding a calc-alkaline basaltic andesite or low-K tholeiite parent, the shield P_2O_5 contents (Fig. 32c) suggest that the melts are derived from low-K tholeiites. Figure 33 depicts the relationship between TiO_2 and K_2O. Like in Figure 31a,b, delayed LKT plagioclase crystallization appears to enrich the FeO^T and TiO_2 to concentrations the above shield concentrations in Figure 33.

While the modeled K_2O contents appear relatively low for Belknap and Mount Washington, the source of this parent composition, Collier Cone, is a cinder cone located at the base of North Sister and shares the NS-type shield characteristics of low K_2O contents for a calc-alkaline basaltic andesite (Schmidt, 2005; Ruscitto, 2010). The fit between North Sister and the primitive-crystallization paths in Figures 31, 32, and 33 suggest that North Sister and Collier Cone are related. Therefore, the polygenetic nature of the shield volcanoes and the monogenetic nature the cinder cones does not reflect a difference in parental magma source composition. Higher K_2O (> 0.8 wt. %), MW-type-monogenetic vents (*e.g.* Sand Mountain and Island Fissure) are found in the central Oregon High Cascades, and primitive compositions modeled from these would better fit the Belknap and Mount Washington compositions. Interestingly, Schmidt (2005) does not find North Sister and Collier Cone to be related by olivine fractionation, but finds incompatible trace element data to suggest the two volcanoes are related.

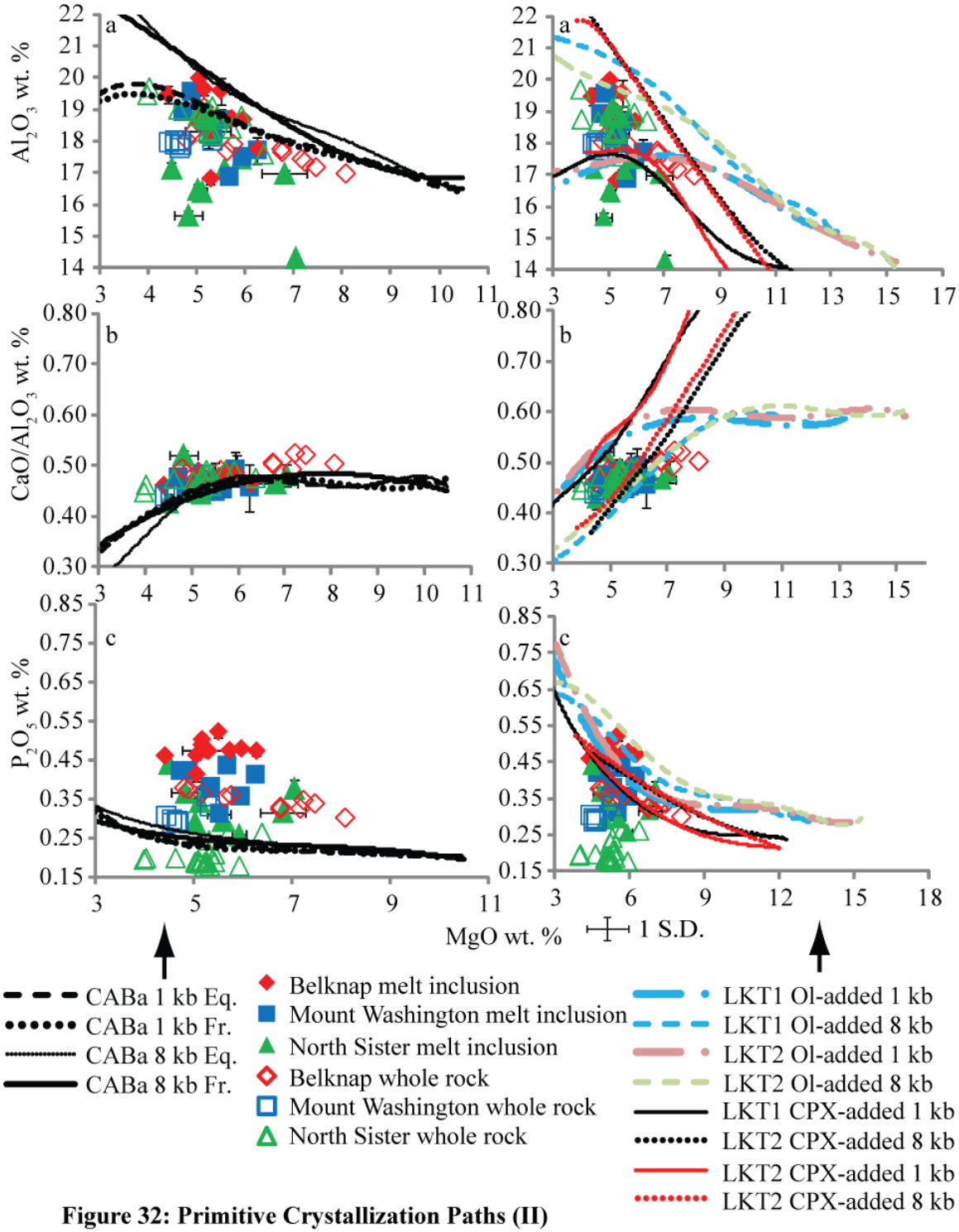

Figure 32: Primitive Crystallization Paths (II)
(a,b,c) Varying crystallization paths can produce a wide range of compositions, for which either a primitive LKT or CABa parent appears possible.

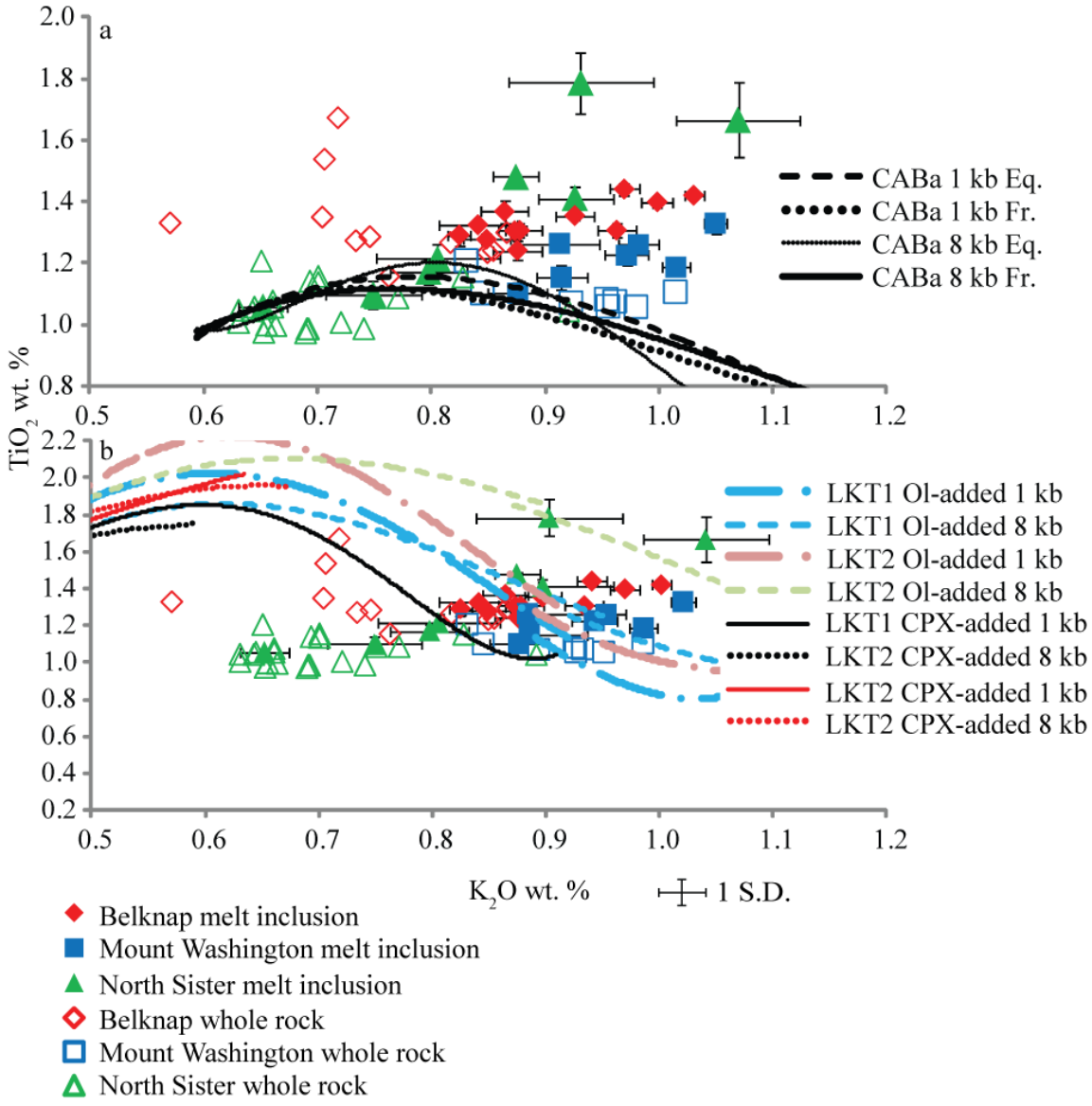

Figure 33: Primitive Crystallization Paths TiO_2 Vs K_2O
(a) Primitive calc-alkaline basaltic andesites are the more likely parents for shield compositions. Though Collier Cone, the CABa choosen for this study, contains relatively low K_2O, other calc-alkaline basaltic andesites with higher K_2O would create crystallization paths that fit well with observed shield compositions. (b) Although a primitive LKT will eventually evolve TiO_2 and K_2O similar to shields, an evolving LKT does not produce the positive correlation between TiO_2 and K_2O at the concentrations found with the shields.

4.6. Postulating Upper Crustal Relations and Eruptive Lifespan

In the Cascades, shield volcano distribution does not cluster or follow a local pattern. Although Mt. Bachelor erupted in a north-south alignment with several smaller monogenetic vents, the composite shield has no distinct geospatial relation to other nearby polygenetic vents (Price, 1990). While many cinder cones display local alignments in the Cascades and other volcanic fields, several cinder cones display no such alignment (Hasenaka, 1994; Sherrod et al., 2004; Hildreth, 2007). The polygenetic and monogenetic vent distribution suggests that some monogenetic cinder cones exploit crustal weaknesses, but these crustal weaknesses are not required for monogenetic activity. The lack of geospatial correlation exhibited by monogenetic vents suggests that upper crustal features do not control monogenetic or polygenetic activity. Instead, monogenetic cinder cones may represent magma bodies of limited magma flux, volume, or buoyancy that cannot develop mature plumbing systems, whereas polygenetic volcanoes are fed by higher flux, larger, and/or more buoyant magma bodies that establish mature plumbing systems.

Hasenaka (1994) supports this reasoning and argues the discontinuity between shield volcano and cinder cone height, volume, and basal diameter implies magma supply, storage and output systems that are different between the two volcanic vent types. Figure 34 compares Belknap, Mount Washington, and North Sister to shield volcanoes found in other volcanic fields. Even including both shields and composite shields, Cascade mafic silicic centers display similar height to width ratios with no notable variation (Table 6). Cinder cones often stand at or near the angle of repose (~35°).

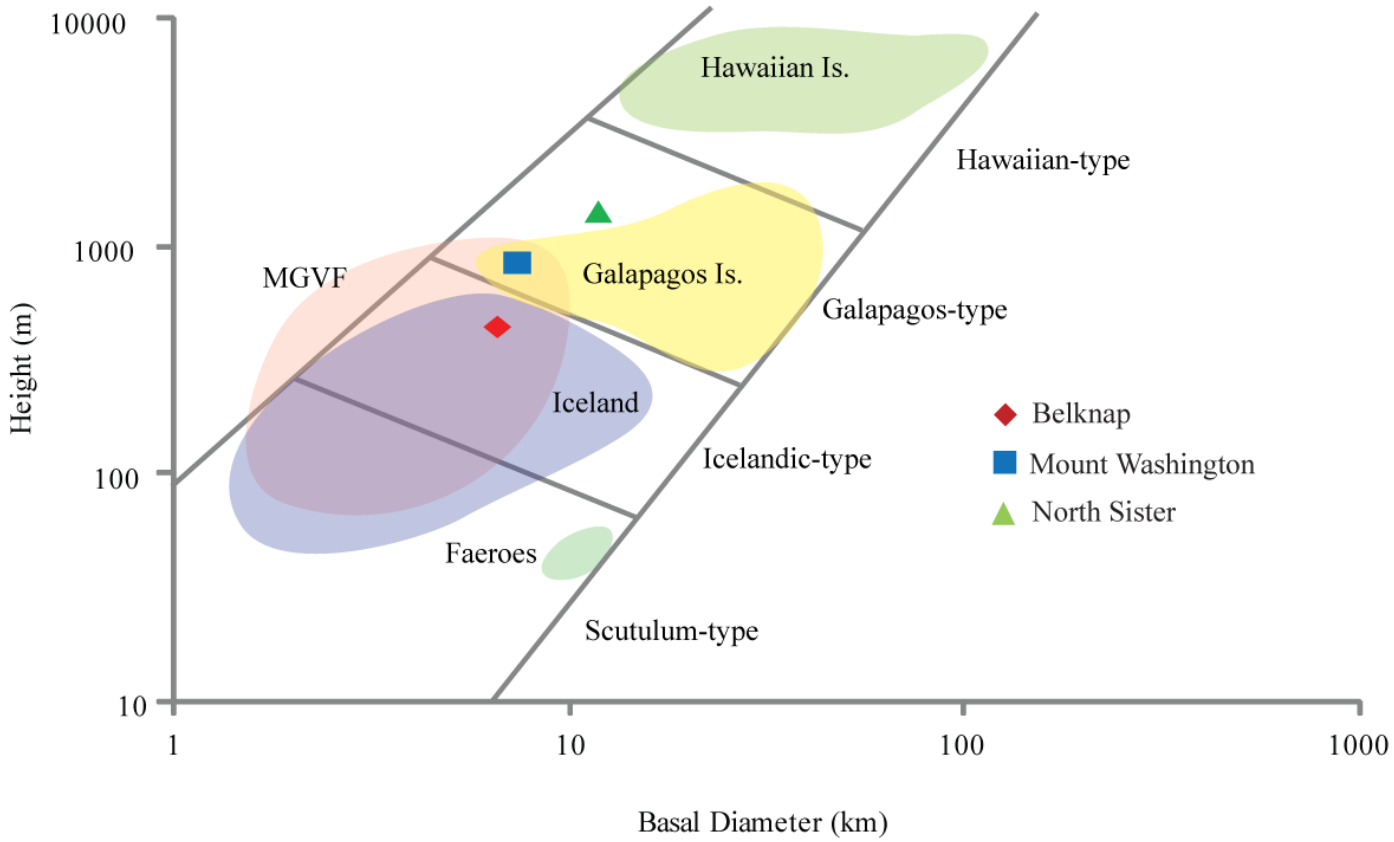

Figure 34: Height-Basal Diameter Relationship of Terrestrial Shield Volcanoes
This figure is modeled after a figure from Hasenaka (1994), in which it was used to compare MGVF height-basal diameter relationships to volcanoes from other fields.

	Height (m)	Diameter (km)	Slope (°)
Belknap	450	6.652	7.71
Mount Washington	850	7.375	12.98
North Sister	1430	11.941	13.47

Table 6: Shield Slope

4.7. Hazard Implications

Because cinder cone and shield volcanism represent the most common types of terrestrial volcanism worldwide (Connor and Conway, 2000) and because these volcanoes are frequently found proximal to population centers, cinder cones and shield volcanoes could disrupt commerce and be potential health hazards (Hansell and Oppenheimer, 2004); therefore, understanding the dynamics of magma transport for these two volcano types could help lead to improved hazard mitigation.

Shallow magma storage is linked to ground deformation. Magma feeding the Mount St. Helens cryptodome crystallized at very shallow conditions (~0.8 wt. % H_2O wt. %). The duration of degassing to these low H_2O concentrations can last days to weeks to months and may accompany eruption precursors (Blundy and Cashman, 2005). Strong degassing, like Figure 15 depicts occurred at Belknap, Mount Washington, and North Sister, often accompanies magma movement adjustment, which has been inferred from seismic activity at Mt. St Helens, Pinatubo, and Montserrat (Weaver et al., 1981; Scandone and Malone, 1985; Edmonds et al., 2003; Saunders et al., 2008). Therefore, seismic evidence of an imminent shield eruption will likely be available in regions where seismic networks are established. Ground deformation may even become observable. Though a shield eruption will not likely be as catastrophic as a stratavolcano, forecasting any eruption near a population center remains paramount to public safety and hazard mitigation.

CHAPTER V

CONCLUSION

I used olivine-hosted melt inclusions to measure volatile and major element concentrations from shield volcanoes to compare to existing data for cinder cones in the central Oregon Cascades. Trapping pressures of the inclusions from shield volcanoes did not display the same distribution as those of cinder cones. The contrast between the higher cinder cone crystallization pressures and the lower shield volcano crystallization pressures suggests that magma is transported and stored differently beneath the two types of volcanoes. Differences in local cinder cone and shield volcano distribution suggest this mechanism to be related to magma flux, volume, or buoyancy and unrelated to upper crustal structure.

The primitive Collier Cone calc-alkaline basaltic andesite crystallization paths better fit observed shield compositions, especially those of North Sister, than primitive Cascade LKT compositions. Primitive shield compositions reconstructed by olivine addition and clinopyroxene addition have SiO_2, TiO_2, and H_2O concentrations that are similar to those in the parent magmas for monogenetic basaltic andesites found in the central Oregon Cascades. The genetic similarity between North Sister and Collier Cone suggests that the two involve the same parental magma despite the differences in edifice size and eruptive longevity.

APPENDIX A

MODEL EXPLANATION

The Danyushevsky (2001) model adjusts the plagioclase liquidus temperature to account for H_2O in the melt and is given by equation 4.

$$T_{plag} = T_{W\&L} + (-.00356345*T_{olivine}^2 + 8.53503 * T_{olivine}-51133.09) \quad (4)$$

In which $T_{W\&L}$ is the plagioclase pseudo-liquidus temperature from Weaver and Langmuir (1990) and $T_{olivine}$ is pseudo-liquidus temperature from Ford et al. (1983).

Danyushevsky (1996) defines temperature in terms of composition by equation 5:

$$T_{W\&L}-T_{olivine} = 56.96 * H_2O-11.72 * (H_2O)^2 \quad (5)$$

and pressure in terms of composition by equation 6:

$$T_{olivine}-T_{clinopyroxene}=5.37*P-.35 \quad (6)$$

in which $T_{clinopyroxene}$ is the pseudo-liquidus temperature of clinopyroxene given by Ariskin et al. (1988), and P is pressure in kilobars. The slope obtained by the equation (6) is consistent with known values on pressure with olivine and clinopyroxene liquidus temperatures (*e.g.* Langmuir et al., 1992).

Although the model defined by Weaver and Langmuir (1990) only defines clinopyroxene in the Danyushevsky models, Weaver and Langmuir calculate the equilibrium state of system given bulk composition and temperature. Weaver and Langmuir (1990) model the olivine, plagioclase, and clinopyroxene liquidi by the stoichiometric equations with Si implicitly assumed as present.

Olivine $MgO + FeO=.67$

Plagioclase $2.5NaO + 1.67CaAl_2O_4 = 1$

Clinopyroxene $2MgO + 2FeO + CaSiO_3 + 2NaAlO_2 + 1.33CaAl_2O_4 + TiO_2 = 1$

Weaver and Langmuir (1990) use the Arrehnius equation 7:

$$\mathrm{Log}K_d = A/(T+B) \qquad (7)$$

in which T is temperature (K), while A and B are experimentally derived coefficients. From the Arrenius equation, $\mathrm{Log}_{10}K_d$ were found to be:

Olivine	MgO	2715/T-1.158
	FeO	4230/T-2.741
Plagioclase	$CaAl_2O_4$	2446/T-(1.122+2.562X)
	$NaAlO_2$	(3195+3283X)/T-(2.318+1.885X)
Clinopyroxene	MgO	3798/T-2.28
	FeO	$.24K_d^{MgO}$
	$CaSiO_3$	1738/T-.753
	$CaAl_2O_4$	2418/T-2.3
	$NaAlO_2$	5087/T-4.48
	TiO_2	1034/T-1.27

in which T temperature (K), X is stoichiometric $CaAl_2O_4/(CaAl_2O_4+NaAlO_2)$ in melt. Ariskin (1988) forwards a clinopyroxene-melt thermometer based on Ariskin (1986) derived by means similar to Weaver and Langmuir (1990). Ariskin (1986) calculates LogKd values, in which:

$$\mathrm{Ln}(K_{En}) = 8521/T-5.16$$

$$\mathrm{Ln}(K_{Fs}) = 13535/T-9.87$$

$$\mathrm{Ln}(K_{Wo}) = 8521/T-1.24$$

$$\mathrm{Ln}(K_{Al}) = 0.2$$

$$K_{En} = X^{CP}_{En}/(X^{NM}_{Mg} * X^{NF}_{Si})$$

$$K_{Fs} = X^{CP}_{Fs}/(X^{NM}_{Fe} * X^{NF}_{Si})$$

$$K_{En} = X^{CP}_{Wo}/(X^{NM}_{Ca} * X^{NF}_{Si})$$

$$K_{En} = X^{CP}_{Al}/X^{NM}_{Al}$$

$$X^{NM}_{Mg(Fe, Ca)} = Mg_{(Fe, Ca)}/(Mg + Fe + Ca + Ti + Mn + Cr + P + Al + Na\text{-}K)$$

$$X^{NM}_{Al} = (Al\text{-}Na\text{-}K)/(Mg + Fe + Ca + Ti + Mn + Cr + P + Al + Na\text{-}K)$$

$$X^{NF}_{Si} = Si / (Si + NA + K)$$

Ford et al. (1983) uses 797 basaltic magma compositions and the Gibbs free energy equation to create an olivine-melt thermometer for olivine. The Gibbs free energy equation is defined by equation 8:

$$\Delta G = 0 = \Delta H° - T\Delta S° + (P-1)\Delta V° + RT\ln K \quad (8)$$

in which, $\Delta H°$,$\Delta S°$, $\Delta V°$ are the enthalpy, entropy, and volume changes, respectively, of pure end-member reactions. T is temperature (K). K is defined as equation 9:

$$K = a^{L}_{Fo}/a^{Ol}_{Fo} \quad (9)$$

in which a^{L}_{Fo} is the activity of forsterite in the melt and a^{Ol}_{Fo} is the activity of forsterite in the solid. To account for bulk comp of magmas, equation 9 becomes equation 10.

$$\ln(X^{Ol}_{i}/X^{L}_{i}) = C_o + C_1/T + C_2(P-1)/T +$$

$$C_3\ln(1.5(X^{L}_{Mg} + X^{L}_{Fe2+} + X^{L}_{Ca} + X^{L}_{Mn} + X^{L}_{Cr2+} + X^{L}_{Ni}) + C_4 * \ln(3X^{L}_{Si}) + \Sigma C_j * \ln(1-X^{L}_{j}) \quad (10)$$

in which X are cation fractions, X_j are X_{Al}, X_{Fe3+}, X_{Ca}, X_{Na+K}, X_{Ti}, and X_P. The C terms are coefficients calculated by least squares multiple linear regression.

Ford et al. (1983) uses equation 11 to find the temperature of the composition.

$$X^{Ol}_{i}/X^{L}_{i} = A - B/T \quad (11)$$

in which T is temperature (K), and A and B are experimentally derived from Leeman and Scheidegger (1977).

To find the melt to solid ratio, Ford et al. (1983) uses equation 12:

$$X^{Ol}_i=(X^{O}i-FX^{L}_i)/(1-F) \quad (12)$$

in which F is fraction of melt remaining, X^{Ol}_i is initial cation fraction of element I, and X^{O}_i and X^{L}_i are cation fractions of each element in olivine and melt.

APPENDIX B

SAMPLE DESCRIPTIONS

During sample collection, I was biased in my sampling preference, avoiding large bombs and selectively collecting medium and fine-grained tephra as these grain sizes contain the loose olivine crystals necessary for this study. In tephra grain sizes finer than medium grained, the tephra olivine phenocryst modal abundance increased with decreasing grain size at Belknap, Mount Washington, and North Sister (Table 7). Single phenocrysts larger than 2 mm were not observed. Because larger olivine crystals allow larger melt inclusions to be trapped during crystallization, the Belknap tephra size and crystal size distribution was ideal for olivine crystal 0.5-1 mm in size. The palagonite tuff from Mount Washington contained more abundant olivine crystals in the 1-2 mm size fraction than Belknap and North Sister, allowing the use of the larger grain sizes for melt inclusion preparation. North Sister had the poorest abundance of olivine with crystals only abundant enough in the 0.25-0.5 mm size fraction.

All melt inclusions appeared clear to light brown, though brown inclusions were more common than clear inclusions. A melt inclusion with a less brown color is shown in Figure 35a below the larger center brown inclusion, whereas inclusions with stronger brown color are shown in Figures 35b,c,d,e,f. Many inclusions initially looked as if they were too dark to be suitable for FTIR analysis, appearing to have devitrified. However, after intersecting these inclusions and polishing the intersected surfaces, several of these inclusions were clearly glassy and, after preparation, were indistinguishable from the other prepared melt inclusion wafers that had a light brown color before sectioning.

The melt inclusions suggested a range crystal growth rates. Figure 35b displays the common ellipsoidal melt inclusion distribution inside olivine. Figures 35c and 35d display a melt inclusion distribution that suggests the olivine crystallized dendritically, indicative of moderate undercooling and rapid crystal growth. Figure 35e displays an olivine crystal with a melt inclusion and several opaque oxide inclusions, which were a common feature in many olivine crystals with and without glassy melt inclusions. Several melt inclusions contained vapor bubbles (Table 2). Figures 35c,d,f provide clear examples of melt inclusions shrinkage bubbles, bubbles formed when the inclusion experiences greater contraction than olivine host during cooling.

Crystals/Tephra Clasts (%)			
Grain Size (mm)	Belknap	Mount Washington	North Sister
< 0.25	80/20	75/25	35/65
0.25-0.5	60/40	60/40	10/90
0.5-1	30/70	20/80	3/97
1-2	< 1/> 99	10/90	< 1/> 99
Olivine/Plag/Cpx (%)			
Grain Size (mm)	Belknap	Mount Washington	North Sister
< 0.25	80/20/< 1	60/40/< 1	60/40/< 1
0.25-0.5	80/20/< 1	80/20/< 1	60/40< 1
0.5-1	20/80/< 1	20/80< 1	10/90< 1
1-2	< 1/> 99/< 1	5/95/< 1	< 1/> 99/< 1

Table 7: Tephra Summary
Individual crystals were not observed >2 mm in size.

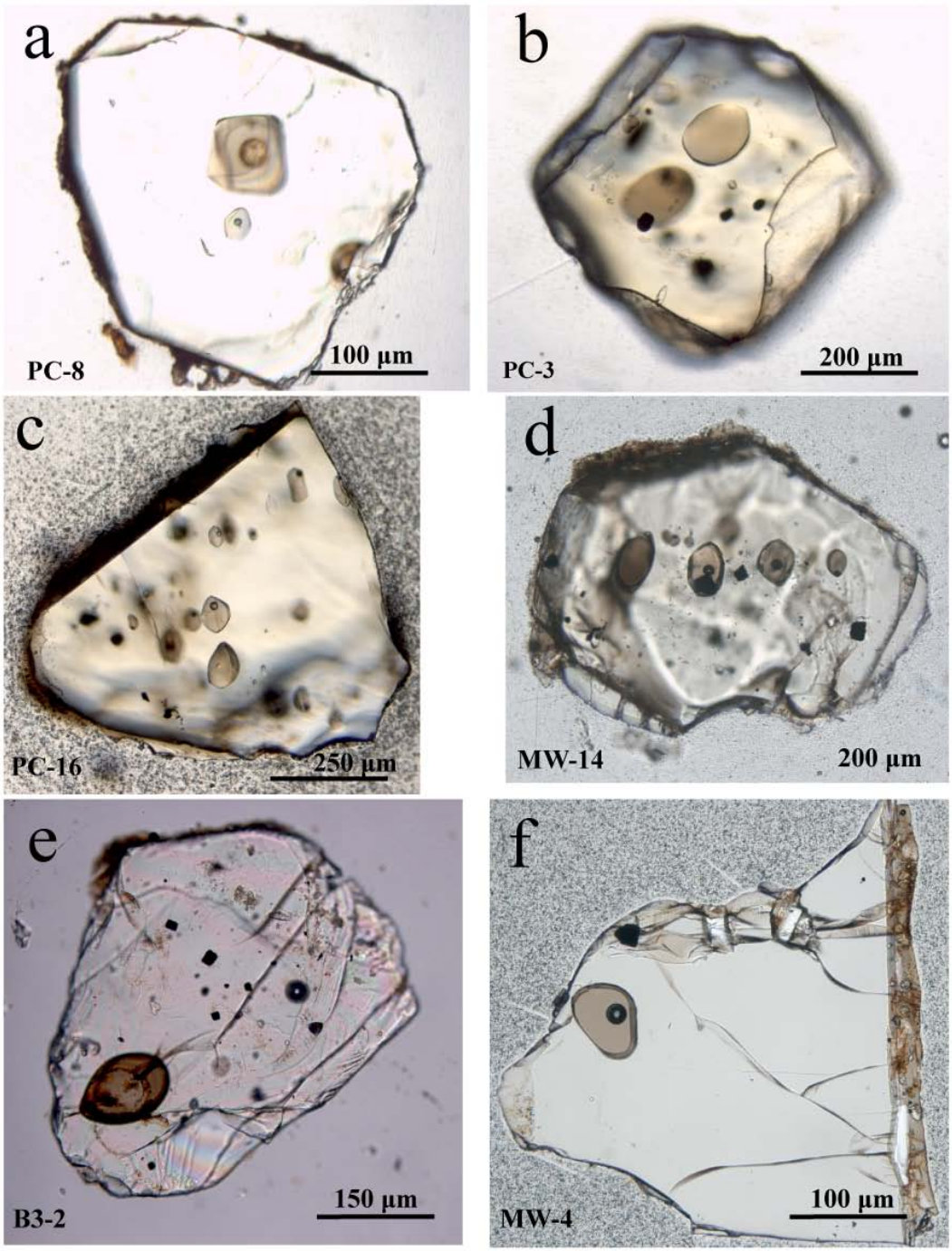

Figure 35: Olivine-Hosted Melt Inclusions from Belknap Crater, Mount Washington and North Sister

a) Faceted, clear glass inclusion with shrinkage bubble; b) ellipsoid inclusions with FeTi oxides; c) Glass inclusions exhibitng a dendritic texture; d) Coplanar inclusions - some with shrinkage bubbles; e) Glass inclusion with several FeTi oxides in same host crystal; f) Glass inclusion with shrinkage bubble

APPENDIX C

SEM ANALYSIS

SEM images of the tephra groundmass of the three volcanoes displayed strong quench crystallization of subhedral plagioclase and anhedral magnetite (Fig. 21) and plagioclase and olivine as the two most common phenocrysts in abundances and sizes that are consistent with late-stage, shallow crystallization. With the exception of one sample from Mount Washington (Fig. 29), mostly euhedral plagioclase predominated the phenocrysts mineral assemblage (Fig. 19, Fig. 20, Fig. 36, Table 8). The Mount Washington clast in question consisted of ~90% groundmass, which were composed of ~95% euhedral to subhedral pyroxene. Subhedral olivine was also present. The groundmass consisted of < 5% glass with the remainder of matrix composed of 60% anhedral magnetite and 40% anhedral pyroxene.

Euhedral to subhedral olivine was always found in modal phenocryst abundances of 5-15%. Olivine grains were seldom observed larger than 100 μm in the tephra clasts. Pyroxene was present in trace abundances with an exception for the one Mount Washington clast. All the samples displayed some level of a diktytaxitic texture from interactions between vesicles and phenocrysts. One large (450 μm), anhedral pryoxene crystal in a North Sister tephra clast appeared separated from another fragment that appeared to have once been part of the larger crystal (Fig. 37). Subhedral plagioclase (200 μm) crystallized in contact with both pieces. In the same tephra clast, one feldspar displays two distinct periods of crystallization with the later crystallization period producing a plagioclase composition similar to that of the plagioclase crystal in contact

with the two pyroxene crystals. The pyroxene crystals appear to have been resorbed, resulting in a subhedral morphology.

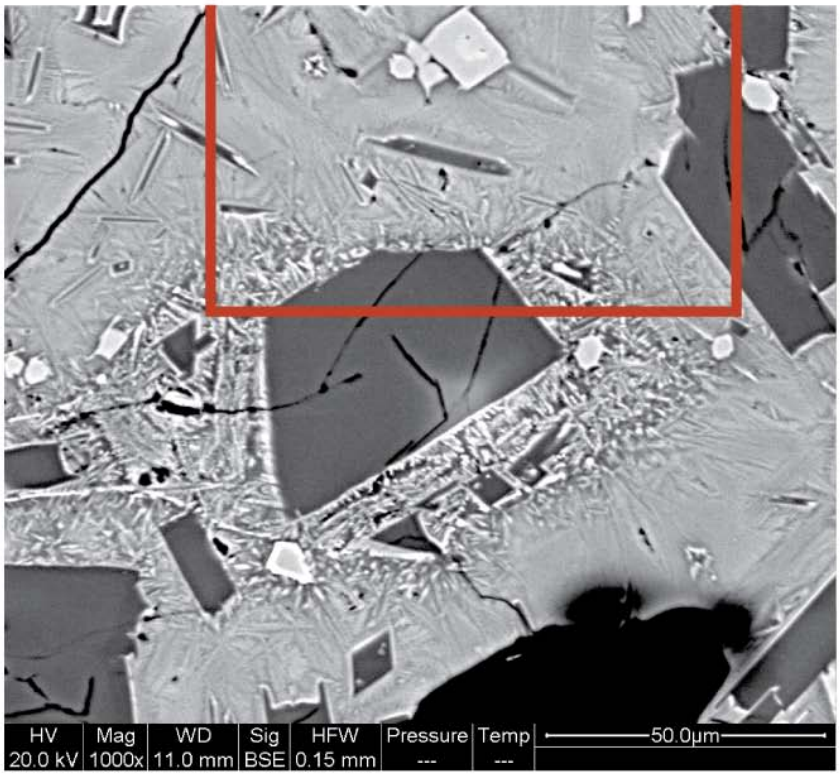

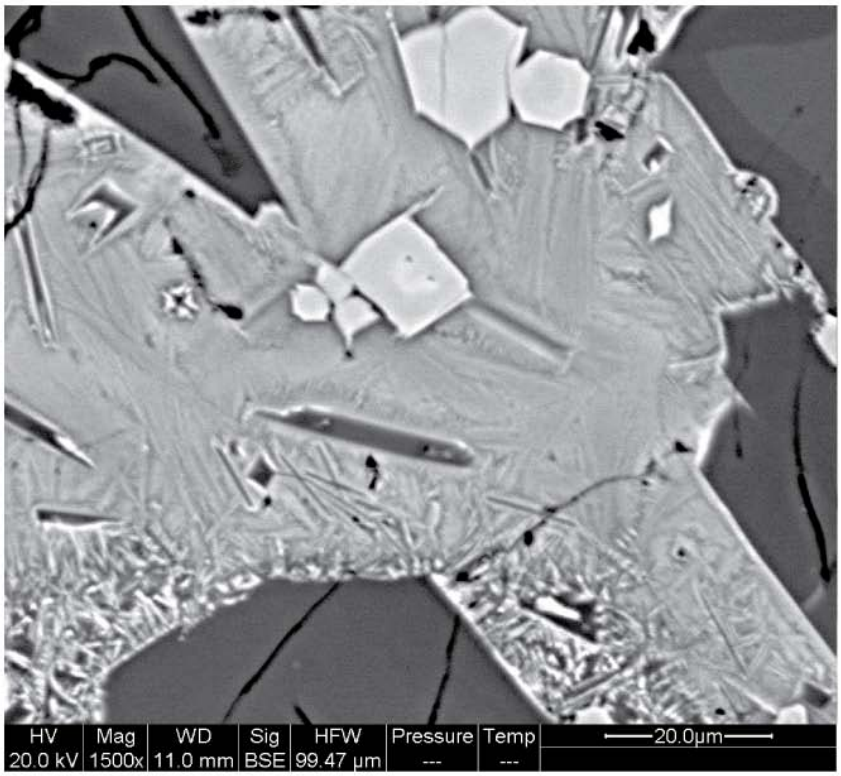

Figure 36: Belknap Tephra Clast
1000x & 1500x

Location of next higher magnification image

Belknap	Modal Abundance	Size (μm)
Phenocrysts	40%	
Plagioclase	70%	50-300
Pyroxene	15%	20-120
Olivine	15%	20-120
Groundmass		
Matrix	60%	
Glass	80%	
Quench Crystals	20%	
Plagioclase	95%	1-10
Magnetite	5%	5-10

North Sister	Modal Abundance	Size (μm)
Phenocrysts	25%	
Plagioclase	95%	20-70
Olivine	5%	20-30
Pyroxene	< 1%	450
Groundmass		
Matrix	75%	
Glass	< 1%	
Quench Crystals	> 99%	
Plagioclase	95%	< 1-5
Magnetite	5%	< 1

Mount Washington	Modal Abundance	Size (μm)
Phenocrysts	30%	
Plagioclase	90%	30-250
Olivine	10%	20-60
Groundmass		
Matrix	70%	
Glass	80%	
Quench Crystals	20%	
Plagioclase	> 99%	< 1-15
Olivine	< 1%	10
Magnetite	< 1%	~3

Mount Washington Pyroxene Cumulate	Modal Abundance	Size (μm)
Phenocrysts	90%	
Pyroxene	95%	50-150
Olivine	5%	50-80
Groundmass		
Matrix	10%	
Glass	< 5%	
Quench Crystals	> 95%	
Magnetite	60%	< 1-10
Pyroxene	40%	< 1-10

Table 8: SEM Image Summary

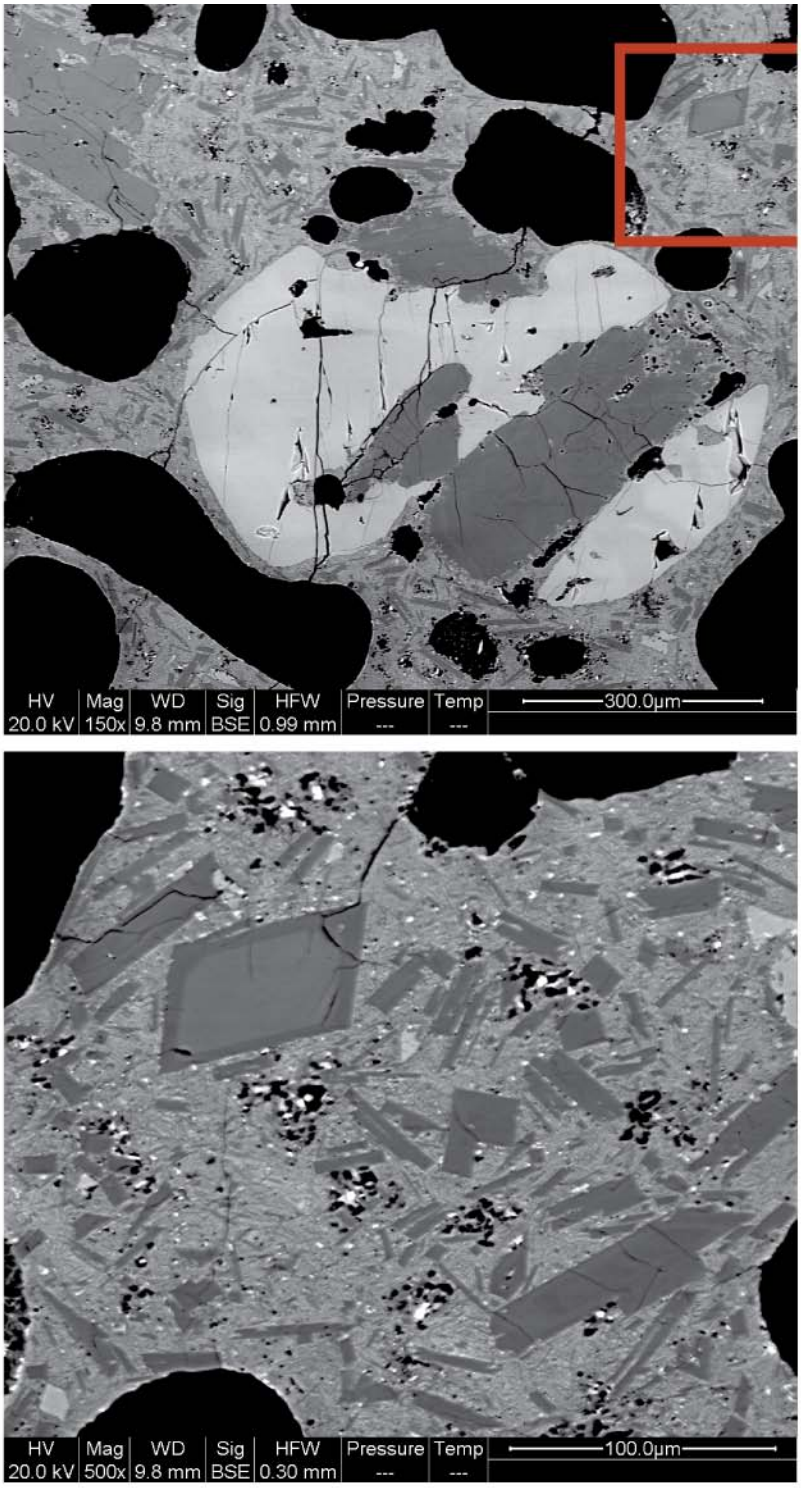

Figure 37: North Sister Tephra Clast
150x & 500x
Top: Pyroxene crystal appears to have been partially resorbed.
Bottom: Zoned plagioclase crystal's outer zone shares similar composition to plagiocase crystal that is between the two pyroxene fragments.

APPENDIX D

MELTS TABLES

Temperature °C	Pressure (bars)	SiO_2	TiO_2	Al_2O_3	Fe_2O_3	FeO	MnO	MgO	CaO	Na_2O	K_2O	P_2O_5
1250	3000	51.19	1.35	17.73	1.80	7.27	0.12	6.26	8.22	4.45	0.92	0.47
1240	2855	51.19	1.35	17.73	1.82	7.25	0.12	6.26	8.22	4.45	0.92	0.47
1230	2710	51.19	1.35	17.73	1.83	7.24	0.12	6.26	8.22	4.45	0.92	0.47
1220	2565	51.19	1.35	17.73	1.84	7.23	0.12	6.26	8.22	4.45	0.92	0.47
1210	2420	51.19	1.35	17.73	1.86	7.22	0.12	6.26	8.22	4.45	0.92	0.47
1200	2275	51.19	1.35	17.73	1.87	7.20	0.12	6.26	8.22	4.45	0.92	0.47
1190	2130	51.19	1.35	17.73	1.89	7.19	0.12	6.26	8.22	4.45	0.92	0.47
1180	1985	51.32	1.41	17.55	1.95	7.31	0.12	5.99	8.16	4.52	0.96	0.49
1170	1840	51.51	1.54	17.02	2.07	7.66	0.13	5.67	7.98	4.65	1.03	0.53
1160	1695	51.64	1.66	16.51	2.19	7.97	0.13	5.38	7.84	4.75	1.10	0.58
1150	1550	51.75	1.79	16.01	2.30	8.27	0.13	5.11	7.73	4.84	1.17	0.62
1140	1405	51.81	1.93	15.51	2.42	8.56	0.14	4.87	7.65	4.90	1.25	0.67
1130	1260	51.85	2.07	15.04	2.54	8.81	0.14	4.64	7.60	4.96	1.32	0.72
1120	1115	51.85	2.21	14.66	2.65	9.05	0.14	4.41	7.49	5.02	1.40	0.77
1110	970	51.85	2.34	14.41	2.74	9.28	0.14	4.16	7.31	5.10	1.48	0.83
1100	825	54.87	1.77	14.54	2.25	7.00	0.16	3.64	6.98	5.54	1.76	1.03
1090	680	55.90	1.64	14.42	2.11	6.31	0.16	3.37	6.83	5.70	1.92	1.15
1080	535	56.75	1.53	14.28	1.97	5.69	0.17	3.14	6.72	5.82	2.09	1.28
1070	390	57.52	1.44	14.14	1.85	5.16	0.17	2.95	6.64	5.89	2.24	1.40
1060	245	58.30	1.36	14.03	1.73	4.68	0.17	2.76	6.48	5.97	2.40	1.44

Table 9: B-34, Equilibrium Crystallization, Initial .29 wt. % H_2O

Temperature °C	Pressure (bars)	SiO_2	TiO_2	Al_2O_3	Fe_2O_3	FeO	MnO	MgO	CaO	Na_2O	K_2O	P_2O_5
1250	3000	51.42	1.36	17.12	1.64	6.97	0.14	8.12	8.62	3.60	0.71	0.30
1240	2855	51.43	1.36	17.12	1.65	6.95	0.14	8.12	8.62	3.60	0.71	0.30
1230	2710	51.43	1.36	17.12	1.66	6.94	0.14	8.12	8.62	3.60	0.71	0.30
1220	2565	51.42	1.36	17.12	1.68	6.93	0.14	8.12	8.62	3.60	0.71	0.30
1210	2420	51.42	1.36	17.12	1.69	6.92	0.14	8.12	8.62	3.60	0.71	0.30
1200	2275	51.49	1.37	17.22	1.70	6.89	0.14	7.88	8.67	3.62	0.71	0.30
1190	2130	51.58	1.38	17.35	1.71	6.84	0.14	7.58	8.74	3.64	0.71	0.31
1180	1985	51.66	1.39	17.48	1.72	6.79	0.14	7.30	8.80	3.67	0.72	0.31
1170	1840	51.75	1.40	17.61	1.73	6.74	0.14	7.03	8.87	3.69	0.72	0.31
1160	1695	51.83	1.41	17.73	1.74	6.69	0.14	6.76	8.92	3.73	0.73	0.31
1150	1550	51.92	1.41	17.85	1.76	6.63	0.14	6.51	8.98	3.75	0.73	0.31
1140	1405	52.00	1.43	17.98	1.77	6.56	0.14	6.25	9.04	3.77	0.74	0.32
1130	1260	52.08	1.44	18.10	1.78	6.50	0.14	6.01	9.10	3.80	0.74	0.32
1120	1115	52.16	1.45	18.21	1.78	6.43	0.14	5.78	9.15	3.82	0.75	0.32
1110	970	52.26	1.46	18.33	1.79	6.34	0.14	5.54	9.21	3.85	0.75	0.32
1100	825	52.35	1.47	18.47	1.79	6.24	0.14	5.26	9.28	3.88	0.76	0.33
1090	680	52.48	1.48	18.64	1.80	6.12	0.13	4.99	9.35	3.91	0.77	0.33
1080	535	53.02	1.60	18.14	1.86	6.20	0.14	4.63	9.12	4.10	0.83	0.36
1070	390	55.35	1.66	17.26	1.86	6.04	0.16	3.85	7.54	4.72	1.08	0.47
1060	245	58.68	1.66	15.60	1.66	5.05	0.18	3.21	6.67	5.00	1.56	0.73

Table 10: Most Primitive Observed Belknap Whole Rock, Equilibrium Crystallization, Initial 2 wt. % H_2O

Temperature °C	SiO_2	TiO_2	Al_2O_3	Fe_2O_3	FeO	MnO	MgO	CaO	Na_2O	K_2O	P_2O_5
1200	52.86	1.28	17.56	1.75	7.04	0.13	6.19	8.01	3.67	0.87	0.41
1190	52.86	1.28	17.56	1.75	7.04	0.13	6.19	8.01	3.67	0.87	0.41
1180	52.86	1.28	17.56	1.76	7.03	0.13	6.19	8.01	3.67	0.87	0.41
1170	52.87	1.28	17.56	1.76	7.02	0.13	6.19	8.01	3.67	0.87	0.41
1160	52.90	1.28	17.59	1.77	7.01	0.13	6.11	8.03	3.67	0.87	0.41
1150	53.00	1.29	17.72	1.77	6.96	0.13	5.84	8.08	3.71	0.87	0.42
1140	53.09	1.29	17.85	1.77	6.89	0.13	5.57	8.14	3.74	0.88	0.42
1130	53.17	1.30	17.98	1.77	6.83	0.13	5.32	8.20	3.76	0.89	0.42
1120	53.27	1.31	18.10	1.76	6.76	0.13	5.08	8.25	3.79	0.89	0.43
1110	53.37	1.32	18.22	1.76	6.68	0.13	4.84	8.30	3.81	0.90	0.43
1100	53.47	1.32	18.34	1.75	6.60	0.13	4.61	8.36	3.84	0.90	0.43
1090	53.58	1.33	18.47	1.75	6.51	0.12	4.39	8.41	3.86	0.91	0.43
1080	53.78	1.32	19.12	1.72	6.53	0.13	4.01	7.63	4.06	0.97	0.46
1070	54.06	1.32	19.27	1.72	6.53	0.14	3.73	7.28	4.19	1.01	0.48
1060	54.71	1.08	19.15	1.76	6.58	0.14	3.42	6.92	4.39	1.07	0.51
1050	55.08	0.98	19.19	1.74	6.43	0.16	3.16	6.65	4.61	1.15	0.54
1040	55.58	0.89	19.29	1.67	6.05	0.18	2.94	6.40	4.86	1.23	0.58
1030	56.22	0.82	19.25	1.60	5.69	0.21	2.71	6.17	5.04	1.30	0.63
1020	56.85	0.76	19.17	1.54	5.37	0.22	2.50	5.97	5.20	1.38	0.66
1010	57.45	0.71	19.08	1.47	5.06	0.23	2.32	5.79	5.34	1.45	0.70
1000	57.99	0.67	18.98	1.42	4.78	0.24	2.15	5.61	5.47	1.53	0.74
990	58.51	0.63	18.89	1.37	4.52	0.25	1.99	5.46	5.58	1.61	0.78
980	58.97	0.59	18.80	1.31	4.27	0.26	1.86	5.31	5.68	1.67	0.82
970	59.41	0.55	18.69	1.26	4.04	0.28	1.73	5.19	5.76	1.75	0.86
960	59.86	0.52	18.61	1.21	3.82	0.29	1.61	5.04	5.85	1.82	0.87
950	60.30	0.49	18.53	1.16	3.61	0.30	1.49	4.88	5.92	1.90	0.88
940	60.69	0.46	18.45	1.12	3.42	0.32	1.39	4.75	5.97	1.98	0.88
930	61.03	0.44	18.37	1.07	3.22	0.34	1.30	4.62	6.03	2.07	0.90
920	61.37	0.42	18.29	1.03	3.05	0.36	1.22	4.51	6.07	2.15	0.92
910	61.67	0.39	18.22	0.99	2.89	0.37	1.14	4.41	6.09	2.23	0.94
900	61.95	0.38	18.15	0.95	2.73	0.39	1.06	4.32	6.11	2.31	0.96

Table 11: MW-8, Equilibrium Crystallization, 2 kbar

Temperature °C	SiO_2	TiO_2	Al_2O_3	Fe_2O_3	FeO	MnO	MgO	CaO	Na_2O	K_2O	P_2O_5
1200	52.86	1.28	17.56	1.75	7.04	0.13	6.19	8.01	3.67	0.87	0.41
1190	52.86	1.28	17.56	1.75	7.04	0.13	6.19	8.01	3.67	0.87	0.41
1180	52.86	1.28	17.56	1.75	7.04	0.13	6.19	8.01	3.67	0.87	0.41
1170	52.86	1.28	17.56	1.75	7.04	0.13	6.19	8.01	3.67	0.87	0.41
1160	52.90	1.28	17.59	1.77	7.01	0.13	6.11	8.03	3.67	0.87	0.41
1150	53.00	1.29	17.72	1.77	6.96	0.13	5.84	8.08	3.71	0.87	0.42
1140	53.08	1.29	17.85	1.77	6.90	0.13	5.57	8.14	3.74	0.88	0.42
1130	53.18	1.30	17.97	1.77	6.85	0.13	5.32	8.20	3.76	0.88	0.42
1120	53.26	1.31	18.09	1.77	6.78	0.13	5.08	8.25	3.78	0.89	0.43
1110	53.35	1.32	18.20	1.77	6.72	0.13	4.83	8.30	3.81	0.90	0.43
1100	53.44	1.32	18.32	1.77	6.66	0.13	4.61	8.35	3.83	0.90	0.43
1090	53.53	1.33	18.43	1.76	6.61	0.13	4.39	8.39	3.85	0.91	0.43
1080	53.78	1.32	19.07	1.75	6.60	0.13	3.86	7.75	4.05	0.96	0.46
1070	54.01	1.33	19.15	1.77	6.71	0.14	3.67	7.31	4.17	1.00	0.47
1060	54.65	1.29	19.18	1.72	6.47	0.15	3.44	6.95	4.32	1.06	0.50
1050	55.52	1.22	19.12	1.64	6.03	0.16	3.15	6.68	4.52	1.12	0.53
1040	56.34	1.16	19.05	1.56	5.63	0.16	2.89	6.44	4.69	1.20	0.57
1030	57.12	1.10	18.94	1.49	5.26	0.17	2.66	6.21	4.85	1.26	0.61
1020	57.84	1.05	18.82	1.42	4.92	0.18	2.45	5.99	5.01	1.33	0.64
1010	58.55	1.00	18.67	1.35	4.61	0.20	2.25	5.79	5.15	1.40	0.67
1000	59.22	0.95	18.51	1.28	4.31	0.21	2.08	5.60	5.28	1.46	0.70
990	59.85	0.91	18.33	1.22	4.04	0.22	1.93	5.41	5.40	1.53	0.73
980	60.46	0.87	18.15	1.17	3.78	0.23	1.79	5.25	5.51	1.59	0.78
970	61.21	0.64	17.73	1.19	3.79	0.24	1.52	5.10	5.64	1.66	0.81
960	61.65	0.59	17.42	1.19	3.76	0.25	1.46	4.94	5.70	1.71	0.84
950	62.25	0.55	17.23	1.14	3.54	0.26	1.35	4.76	5.80	1.78	0.84
940	62.83	0.53	17.03	1.11	3.34	0.27	1.25	4.58	5.88	1.85	0.84
930	63.38	0.50	16.83	1.05	3.14	0.28	1.16	4.40	5.96	1.91	0.85
920	63.93	0.47	16.63	1.02	2.96	0.29	1.07	4.23	6.03	1.97	0.86
910	64.44	0.45	16.42	0.96	2.79	0.30	0.99	4.07	6.09	2.03	0.87
900	64.93	0.43	16.21	0.92	2.63	0.32	0.91	3.92	6.15	2.10	0.88

Table 12: MW-8, Fractional Crystallization, 2 kbar

Temperature °C	SiO_2	TiO_2	Al_2O_3	Fe_2O_3	FeO	MnO	MgO	CaO	Na_2O	K_2O	P_2O_5
1280	52.10	0.96	16.43	1.58	6.32	0.09	10.49	7.66	3.57	0.59	0.20
1270	52.13	0.96	16.48	1.59	6.31	0.09	10.37	7.68	3.58	0.59	0.20
1260	52.25	0.97	16.66	1.59	6.28	0.09	9.97	7.76	3.62	0.59	0.20
1250	52.38	0.98	16.83	1.59	6.25	0.09	9.58	7.84	3.66	0.60	0.20
1240	52.50	0.99	17.00	1.59	6.21	0.09	9.20	7.91	3.70	0.60	0.20
1230	52.61	1.00	17.16	1.59	6.17	0.09	8.84	7.98	3.73	0.62	0.21
1220	52.72	1.01	17.32	1.59	6.13	0.09	8.48	8.06	3.76	0.63	0.22
1210	52.84	1.01	17.48	1.59	6.08	0.09	8.13	8.13	3.80	0.63	0.22
1200	52.95	1.03	17.64	1.59	6.02	0.09	7.80	8.19	3.84	0.64	0.22
1190	53.08	1.04	17.79	1.58	5.96	0.09	7.48	8.27	3.87	0.64	0.22
1180	53.19	1.05	17.94	1.58	5.90	0.09	7.16	8.33	3.90	0.65	0.22
1170	53.30	1.06	18.09	1.57	5.83	0.09	6.87	8.40	3.93	0.65	0.22
1160	53.42	1.07	18.24	1.56	5.75	0.08	6.57	8.47	3.96	0.66	0.23
1150	53.53	1.07	18.39	1.56	5.67	0.08	6.29	8.53	3.99	0.66	0.23
1140	53.65	1.08	18.53	1.55	5.59	0.08	6.02	8.60	4.03	0.67	0.23
1130	53.75	1.09	18.67	1.54	5.49	0.08	5.76	8.66	4.06	0.67	0.23
1120	53.87	1.10	18.81	1.52	5.40	0.08	5.51	8.72	4.09	0.68	0.23
1110	53.98	1.11	18.95	1.51	5.30	0.08	5.26	8.78	4.12	0.68	0.23
1100	54.09	1.11	19.08	1.50	5.20	0.08	5.02	8.84	4.15	0.69	0.24
1090	54.21	1.12	19.21	1.48	5.09	0.08	4.80	8.90	4.18	0.69	0.24
1080	54.42	1.11	19.64	1.45	5.00	0.08	4.51	8.54	4.30	0.71	0.24
1070	54.84	1.13	19.74	1.44	4.97	0.08	4.19	8.11	4.48	0.75	0.26
1060	55.34	1.15	19.76	1.43	4.91	0.08	3.91	7.70	4.66	0.79	0.27
1050	55.84	1.15	19.77	1.43	4.84	0.09	3.65	7.31	4.83	0.83	0.28
1040	56.37	1.13	19.76	1.41	4.74	0.09	3.40	6.94	4.99	0.87	0.30
1030	56.92	1.10	19.73	1.39	4.63	0.09	3.17	6.60	5.15	0.91	0.31
1020	57.53	1.05	19.67	1.36	4.49	0.09	2.95	6.28	5.29	0.96	0.33
1010	58.64	1.00	19.29	1.29	4.20	0.09	2.72	5.87	5.49	1.04	0.36
1000	59.63	0.51	18.54	1.37	4.29	0.10	2.38	5.46	6.05	1.23	0.44
990	60.00	0.46	18.20	1.39	4.20	0.11	2.16	5.13	6.44	1.42	0.51
980	60.43	0.42	17.86	1.37	3.98	0.13	1.95	4.86	6.77	1.64	0.60
970	60.89	0.39	17.55	1.29	3.63	0.15	1.78	4.66	7.04	1.89	0.73
960	61.38	0.35	17.26	1.21	3.29	0.16	1.64	4.46	7.24	2.20	0.81
950	61.97	0.33	17.05	1.12	2.95	0.17	1.49	4.17	7.37	2.58	0.80

Table 13: Collier Cone Equilibrium Crystallization, 1 kbar

Temperature °C	SiO_2	TiO_2	Al_2O_3	Fe_2O_3	FeO	MnO	MgO	CaO	Na_2O	K_2O	P_2O_5
1280	52.10	0.96	16.43	1.58	6.32	0.09	10.49	7.66	3.57	0.59	0.20
1270	52.13	0.96	16.48	1.59	6.31	0.09	10.37	7.68	3.58	0.59	0.20
1260	52.25	0.97	16.66	1.59	6.28	0.09	9.97	7.76	3.63	0.59	0.20
1250	52.37	0.98	16.83	1.59	6.26	0.09	9.58	7.84	3.66	0.60	0.20
1240	52.50	0.99	16.99	1.59	6.22	0.09	9.20	7.91	3.70	0.60	0.20
1230	52.59	1.00	17.16	1.60	6.19	0.09	8.83	7.98	3.73	0.61	0.20
1220	52.71	1.00	17.30	1.60	6.16	0.09	8.48	8.05	3.76	0.63	0.22
1210	52.82	1.02	17.46	1.60	6.12	0.09	8.13	8.12	3.79	0.63	0.22
1200	52.92	1.03	17.61	1.60	6.09	0.09	7.80	8.18	3.82	0.64	0.22
1190	53.03	1.04	17.75	1.60	6.05	0.09	7.48	8.26	3.86	0.64	0.22
1180	53.13	1.05	17.89	1.60	6.01	0.09	7.16	8.32	3.89	0.65	0.22
1170	53.24	1.05	18.03	1.60	5.96	0.09	6.87	8.38	3.92	0.65	0.22
1160	53.33	1.06	18.17	1.60	5.92	0.09	6.57	8.44	3.95	0.65	0.23
1150	53.42	1.07	18.30	1.60	5.87	0.09	6.28	8.50	3.98	0.66	0.23
1140	53.52	1.08	18.43	1.60	5.83	0.09	6.01	8.55	4.00	0.66	0.23
1130	53.61	1.08	18.55	1.60	5.78	0.09	5.75	8.60	4.04	0.67	0.23
1120	53.70	1.09	18.67	1.60	5.73	0.09	5.49	8.67	4.06	0.67	0.23
1110	53.79	1.10	18.79	1.60	5.68	0.08	5.25	8.72	4.09	0.68	0.23
1100	53.88	1.10	18.91	1.60	5.63	0.08	5.00	8.78	4.11	0.68	0.23
1090	53.97	1.11	19.02	1.60	5.57	0.08	4.78	8.82	4.14	0.68	0.23
1080	54.11	1.10	19.37	1.59	5.56	0.09	4.48	8.51	4.24	0.70	0.24
1070	54.41	1.12	19.50	1.62	5.63	0.09	4.17	8.08	4.40	0.73	0.25
1060	54.78	1.14	19.48	1.65	5.72	0.09	3.88	7.67	4.55	0.77	0.26
1050	55.16	1.16	19.44	1.67	5.80	0.10	3.60	7.27	4.70	0.81	0.28
1040	55.98	1.09	19.42	1.61	5.52	0.10	3.34	6.90	4.89	0.85	0.29
1030	56.86	1.01	19.36	1.53	5.17	0.11	3.11	6.56	5.08	0.89	0.31
1020	57.72	0.92	19.29	1.45	4.85	0.11	2.90	6.23	5.26	0.95	0.32
1010	58.66	0.86	19.06	1.39	4.54	0.11	2.69	5.89	5.44	1.00	0.34
1000	59.83	0.81	18.65	1.32	4.21	0.14	2.40	5.47	5.71	1.08	0.37
990	60.95	0.76	18.22	1.25	3.90	0.15	2.14	5.09	5.96	1.18	0.41
980	61.99	0.72	17.80	1.19	3.61	0.16	1.93	4.73	6.18	1.26	0.45
970	63.10	0.46	17.09	1.24	3.69	0.17	1.64	4.43	6.37	1.35	0.48
960	63.91	0.42	16.64	1.22	3.57	0.18	1.49	4.14	6.51	1.43	0.51
950	64.84	0.39	16.19	1.16	3.32	0.19	1.35	3.86	6.65	1.52	0.54

Table 14: Collier Cone Fractional Crystallization, 1 kbar

Temperature °C	SiO_2	TiO_2	Al_2O_3	Fe_2O_3	FeO	MnO	MgO	CaO	Na_2O	K_2O	P_2O_5
1340	52.12	0.96	16.44	1.23	6.63	0.09	10.49	7.66	3.57	0.59	0.20
1330	52.09	0.96	16.55	1.24	6.64	0.09	10.32	7.71	3.60	0.59	0.20
1320	52.03	0.98	16.79	1.25	6.64	0.09	9.91	7.84	3.67	0.60	0.20
1310	51.98	0.99	17.04	1.25	6.63	0.09	9.50	7.96	3.73	0.62	0.21
1300	51.91	1.00	17.28	1.26	6.62	0.09	9.12	8.08	3.79	0.63	0.22
1290	51.86	1.03	17.52	1.26	6.61	0.09	8.73	8.20	3.86	0.64	0.22
1280	51.82	1.04	17.75	1.26	6.58	0.10	8.35	8.30	3.93	0.65	0.22
1270	51.77	1.05	17.98	1.26	6.55	0.10	8.00	8.42	3.99	0.66	0.23
1260	51.74	1.06	18.21	1.26	6.51	0.10	7.64	8.52	4.06	0.67	0.23
1250	51.71	1.07	18.44	1.26	6.46	0.10	7.30	8.63	4.12	0.68	0.23
1240	51.68	1.09	18.67	1.26	6.40	0.10	6.96	8.73	4.18	0.69	0.24
1230	51.65	1.10	18.89	1.26	6.34	0.10	6.64	8.82	4.25	0.70	0.24
1220	51.63	1.11	19.11	1.26	6.28	0.11	6.33	8.92	4.31	0.71	0.24
1210	51.61	1.12	19.34	1.26	6.20	0.11	6.02	9.00	4.37	0.72	0.25
1200	51.60	1.13	19.57	1.25	6.11	0.11	5.72	9.09	4.44	0.73	0.25
1190	51.59	1.14	19.80	1.24	6.01	0.11	5.44	9.17	4.51	0.74	0.26
1180	51.59	1.16	20.03	1.23	5.90	0.11	5.15	9.23	4.58	0.75	0.26
1170	51.59	1.18	20.28	1.21	5.79	0.11	4.89	9.29	4.64	0.76	0.26
1160	51.58	1.19	20.52	1.20	5.66	0.12	4.62	9.34	4.71	0.78	0.27
1150	52.53	1.08	22.02	1.13	5.62	0.13	3.84	7.10	5.35	0.90	0.30
1140	52.76	1.05	22.41	1.10	5.46	0.15	3.55	6.78	5.51	0.93	0.31
1130	53.03	1.01	22.77	1.06	5.29	0.15	3.27	6.48	5.66	0.96	0.32
1120	53.30	0.97	23.11	1.03	5.11	0.16	3.02	6.19	5.81	0.99	0.33
1110	53.58	0.93	23.42	0.99	4.91	0.16	2.78	5.90	5.97	1.02	0.34
1100	54.30	0.63	23.56	0.96	4.68	0.16	2.52	5.64	6.15	1.05	0.35
1090	54.61	0.56	23.80	0.92	4.47	0.17	2.33	5.40	6.29	1.09	0.37
1080	54.93	0.50	24.04	0.88	4.26	0.17	2.15	5.16	6.43	1.11	0.38
1070	55.58	0.46	23.89	0.83	3.96	0.18	1.99	4.93	6.65	1.15	0.39
1060	56.33	0.43	23.65	0.78	3.63	0.18	1.83	4.71	6.87	1.20	0.41
1050	57.04	0.40	23.39	0.72	3.32	0.19	1.70	4.49	7.09	1.24	0.42
1040	57.73	0.37	23.13	0.67	3.03	0.19	1.58	4.30	7.30	1.27	0.43
1030	58.40	0.34	22.86	0.63	2.76	0.20	1.46	4.11	7.49	1.32	0.44
1020	59.03	0.32	22.60	0.58	2.51	0.20	1.36	3.92	7.68	1.35	0.45
1010	59.64	0.30	22.33	0.54	2.28	0.21	1.27	3.75	7.84	1.38	0.46
1000	60.23	0.27	22.06	0.50	2.06	0.21	1.18	3.58	8.00	1.42	0.48
990	60.79	0.25	21.79	0.46	1.86	0.22	1.10	3.43	8.16	1.45	0.49
980	61.36	0.23	21.54	0.41	1.69	0.22	1.03	3.26	8.31	1.47	0.48
970	61.69	0.21	21.33	0.39	1.57	0.23	0.97	3.15	8.44	1.54	0.48
960	62.01	0.19	21.12	0.37	1.47	0.25	0.92	3.03	8.56	1.60	0.49
950	62.30	0.18	20.92	0.35	1.38	0.26	0.87	2.93	8.67	1.66	0.49

Table 15: Collier Cone Equilibrium Crystallization, 8 kbar

Temperature °C	SiO_2	TiO_2	Al_2O_3	Fe_2O_3	FeO	MnO	MgO	CaO	Na_2O	K_2O	P_2O_5
1340	52.12	0.96	16.44	1.23	6.63	0.09	10.49	7.66	3.57	0.59	0.20
1330	52.09	0.96	16.55	1.24	6.64	0.09	10.32	7.71	3.60	0.59	0.20
1320	52.03	0.98	16.79	1.25	6.64	0.09	9.91	7.84	3.67	0.60	0.20
1310	51.97	0.99	17.04	1.25	6.64	0.09	9.50	7.96	3.73	0.62	0.21
1300	51.91	1.00	17.27	1.26	6.63	0.09	9.11	8.08	3.79	0.63	0.22
1290	51.85	1.03	17.51	1.26	6.63	0.09	8.73	8.20	3.86	0.64	0.22
1280	51.80	1.04	17.73	1.27	6.62	0.10	8.35	8.30	3.92	0.65	0.22
1270	51.74	1.05	17.96	1.27	6.61	0.10	7.99	8.42	3.98	0.66	0.23
1260	51.70	1.06	18.18	1.28	6.59	0.10	7.63	8.52	4.04	0.67	0.23
1250	51.65	1.07	18.40	1.28	6.57	0.10	7.28	8.63	4.10	0.68	0.23
1240	51.61	1.09	18.60	1.29	6.56	0.10	6.95	8.72	4.15	0.69	0.24
1230	51.57	1.10	18.81	1.30	6.53	0.10	6.62	8.83	4.20	0.70	0.24
1220	51.53	1.11	19.02	1.30	6.50	0.10	6.31	8.93	4.27	0.70	0.24
1210	51.50	1.12	19.22	1.30	6.47	0.11	6.00	9.01	4.32	0.71	0.24
1200	51.45	1.13	19.41	1.31	6.44	0.11	5.70	9.11	4.37	0.72	0.25
1190	51.43	1.14	19.60	1.31	6.40	0.11	5.41	9.19	4.43	0.73	0.25
1180	51.40	1.15	19.79	1.31	6.36	0.11	5.12	9.28	4.48	0.74	0.25
1170	51.36	1.16	19.99	1.31	6.32	0.11	4.85	9.35	4.53	0.75	0.26
1160	51.34	1.17	20.17	1.31	6.28	0.11	4.59	9.44	4.59	0.75	0.26
1150	51.96	1.11	21.98	1.26	6.26	0.13	3.20	7.68	5.23	0.88	0.30
1140	52.11	1.09	22.34	1.25	6.26	0.13	2.92	7.33	5.36	0.90	0.30
1130	52.26	1.07	22.67	1.24	6.24	0.15	2.68	6.98	5.48	0.92	0.31
1120	52.40	1.04	22.99	1.24	6.22	0.15	2.44	6.65	5.61	0.94	0.32
1110	52.58	1.01	23.29	1.23	6.19	0.15	2.22	6.33	5.71	0.97	0.33
1100	52.75	0.97	23.57	1.22	6.16	0.15	2.03	6.02	5.82	0.99	0.33
1090	52.92	0.93	23.82	1.21	6.12	0.16	1.84	5.72	5.93	1.01	0.34
1080	53.13	0.87	24.03	1.20	6.07	0.16	1.68	5.45	6.04	1.03	0.34
1070	53.58	0.80	24.13	1.17	5.85	0.16	1.43	5.26	6.22	1.05	0.35
1060	54.03	0.74	24.21	1.14	5.61	0.17	1.19	5.08	6.38	1.09	0.37
1050	54.44	0.70	24.24	1.11	5.41	0.17	1.00	4.88	6.56	1.12	0.38
1040	54.81	0.68	24.17	1.10	5.30	0.18	0.86	4.61	6.73	1.16	0.40
1030	55.16	0.67	24.10	1.09	5.20	0.19	0.73	4.34	6.90	1.21	0.41
1020	55.47	0.66	24.02	1.08	5.10	0.19	0.63	4.10	7.07	1.25	0.43
1010	55.80	0.65	23.95	1.07	5.00	0.20	0.53	3.85	7.22	1.28	0.44
1000	56.08	0.64	23.88	1.07	4.90	0.21	0.44	3.62	7.37	1.33	0.45
990	56.39	0.64	23.83	1.05	4.79	0.21	0.37	3.39	7.51	1.37	0.45
980	56.82	0.61	23.80	1.01	4.52	0.22	0.32	3.18	7.65	1.42	0.46
970	57.21	0.59	23.78	0.97	4.28	0.23	0.28	2.96	7.79	1.46	0.46
960	57.57	0.56	23.75	0.92	4.04	0.23	0.24	2.77	7.91	1.52	0.47
950	57.91	0.53	23.75	0.88	3.82	0.25	0.21	2.59	8.03	1.57	0.47

Table 16: Collier Cone Fractional Crystallization, 8 kbar

Temperature °C	SiO_2	TiO_2	Al_2O_3	Fe_2O_3	FeO	MnO	MgO	CaO	Na_2O	K_2O	P_2O_5
1340	48.14	1.34	15.11	1.47	8.40	0.16	13.21	8.77	2.74	0.35	0.29
1330	48.14	1.34	15.11	1.48	8.40	0.16	13.20	8.77	2.74	0.35	0.29
1320	48.22	1.36	15.30	1.48	8.39	0.16	12.75	8.88	2.78	0.36	0.30
1310	48.32	1.38	15.50	1.50	8.38	0.16	12.30	8.98	2.81	0.36	0.30
1300	48.41	1.39	15.68	1.51	8.37	0.16	11.87	9.09	2.84	0.37	0.30
1290	48.50	1.41	15.86	1.51	8.35	0.16	11.45	9.19	2.88	0.37	0.31
1280	48.59	1.43	16.05	1.52	8.33	0.16	11.03	9.30	2.91	0.37	0.31
1270	48.69	1.45	16.22	1.53	8.30	0.16	10.63	9.39	2.94	0.38	0.31
1260	48.77	1.47	16.40	1.53	8.27	0.16	10.24	9.49	2.97	0.38	0.32
1250	48.86	1.48	16.57	1.54	8.24	0.16	9.86	9.58	3.00	0.39	0.32
1240	48.95	1.50	16.74	1.54	8.20	0.16	9.48	9.68	3.03	0.39	0.32
1230	49.03	1.51	16.91	1.55	8.16	0.16	9.12	9.77	3.06	0.39	0.33
1220	49.12	1.52	17.07	1.55	8.12	0.16	8.77	9.86	3.09	0.40	0.33
1210	49.21	1.54	17.22	1.56	8.08	0.15	8.43	9.95	3.13	0.40	0.33
1200	49.30	1.55	17.38	1.56	8.03	0.15	8.09	10.04	3.15	0.41	0.33
1190	49.38	1.56	17.54	1.57	7.98	0.15	7.77	10.12	3.18	0.41	0.34
1180	49.45	1.58	17.69	1.57	7.93	0.15	7.46	10.21	3.21	0.41	0.34
1170	49.53	1.59	17.83	1.58	7.88	0.15	7.15	10.29	3.23	0.42	0.34
1160	49.62	1.60	17.97	1.58	7.82	0.15	6.85	10.36	3.26	0.43	0.35
1150	49.70	1.62	18.12	1.58	7.76	0.15	6.57	10.44	3.28	0.43	0.35
1140	49.94	1.71	17.76	1.64	7.97	0.16	6.24	10.36	3.38	0.46	0.37
1130	50.21	1.82	17.32	1.71	8.22	0.16	5.92	10.26	3.50	0.48	0.40
1120	50.43	1.93	17.15	1.78	8.50	0.17	5.55	9.90	3.65	0.52	0.43
1110	50.65	2.02	17.10	1.83	8.78	0.18	5.16	9.46	3.82	0.55	0.46
1100	50.88	2.09	17.05	1.88	9.04	0.19	4.79	9.02	3.99	0.58	0.49
1090	51.12	2.16	17.00	1.93	9.28	0.19	4.43	8.59	4.15	0.62	0.52
1080	51.93	2.04	16.98	1.92	9.10	0.21	4.05	8.15	4.38	0.67	0.56
1070	53.22	1.78	16.98	1.84	8.56	0.22	3.67	7.73	4.66	0.73	0.62
1060	54.38	1.55	16.93	1.77	8.07	0.25	3.34	7.35	4.90	0.79	0.67
1050	55.46	1.37	16.83	1.71	7.61	0.26	3.05	7.02	5.13	0.84	0.72
1040	56.44	1.21	16.70	1.65	7.20	0.28	2.80	6.71	5.34	0.89	0.77
1030	57.38	1.08	16.56	1.59	6.81	0.29	2.57	6.43	5.52	0.95	0.82
1020	58.25	0.97	16.38	1.54	6.45	0.30	2.37	6.19	5.69	1.00	0.86
1010	59.10	0.87	16.20	1.48	6.11	0.31	2.19	5.94	5.86	1.05	0.90
1000	59.98	0.77	16.02	1.44	5.79	0.33	1.99	5.67	6.03	1.11	0.87

Table 17: FLR-03-1 Whole Rock, Olivine Restored, Fractional Crystallization, 1 kbar

Temperature °C	SiO_2	TiO_2	Al_2O_3	Fe_2O_3	FeO	MnO	MgO	CaO	Na_2O	K_2O	P_2O_5
1390	48.14	1.34	15.11	1.37	8.51	0.16	13.21	8.77	2.74	0.35	0.29
1380	48.11	1.35	15.14	1.38	8.50	0.16	13.17	8.79	2.75	0.35	0.29
1370	47.96	1.37	15.39	1.39	8.55	0.16	12.76	8.95	2.80	0.36	0.30
1360	47.81	1.39	15.63	1.41	8.59	0.17	12.35	9.10	2.86	0.37	0.30
1350	47.65	1.42	15.86	1.43	8.63	0.17	11.95	9.27	2.91	0.38	0.31
1340	47.52	1.45	16.10	1.45	8.66	0.17	11.56	9.42	2.96	0.38	0.32
1330	47.37	1.47	16.34	1.47	8.69	0.18	11.17	9.57	3.02	0.39	0.32
1320	47.23	1.49	16.56	1.49	8.71	0.18	10.80	9.73	3.07	0.40	0.33
1310	47.12	1.51	16.79	1.50	8.74	0.18	10.43	9.87	3.13	0.40	0.33
1300	46.98	1.54	17.01	1.52	8.76	0.18	10.06	10.01	3.18	0.41	0.34
1290	46.85	1.56	17.23	1.53	8.77	0.19	9.70	10.16	3.24	0.42	0.34
1280	46.73	1.58	17.45	1.55	8.78	0.19	9.35	10.30	3.29	0.43	0.35
1270	46.60	1.60	17.66	1.56	8.80	0.19	9.01	10.45	3.34	0.44	0.36
1260	46.48	1.62	17.88	1.58	8.80	0.20	8.66	10.58	3.39	0.45	0.36
1250	46.36	1.64	18.09	1.59	8.80	0.20	8.33	10.71	3.44	0.45	0.37
1240	46.25	1.66	18.30	1.61	8.79	0.20	8.01	10.85	3.49	0.46	0.37
1230	45.89	1.75	19.87	1.63	9.22	0.23	6.85	9.63	3.97	0.53	0.44
1220	46.05	1.78	20.26	1.65	9.32	0.25	6.31	9.18	4.18	0.56	0.46
1210	46.45	1.80	20.48	1.66	9.35	0.26	5.71	8.77	4.43	0.59	0.49
1200	46.87	1.82	20.66	1.66	9.36	0.28	5.17	8.37	4.66	0.63	0.52
1190	47.31	1.82	20.83	1.66	9.34	0.30	4.66	7.98	4.89	0.66	0.55
1180	47.77	1.81	20.97	1.66	9.29	0.32	4.20	7.62	5.10	0.69	0.57
1170	48.24	1.80	21.09	1.66	9.21	0.33	3.78	7.26	5.31	0.72	0.60
1160	48.74	1.77	21.19	1.65	9.12	0.34	3.39	6.92	5.50	0.76	0.62
1150	49.25	1.73	21.27	1.65	9.00	0.35	3.04	6.60	5.69	0.79	0.64
1140	49.78	1.67	21.32	1.64	8.87	0.37	2.72	6.29	5.88	0.81	0.66
1130	50.41	1.56	21.35	1.63	8.71	0.38	2.45	5.96	6.06	0.84	0.68
1120	51.12	1.44	21.37	1.61	8.54	0.39	2.19	5.60	6.24	0.86	0.63
1110	51.79	1.34	21.39	1.59	8.33	0.40	1.97	5.28	6.41	0.89	0.60
1100	52.42	1.23	21.42	1.57	8.14	0.41	1.72	4.98	6.61	0.92	0.56
1090	52.98	1.16	21.48	1.55	7.91	0.43	1.45	4.71	6.84	0.95	0.53
1080	53.74	1.11	21.30	1.51	7.53	0.45	1.31	4.43	7.09	1.01	0.51
1070	54.50	1.05	21.14	1.46	7.12	0.48	1.18	4.17	7.33	1.06	0.49
1060	55.19	0.99	20.99	1.41	6.73	0.52	1.08	3.92	7.56	1.12	0.48
1050	55.85	0.94	20.84	1.36	6.36	0.55	0.99	3.68	7.78	1.18	0.48
1040	56.48	0.88	20.70	1.33	6.01	0.58	0.90	3.44	7.98	1.23	0.47
1030	57.06	0.83	20.56	1.28	5.69	0.61	0.82	3.23	8.19	1.29	0.46
1020	57.59	0.78	20.43	1.23	5.37	0.64	0.76	3.01	8.37	1.35	0.46
1010	58.11	0.73	20.32	1.19	5.08	0.68	0.69	2.81	8.54	1.41	0.45
1000	58.58	0.69	20.19	1.15	4.80	0.71	0.64	2.63	8.70	1.46	0.45

Table 18: FLR-03-1 Whole Rock, Olivine Restored, Fractional Crystallization, 8 kbar

Temperature °C	SiO_2	TiO_2	Al_2O_3	Fe_2O_3	FeO	MnO	MgO	CaO	Na_2O	K_2O	P_2O_5
1370	46.37	1.42	14.20	1.61	9.77	0.13	15.31	8.49	2.05	0.36	0.28
1360	46.40	1.43	14.30	1.62	9.78	0.13	15.08	8.54	2.07	0.36	0.28
1350	46.48	1.44	14.51	1.63	9.79	0.13	14.60	8.67	2.09	0.37	0.29
1340	46.57	1.47	14.70	1.64	9.80	0.13	14.12	8.78	2.12	0.37	0.29
1330	46.65	1.49	14.91	1.65	9.80	0.13	13.65	8.90	2.15	0.38	0.29
1320	46.72	1.51	15.10	1.66	9.80	0.13	13.20	9.01	2.18	0.38	0.30
1310	46.80	1.53	15.29	1.67	9.80	0.13	12.75	9.13	2.21	0.39	0.30
1300	46.88	1.55	15.49	1.68	9.80	0.13	12.31	9.23	2.23	0.39	0.31
1290	46.95	1.57	15.67	1.69	9.79	0.13	11.88	9.34	2.26	0.40	0.31
1280	47.03	1.59	15.86	1.69	9.78	0.13	11.47	9.44	2.30	0.40	0.31
1270	47.11	1.60	16.04	1.70	9.76	0.13	11.06	9.55	2.32	0.41	0.32
1260	47.18	1.62	16.21	1.71	9.74	0.13	10.66	9.66	2.35	0.41	0.32
1250	47.26	1.64	16.40	1.72	9.71	0.13	10.27	9.75	2.37	0.42	0.32
1240	47.33	1.66	16.57	1.73	9.68	0.13	9.89	9.85	2.40	0.42	0.33
1230	47.41	1.67	16.74	1.73	9.65	0.13	9.52	9.96	2.42	0.44	0.33
1220	47.50	1.69	16.91	1.74	9.61	0.13	9.16	10.05	2.44	0.44	0.33
1210	47.56	1.71	17.07	1.75	9.57	0.13	8.81	10.14	2.47	0.44	0.34
1200	47.63	1.72	17.24	1.76	9.53	0.13	8.47	10.24	2.49	0.45	0.34
1190	47.71	1.74	17.40	1.76	9.48	0.13	8.14	10.34	2.51	0.45	0.34
1180	47.78	1.75	17.55	1.77	9.43	0.13	7.81	10.42	2.54	0.46	0.35
1170	47.86	1.77	17.71	1.77	9.39	0.13	7.49	10.51	2.56	0.46	0.35
1160	47.93	1.78	17.87	1.78	9.33	0.12	7.19	10.60	2.58	0.46	0.35
1150	48.00	1.80	18.02	1.79	9.27	0.12	6.89	10.68	2.60	0.47	0.36
1140	48.13	1.84	17.99	1.81	9.32	0.12	6.59	10.71	2.64	0.48	0.36
1130	48.32	1.97	17.57	1.90	9.62	0.13	6.26	10.61	2.73	0.51	0.40
1120	48.52	2.09	17.15	1.97	9.91	0.13	5.95	10.51	2.81	0.54	0.42
1110	48.67	2.19	17.01	2.03	10.25	0.14	5.58	10.18	2.93	0.57	0.45
1100	48.83	2.28	17.00	2.08	10.58	0.15	5.19	9.74	3.06	0.61	0.48
1090	49.02	2.35	16.99	2.14	10.88	0.15	4.82	9.31	3.19	0.64	0.51
1080	50.52	2.01	17.19	2.04	10.15	0.17	4.33	8.84	3.46	0.71	0.57
1070	51.89	1.74	17.32	1.94	9.49	0.18	3.91	8.41	3.71	0.79	0.62
1060	53.12	1.52	17.37	1.85	8.90	0.20	3.56	8.02	3.92	0.85	0.69
1050	54.25	1.32	17.38	1.78	8.36	0.22	3.25	7.66	4.12	0.91	0.74
1040	55.31	1.17	17.34	1.71	7.87	0.23	2.97	7.34	4.31	0.98	0.78
1030	56.29	1.04	17.26	1.64	7.41	0.24	2.73	7.04	4.48	1.04	0.83
1020	57.21	0.92	17.17	1.58	6.99	0.25	2.51	6.76	4.63	1.09	0.89
1010	58.04	0.83	17.04	1.52	6.59	0.27	2.29	6.55	4.78	1.16	0.94
1000	58.95	0.75	16.93	1.46	6.21	0.28	2.09	6.27	4.94	1.22	0.91

Table 19: FLR-03-1 Melt Inclusion, Olivine Restored, Fractional Crystallization, 1 kbar

Temperature °C	SiO_2	TiO_2	Al_2O_3	Fe_2O_3	FeO	MnO	MgO	CaO	Na_2O	K_2O	P_2O_5
1420	46.37	1.42	14.20	1.49	9.87	0.13	15.31	8.49	2.05	0.36	0.28
1410	46.41	1.42	14.29	1.51	9.87	0.13	15.11	8.55	2.06	0.36	0.28
1400	46.48	1.44	14.49	1.52	9.88	0.13	14.63	8.67	2.09	0.37	0.29
1390	46.56	1.46	14.70	1.53	9.89	0.13	14.15	8.78	2.12	0.37	0.29
1380	46.65	1.49	14.90	1.53	9.89	0.13	13.69	8.89	2.15	0.38	0.29
1370	46.73	1.51	15.09	1.54	9.88	0.13	13.24	9.02	2.18	0.38	0.30
1360	46.57	1.54	15.33	1.56	9.95	0.13	12.83	9.18	2.22	0.39	0.30
1350	46.42	1.56	15.57	1.58	10.00	0.13	12.42	9.34	2.26	0.40	0.31
1340	46.25	1.59	15.80	1.60	10.05	0.14	12.02	9.49	2.32	0.41	0.32
1330	46.11	1.62	16.03	1.62	10.10	0.14	11.63	9.66	2.36	0.41	0.32
1320	45.95	1.64	16.26	1.64	10.15	0.14	11.26	9.81	2.40	0.42	0.33
1310	45.80	1.66	16.49	1.65	10.19	0.14	10.89	9.97	2.44	0.44	0.33
1300	45.64	1.69	16.71	1.67	10.22	0.15	10.53	10.12	2.48	0.45	0.34
1290	45.49	1.71	16.93	1.69	10.26	0.15	10.18	10.28	2.52	0.45	0.35
1280	45.34	1.74	17.14	1.71	10.29	0.15	9.82	10.43	2.57	0.46	0.35
1270	45.19	1.76	17.36	1.73	10.31	0.15	9.48	10.57	2.61	0.47	0.36
1260	45.06	1.78	17.56	1.75	10.33	0.16	9.14	10.72	2.65	0.48	0.36
1250	44.91	1.81	17.78	1.76	10.35	0.16	8.80	10.86	2.70	0.48	0.37
1240	44.58	1.89	18.55	1.78	10.64	0.17	8.21	10.38	2.87	0.52	0.41
1230	44.54	1.94	19.01	1.81	10.84	0.18	7.65	10.01	3.04	0.55	0.43
1220	44.84	2.00	19.25	1.83	10.98	0.19	6.98	9.64	3.24	0.59	0.46
1210	45.17	2.05	19.46	1.85	11.07	0.21	6.35	9.27	3.45	0.63	0.49
1200	45.54	2.09	19.66	1.86	11.13	0.22	5.76	8.89	3.65	0.67	0.52
1190	45.93	2.11	19.83	1.88	11.15	0.23	5.22	8.53	3.84	0.71	0.55
1180	46.37	2.12	19.98	1.88	11.15	0.26	4.72	8.16	4.03	0.76	0.58
1170	46.85	2.12	20.12	1.88	11.09	0.27	4.24	7.82	4.22	0.79	0.61
1160	47.36	2.10	20.23	1.88	10.99	0.28	3.81	7.48	4.41	0.83	0.64
1150	47.95	2.05	20.32	1.86	10.83	0.29	3.42	7.15	4.59	0.87	0.68
1140	48.61	1.98	20.41	1.84	10.60	0.31	3.05	6.82	4.76	0.90	0.71
1130	49.48	1.80	20.74	1.76	10.00	0.32	2.73	6.51	4.98	0.94	0.73
1120	50.42	1.64	21.03	1.69	9.47	0.33	2.42	6.15	5.18	0.99	0.68
1110	51.27	1.49	21.29	1.62	8.96	0.34	2.17	5.82	5.36	1.03	0.65
1100	52.06	1.36	21.40	1.58	8.58	0.36	1.87	5.54	5.57	1.07	0.61
1090	52.83	1.26	21.47	1.55	8.20	0.37	1.58	5.28	5.79	1.11	0.57
1080	53.55	1.16	21.55	1.50	7.82	0.38	1.31	5.03	6.00	1.16	0.54
1070	54.21	1.07	21.62	1.46	7.44	0.40	1.08	4.81	6.20	1.20	0.51
1060	54.90	1.01	21.58	1.41	7.05	0.41	0.93	4.58	6.39	1.24	0.50
1050	55.63	0.96	21.43	1.36	6.65	0.44	0.84	4.33	6.58	1.31	0.48
1040	56.31	0.91	21.30	1.31	6.27	0.47	0.75	4.09	6.74	1.37	0.48
1030	56.97	0.87	21.18	1.26	5.90	0.49	0.68	3.86	6.90	1.42	0.47
1020	57.59	0.83	21.05	1.21	5.56	0.51	0.60	3.64	7.06	1.49	0.46
1010	58.17	0.78	20.94	1.16	5.24	0.53	0.54	3.42	7.20	1.55	0.46
1000	58.72	0.74	20.82	1.11	4.94	0.56	0.49	3.22	7.33	1.61	0.46

Table 20: FLR-03-1 Melt Inclusion, Olivine Restored, Fractional Crystallization, 8 kbar

Temperature °C	SiO_2	TiO_2	Al_2O_3	Fe_2O_3	FeO	MnO	MgO	CaO	Na_2O	K_2O	P_2O_5
1290	50.03	1.15	13.60	1.37	6.91	0.17	12.30	11.64	2.28	0.29	0.24
1280	50.11	1.16	13.72	1.38	6.89	0.17	11.98	11.75	2.30	0.29	0.24
1270	50.23	1.17	13.88	1.38	6.85	0.17	11.58	11.87	2.33	0.29	0.24
1260	50.33	1.18	14.03	1.39	6.82	0.17	11.17	11.99	2.35	0.30	0.24
1250	50.43	1.20	14.18	1.39	6.79	0.17	10.78	12.11	2.37	0.30	0.25
1240	50.53	1.21	14.33	1.40	6.75	0.17	10.41	12.24	2.40	0.30	0.25
1230	50.64	1.22	14.47	1.40	6.71	0.17	10.03	12.36	2.43	0.31	0.25
1220	50.74	1.23	14.62	1.42	6.66	0.16	9.67	12.47	2.46	0.31	0.25
1210	50.85	1.24	14.76	1.42	6.62	0.16	9.32	12.59	2.48	0.31	0.25
1200	50.95	1.25	14.89	1.42	6.57	0.16	8.98	12.70	2.50	0.31	0.26
1190	51.04	1.27	15.02	1.43	6.52	0.16	8.64	12.81	2.52	0.32	0.26
1180	51.13	1.28	15.16	1.43	6.47	0.16	8.32	12.92	2.55	0.32	0.26
1170	51.12	1.33	15.75	1.44	6.58	0.17	7.83	12.48	2.67	0.34	0.28
1160	51.11	1.37	16.38	1.45	6.70	0.18	7.34	12.00	2.81	0.36	0.29
1150	51.12	1.41	16.99	1.45	6.81	0.19	6.87	11.52	2.96	0.37	0.31
1140	51.16	1.44	17.58	1.46	6.89	0.20	6.42	11.04	3.09	0.40	0.32
1130	51.43	1.53	17.56	1.50	7.16	0.21	6.01	10.55	3.27	0.43	0.36
1120	51.70	1.62	17.54	1.55	7.40	0.22	5.60	10.09	3.43	0.47	0.39
1110	51.99	1.70	17.50	1.60	7.62	0.24	5.22	9.64	3.59	0.50	0.41
1100	52.27	1.77	17.45	1.64	7.83	0.25	4.85	9.22	3.75	0.53	0.44
1090	52.56	1.83	17.40	1.68	8.02	0.27	4.51	8.81	3.89	0.56	0.47
1080	52.87	1.90	17.34	1.72	8.20	0.28	4.17	8.41	4.03	0.59	0.49
1070	53.19	1.95	17.27	1.76	8.35	0.29	3.85	8.02	4.17	0.62	0.52
1060	54.28	1.76	17.25	1.70	7.93	0.31	3.52	7.64	4.39	0.67	0.56
1050	55.39	1.56	17.19	1.63	7.47	0.33	3.23	7.28	4.59	0.72	0.60
1040	56.44	1.39	17.10	1.56	7.05	0.35	2.97	6.95	4.79	0.76	0.65
1030	57.42	1.24	16.99	1.50	6.66	0.36	2.73	6.66	4.95	0.81	0.68
1020	58.29	1.12	16.86	1.45	6.29	0.38	2.51	6.39	5.12	0.86	0.72
1010	59.12	1.01	16.70	1.39	5.94	0.40	2.30	6.17	5.29	0.91	0.76

Table 21: FLR-03-1 Whole Rock, CPX Restored, Fractional Crystallization, 1 kbar

Temperature °C	SiO_2	TiO_2	Al_2O_3	Fe_2O_3	FeO	MnO	MgO	CaO	Na_2O	K_2O	P_2O_5
1350	50.01	1.15	13.68	1.28	7.00	0.17	12.18	11.71	2.29	0.29	0.24
1340	49.89	1.17	13.89	1.29	7.01	0.17	11.79	11.89	2.34	0.29	0.24
1330	49.77	1.19	14.11	1.30	7.02	0.18	11.41	12.07	2.38	0.30	0.25
1320	49.66	1.21	14.32	1.32	7.02	0.18	11.03	12.26	2.43	0.31	0.25
1310	49.57	1.23	14.54	1.33	7.03	0.18	10.64	12.44	2.47	0.31	0.25
1300	49.43	1.27	14.89	1.34	7.06	0.19	10.22	12.47	2.54	0.32	0.26
1290	49.24	1.34	15.59	1.36	7.20	0.20	9.59	12.16	2.70	0.34	0.28
1280	49.06	1.40	16.28	1.38	7.32	0.21	9.00	11.82	2.86	0.36	0.30
1270	48.90	1.46	16.95	1.39	7.45	0.23	8.43	11.46	3.01	0.40	0.32
1260	48.80	1.51	17.61	1.39	7.56	0.24	7.88	11.09	3.17	0.42	0.33
1250	48.69	1.56	18.25	1.40	7.66	0.25	7.36	10.70	3.33	0.44	0.36
1240	48.62	1.62	18.85	1.40	7.75	0.26	6.87	10.31	3.48	0.46	0.38
1230	48.55	1.66	19.44	1.41	7.84	0.28	6.39	9.92	3.64	0.48	0.40
1220	48.52	1.69	20.01	1.41	7.90	0.30	5.94	9.52	3.78	0.51	0.41
1210	48.52	1.71	20.55	1.42	7.96	0.31	5.51	9.13	3.94	0.53	0.43
1200	48.53	1.73	21.06	1.42	8.01	0.32	5.10	8.75	4.09	0.55	0.45
1190	48.56	1.74	21.55	1.41	8.04	0.34	4.72	8.37	4.23	0.57	0.47
1180	48.67	1.75	21.98	1.41	8.05	0.35	4.35	8.00	4.38	0.59	0.48
1170	49.13	1.76	22.15	1.40	7.97	0.36	3.91	7.67	4.54	0.61	0.50
1160	49.58	1.74	22.30	1.39	7.87	0.38	3.51	7.36	4.71	0.64	0.52
1150	50.05	1.72	22.44	1.38	7.75	0.39	3.14	7.05	4.87	0.66	0.54
1140	50.54	1.69	22.55	1.36	7.63	0.40	2.82	6.75	5.02	0.69	0.56
1130	51.06	1.63	22.63	1.35	7.49	0.42	2.52	6.45	5.16	0.71	0.58
1120	51.66	1.51	22.67	1.33	7.35	0.43	2.27	6.15	5.31	0.74	0.59
1110	52.18	1.40	22.76	1.31	7.16	0.44	1.96	5.90	5.50	0.76	0.63
1100	52.75	1.35	22.75	1.32	7.04	0.46	1.70	5.55	5.71	0.80	0.59
1090	53.27	1.33	22.67	1.31	6.97	0.49	1.47	5.19	5.92	0.83	0.57
1080	53.74	1.31	22.58	1.31	6.88	0.52	1.28	4.85	6.11	0.88	0.55
1070	54.19	1.29	22.50	1.31	6.81	0.54	1.10	4.53	6.28	0.92	0.53

Table 22: FLR-03-1 Whole Rock, CPX Restored, Fractional Crystallization, 8 kbar

Temperature °C	SiO_2	TiO_2	Al_2O_3	Fe_2O_3	FeO	MnO	MgO	CaO	Na_2O	K_2O	P_2O_5
1260	49.66	1.18	12.72	1.48	7.14	0.15	12.00	13.52	1.65	0.28	0.21
1250	49.76	1.19	12.86	1.50	7.11	0.15	11.61	13.66	1.66	0.28	0.22
1240	49.86	1.21	12.99	1.50	7.08	0.15	11.23	13.79	1.68	0.28	0.22
1230	49.95	1.22	13.14	1.51	7.04	0.15	10.85	13.93	1.70	0.28	0.22
1220	50.06	1.23	13.27	1.52	7.00	0.15	10.48	14.07	1.71	0.29	0.22
1210	50.16	1.24	13.40	1.52	6.95	0.15	10.12	14.21	1.73	0.29	0.22
1200	50.26	1.25	13.52	1.53	6.90	0.15	9.77	14.33	1.75	0.29	0.23
1190	50.22	1.30	13.97	1.54	7.01	0.16	9.31	14.11	1.82	0.31	0.24
1180	50.12	1.36	14.64	1.56	7.19	0.17	8.79	13.65	1.93	0.33	0.25
1170	50.04	1.42	15.29	1.57	7.36	0.18	8.28	13.18	2.05	0.35	0.27
1160	49.98	1.47	15.92	1.59	7.52	0.19	7.79	12.73	2.15	0.37	0.28
1150	49.94	1.51	16.53	1.60	7.67	0.20	7.33	12.26	2.26	0.39	0.30
1140	49.93	1.55	17.12	1.60	7.81	0.21	6.87	11.80	2.38	0.41	0.31
1130	49.92	1.58	17.69	1.62	7.93	0.22	6.44	11.34	2.49	0.43	0.34
1120	50.14	1.68	17.71	1.67	8.22	0.23	6.03	10.89	2.61	0.47	0.36
1110	50.37	1.76	17.72	1.71	8.48	0.24	5.63	10.46	2.74	0.50	0.39
1100	50.59	1.85	17.72	1.75	8.74	0.27	5.25	10.03	2.86	0.53	0.42
1090	50.85	1.91	17.72	1.80	8.96	0.28	4.88	9.62	2.99	0.56	0.44
1080	51.11	1.97	17.71	1.84	9.17	0.29	4.53	9.22	3.11	0.59	0.47
1070	51.44	2.01	17.71	1.87	9.32	0.30	4.19	8.81	3.22	0.63	0.49
1060	52.71	1.76	17.81	1.78	8.73	0.33	3.81	8.41	3.42	0.69	0.54
1050	53.87	1.56	17.85	1.71	8.21	0.35	3.49	8.03	3.61	0.74	0.59
1040	54.97	1.38	17.86	1.63	7.72	0.37	3.20	7.68	3.78	0.79	0.63
1030	55.99	1.24	17.83	1.56	7.27	0.38	2.95	7.36	3.93	0.84	0.66
1020	56.93	1.11	17.76	1.50	6.86	0.40	2.72	7.06	4.07	0.89	0.70
1010	57.80	0.99	17.69	1.44	6.46	0.42	2.49	6.81	4.21	0.93	0.75
1000	58.61	0.90	17.56	1.38	6.09	0.46	2.29	6.59	4.34	0.98	0.79
990	59.42	0.82	17.42	1.32	5.72	0.48	2.10	6.39	4.47	1.03	0.83
980	60.45	0.75	17.08	1.27	5.35	0.51	1.88	6.10	4.62	1.10	0.88

Table 23: FLR-03-1 Melt Inclusion, CPX Restored, Fractional Crystallization, 1 kbar

Temperature °C	SiO_2	TiO_2	Al_2O_3	Fe_2O_3	FeO	MnO	MgO	CaO	Na_2O	K_2O	P_2O_5
1330	49.47	1.18	12.72	1.38	7.28	0.16	12.14	13.52	1.65	0.28	0.21
1320	49.34	1.20	12.92	1.39	7.30	0.16	11.76	13.73	1.68	0.28	0.22
1310	49.07	1.28	13.62	1.42	7.48	0.17	11.13	13.50	1.79	0.30	0.23
1300	48.82	1.36	14.33	1.44	7.67	0.18	10.52	13.21	1.90	0.32	0.25
1290	48.57	1.43	15.02	1.46	7.86	0.20	9.92	12.89	2.03	0.35	0.27
1280	48.36	1.50	15.70	1.48	8.04	0.21	9.35	12.55	2.14	0.37	0.29
1270	48.18	1.57	16.36	1.49	8.21	0.22	8.81	12.19	2.26	0.40	0.30
1260	48.00	1.63	17.01	1.50	8.37	0.24	8.28	11.84	2.39	0.42	0.32
1250	47.86	1.70	17.64	1.51	8.51	0.25	7.77	11.46	2.50	0.45	0.35
1240	47.74	1.75	18.24	1.53	8.65	0.26	7.28	11.09	2.62	0.47	0.37
1230	47.65	1.80	18.85	1.53	8.78	0.27	6.81	10.71	2.74	0.49	0.38
1220	47.55	1.84	19.42	1.54	8.89	0.30	6.37	10.32	2.86	0.52	0.40
1210	47.50	1.89	19.97	1.54	8.99	0.31	5.93	9.93	2.98	0.54	0.42
1200	47.47	1.91	20.50	1.54	9.08	0.32	5.52	9.55	3.10	0.56	0.44
1190	47.46	1.93	21.02	1.54	9.16	0.34	5.13	9.16	3.22	0.59	0.46
1180	47.48	1.95	21.51	1.54	9.22	0.35	4.75	8.78	3.33	0.61	0.47
1170	47.91	1.95	21.72	1.53	9.16	0.37	4.29	8.45	3.47	0.64	0.50
1160	48.37	1.96	21.89	1.53	9.08	0.38	3.85	8.13	3.62	0.68	0.52
1150	48.86	1.94	22.06	1.51	8.96	0.40	3.47	7.81	3.75	0.70	0.54
1140	49.38	1.91	22.19	1.50	8.84	0.41	3.10	7.49	3.88	0.73	0.56
1130	49.96	1.83	22.29	1.48	8.69	0.43	2.78	7.17	4.02	0.76	0.59
1120	50.62	1.70	22.35	1.46	8.54	0.44	2.51	6.85	4.14	0.78	0.61
1110	51.22	1.58	22.45	1.44	8.33	0.46	2.15	6.60	4.33	0.81	0.63
1100	51.86	1.47	22.54	1.42	8.08	0.48	1.80	6.33	4.52	0.86	0.63

Table 24: FLR-03-1 Melt Inclusion, CPX Restored, Fractional Crystallization, 8 kbar

REFERENCES CITED

Anderson AT, Brown GG (1993) CO_2 contents and formation pressures of some Kilauean melt inclusions. American Mineralogist 78: 794-803.

Ariskin AA, Barmina GS, Frenkel MY (1986) Computer simulation of crystallization of basaltic melts under conditions of fixed oxygen fugacity. Geokhimiya 11: 1614-1628.

Ariskin AA, Barima GS, Freknal MY (1988) Simulating low-pressure tholeiite-magma crystallization at a fixed oxygen fugacity. Geochemistry International 25(4): 21-38.

Asimow PD, Ghiorso MS (1998) Algorithmic modifications extending MELTS to calculate subsolidus rhase relations. American Mineralogist 83: 1127-1131.

Bacon CR (1983) Eruptive history of Mount Mazama and Crater Lake Caldera, Cascade Range, USA. Journal of Volcanology and Geothermal Research 35.3: 57-115.

Bacon CR, Bruggman PE, Christiansen RL, Clynne MA, Donnelly-Nolan JM, Hildreth W (1997) Primitive magmas at five Cascade volcanic fields: melts from hot, heterogenous sub-arc mantle. Canadian Mineralogist 35. 397-423.

Bevington PR (1969) Data reduction and error analysis for the physical sciences. McGraw-Hill, New York. Ch. 4 & 5.

Blundy J, Cashman K (2005) Rapid decompression-driven crystallization recoded by melt inclusions from Mount St. Helens volcano. Geology 33(10): 793-796.

Borg LE (1995) The origin and evolution of magmas from the Lassen region of the southernmost Cascades, California. PhD Thesis. University of Oregon, Oregon.

Borg LE, Clynne MA, Bullen TD (1997) The variable role of slab-derived fluids in generation of a suite of primitive calc-alkaline lavas from the southernmost Cascades, California. Canadian Mineralogist 35. 425-452.

Clague DA, Moore JG, Dixon JE, Friesen WB (1995) Petrology of submarine lavas from Kilauea's Puna Ridge, Hawaii. Journal of Petrology 36(2): 299-349.

Clark JG (1983) Geology and petrology of South Sister volcano, High Cascade Range, Oregon. Phd Thesis. University of Oregon, Oregon.

Connor CB, Conway FM (2000) Basaltic volcanic cones. In: Sigurdsson, H., Houghton, B.F., McNutt, S.R., Rymer, H., Stix, J. (Eds.) Encyclopedia of Volcanoes. Academic Press, San Diego. 331-343.

Conrey RM, Sherrod DR, Hooper PR, Swanson DA (1997) Diverse primitive magmas in the Cascade arc, northern Oregon and southern Washington. Canadian Mineralogist 35. 367-396.

Conrey RM, Sherrod DR, Donnelly-Nolan JM, Taylor EM (2000) The north-central Oregon Cascade margin: Exploring petrologic and tectonic intimacy in a propagating intra-arc rift: MARGINS 2000 Field Trip.

Conrey RM, Hooper PR, Larson PB, Chesley J, Ruiz J (2001) Trace elements and isotopic evidence for two types of crustal melting beneath a High Cascade volcanic center, Mt. Jefferson, Oregon. Contributions to Mineralogy and Petrology 141: 710-732.

Conrey RM, Taylor EM, Donnelly-Nolan JM, Sherrod DR (2002) North-central Oregon Cascades: exploring petrologic and tectonic intimacy in a propagating intra-arc rift. Oregon Department of Geology and Mineral Industries. Special Paper 36: 47-90.

Conrey RM, Grunder AL, Schmidt ME (2004) SOTA field trip guide — state of the Cascade arc: stratocone persistence, mafic lava shields, and pyroclastic volcanism associated with intra-arc rift propagation. DOGAMI Open File Report: O-04-04.

Danyushevsky LV, Sobolev AV, Dmitriev LV (1996) Estimation of the pressure of crystallization and H_2O content of the MORB and BABB glasses: calibration of an empirical technique. Mineralogy and Petrology 57: 185-204.

Danyushevsky LV, Della-Pasqa FN, Sokolov S (2000) Re-equilibration of melt inclusions trapped by magnesium olivine phenocrysts from subduction-related magmas: petrological implications. Contributions to Mineralogy and Petrology 138: 68-83.

Danyushevsky LV (2001) The effect of small amounts of H_2O on crystallization of mid-ocean ridge and backarc basin magmas. The Journal of Volcanology and Geothermal Research 110 (3-4): 265-280.

Delmelle P, Stix J (2000) Volcanic Gases. In: Sigurdsson, H., Houghton, B.F., McNutt, S.R., Rymer, H., Stix, J. (Eds.) Encyclopedia of Volcanoes. Academic Press, San Diego. 331-343.

Edmonds M, Herd RA, Galle B, Oppenheimer CM (2003) Automated, high time-resolution measurements of CO_2 flux at Soufriere Hills Volcano, Montserrat. Bulletin of Volcanology 65: 578-586.

Ford CE, Russel DG, Groven JA, Fisk MR (1983) Distribution coefficients of Mg^{2+}, Fe^{2+}, Ca^{2+}, and Mn^{2+} between olivine and melt. Journal of Petrology 24: 256-265.

Ghiorso MS, Sack RO (1995) Chemical mass transfer in magmatic processes. IV. A revised and internally consistent thermodynamic model for the interpolation and extrapolation of liquid-solid equilibria in magmatic systems at elevated temperatures and pressures. Contributions to Mineralogy and Petrology 119: 197-212.

Gill JB (1981) Orogenic andesites and plate tectonics. Springer-Verlag, Berlin.

Grove TL, Parman SW, Bowring SA, Price RC, Baker MG (2002) The role of an H_2O-rich fluid component in the generation of primitive basaltic andesites. Contributions to Mineralogy and Petrology 142. 375.

Guffanti M, Weaver GS (1988) Distribution of Late Cenozoic volcanic vents in the Cascade range: volcanic arc segmentation and regional tectonic considerations. Journal of Geophysics 93: 6513-6529.

Hansell A, Oppenheimer C (2004) Health hazards from volcanic gases: A systemic literature review. Environmental Health 59(12): 628-639.

Hasenaka, T (1994) Size, distribution, and magma output rate for shield volcanoes of the Michoacan-Guanajuato volcanic field, Central Mexico. Journal of Volcanology and Geothermal Research 63: 13-31.

Hildreth W (2007) Quaternary magmatism in the Cascades—geologic perspectives. U.S. Geological Survey Professional Paper 1744.

Hughes SS, Taylor EM (1986) Geochemistry, petrogenesis, and tectonic implications of central High Cascade mafic platform lavas. Geological Society of America Bulletin 97: 1024- 1036.

Irvine TN, Baragar WRA (1971) A guide to the chemical classification of the common rocks. Canadian Journal of Earth Science 8: 523-548.

Johnson ER, Wallace PJ, Cashman KV, Delgado Granados H, Kent AJR (2008) Magmatic volatile contents and degassing-induced crystallization at Volcan Jorullo, Mexico: implications for melt evolution and the plumbing systems of monogenetic volcanoes. Earth and Planetary Science Letters 269 (3-4): 478-487.

Johnson ER, Wallace PJ, Delgado Granadaos H, Manea VC, Kent AJR, Bindeman IN, Donegan CS (2009) Subduction-related volatile recycling and magma generation beneath Central Mexico: insights from melt inclusions, oxygen isotopes and geodynamic models. Journal of Petrology 50(9): 1729-1764.

Johnson ER, Wallace PJ, Cashman KV, Delgado Granados H (2010) Degassing of volatiles (H_2O, CO_2, S, Cl) during ascent, crystallization, and eruption at mafic monogenetic volcanoes in central Mexico. Journal of Volcanology and Geothermal Research 197: 225- 238.

Krauskopf K (1948) Mechanism of eruption at Paricutin volcano, Mexico. Geological Society of America Bulletin 8: 711-732.

Langmuir CH, Klein EM, Plank T (1992) Petrological systematic of mid-ocean ridge basalts: constraints on melt generation beneath ocean ridges. In: Mantle flow and melt generation at mid-ocean ridges. AGU Geophysical Monograph 71: 183-280.

Lawrence RL (1976) Strike-slip faulting terminates the Basin and Range province in Oregon. Geological Society of America Bulletin 87. 846-850.

Leeman WP, Lewis JF, Evarts RC, Conrey RM, Streck MJ (2005) Petrologic constraints on the thermal structure of the Cascade arc. Journal of Volcanology and Geothermal Research 140: 67-105.

Leeman WP, Scheidegger KF (1977) Olivine/liquid distribution coefficients and a test for crystal-liquid equilibrium. Earth and Planetary Science Letters 35: 247-257.

Licciardi J, Kurz M, Clark P, Brook E (1999) Calibration of cosmogenic ^{3}He production rates from Holocene Lava flows in Oregon, USA, and effects of the Earth's magnetic field. Earth and Planetary Science Letters 172: 261-271.

Luhr JF (2001) Glass inclusions and melt volatile contents at Particutin Volcano, Mexico. Contributions to Mineralogy and Petrology 142(26): 261-283.

McBirney AR, White CM (1982) The Cascade province. In: Thorpe RS (Eds.) Andesites. John Wileys and Sons, New York. 115-135.

Mercer CN, Johnston AD (2008) Experimental studies of the P-T-H2O near-liquidus phase relations of basaltic andesite from North Sister volcano, High Oregon Cascades: constraints on lower-crustal mineral assemblages. Contributions to Mineralogy and Petrology 155: 5571-951.

Mercer CN (2009) Mineralogical indicators of magmatic and hydrothermal process in continental arc crust. PhD Thesis. University of Oregon, Oregon.

Métrich N, Wallace PJ (2008) Volatile abundances in basaltic magmas and their degassing paths tracked by melt inclusions. In: Putirka KD, Tepley FJ (Eds.) Minerals, Inclusions and Volcanic Processes. Mineralogical Society of America and Geochemical Society 69. 364-402.

Mitchener CB (1998) Central Oregon High Cascade volcanism at McKenzie Pass. Masters Thesis. Baylor University, Texas.

Moore G, Carmichael ISE (1998) The hydrous phase equilibria (to 3 kbar) of an andesite and basaltic andesite from western Mexico: constraints on water content and conditions of phenocryst growth. Contributions to Mineralogy and Petrology 130: 304-319.

Newman S, Lowenstern JB (2002) VolatileCalc: a silicate melt-H_2O-CO_2 solution model written in Visual Basic for Excel: Computers and Geosciences 28(5): 597-604.

Nielsen RL, Dungan MA (1983) Low pressure mineral-melt equilibria in natural anhydrous mafic systems. Contributions to Mineralogy and Petrology 84: 310-326.

Pioli L, Erlund E, Johnson E, Cashman K, Wallace P, Rosi M, Delgado Granados H (2008) Explosive dynamics of violent Strombolian eruptions: the eruption of Paricutin Volcano 1943-1952 (Mexico). Earth and Planetary Science Letters 271: 359-368.

Price JD (1990) Geology of Mt. Bachelor, Central High Cascade Range, Oregon. Senior Thesis. Baylor University, Texas.

Priest GR, Vogt BF (1982) Geology and geothermal resources of the Cascades, Oregon. Oregon Department of Geology and Mineral Industries Open-File Report 0-82-7. 205.

Priest GR (1990) Volcanic and tectonic evolution of the Cascade volcanic arc, central Oregon. Journal of Geophysical Research 95 (19): 583- 599.

Rasmussen D (2012) Cascade arc magma genesis: volatiles and major element indicators in primitive basalts from the Lassen region. Senior Thesis. University of Oregon, Oregon.

Riker, J (2005) The 1859 eruption of Mauna Loa volcano, Hawai'i: controls on the development of long lava channels. Masters Thesis. University of Oregon, Oregon.

Roeder PL, Emslie RF (1970) Olivine-liquid equilibrium. Contributions to Mineralogy and Petrology 29: 275-289.

Roggensack K, Hervig RL, McKnight SB, Williams SN (1997) Explosive basaltic volcanism from Cerror Negro volcano: influence of volatiles on eruption style. Science 277: 1639-1642.

Rowe MC, Kent AJR, Nielsen RL (2009) Subduction influence on oxygen fugacity and trace and volatile elements in basalts across the Cascade volcanic arc. Journal of Petrology 50(1): 61-90.

Ruscitto DM (2010) Magmatic volatile contents and explosive cinder cone eruptions in the high Cascades: recent volcanism in central Oregon and Northern California. PhD Thesis. University of Oregon, Oregon.

Ruscitto DM, Wallace PJ, Johnson ER, Kent AJR, Bindeman IN (2010) Volatile contents of mafic magmas from cinder cones in the Central Oregon High Cascades: implications for magma formation and mantle conditions in a hot arc. Earth and Planetary Science Letters 298: 153-161.

Ruscitto DM, Wallace PJ, McKay D, Cashman KV (2012) A melt inclusion investigation into the plumbing systems of two explosive mafic eruptions in the central Oregon High Cascades. Journal of Volcanology and Geothermal Research, in review.

Ryan MP, Sammis CG (1981) The glass transition in basalt. Journal of Geophysical Research 86: 9519-9535.

Sadofsky SJ, Portnyagin M, Hoernle K, van den Bogaard P (2008) Subduction of recycling volatiles and trace elements through the Central American volcanic arc: evidence from melt inclusions. Contributions to Mineralogy and Petrology 155: 433-456.

Saunders K, Blundy J, Dohmen R, Cashman K (2012) Linking petrology and seismology at an active volcano. Science 336: 1023-1027.

Scandone R, Malone SD (1985) Magma supply, magma discharge and readjustment of the feeding system of Mount St. Helens during 1980. Journal of Volcanology and Geothermal Research 23: 239-262.

Schick JD (1994) Origin of compositional variability of the lavas at Collier Cone, High Cascades, Oregon. Masters Thesis, University of Oregon, Oregon.

Schmidt ME (2005) Deep crustal and mantle inputs to North Sister volcano, Oregon High Cascade Range. PhD Thesis, Oregon State University, Oregon.

Schmidt ME, Grunder AL (2009) The evolution of North Sister: A volcano shaped by extension and ice in the central Oregon Cascade Arc. Geol. Soc. Am. Bull. 121, 643-662.

Schmidt ME, Grunder AL (2011) Deep mafic roots to arc volcanoes: mafic recharge and differentiation of basaltic andesite at North Sister Volcano, Oregon Cascades. Journal of Petrology. 52(3) 603-641.

Scott WE (1977) Quaternary glaciation and volcanism, Metolius River area, Oregon. Geological Society of America Bulletin 88: 113-124.

Scott WE (1990) Temporal relations between eruptions of the Mount Bachelor volcanic chain and fluctuation of late Quaternary glaciers. Oregon Geology 52: 114-117.

Shaw SD (2011) H_2O Contents in olivine-hosted melt inclusions from primitive magmas in the northern Cascade arc. Masters Thesis. Western Washington University, Washington.

Sherrod DR, Taylor EM, Ferns ML, Scott WE, Conrey RM, Smith GA (2004) Geologic map of the Bend 30- x 60-minute quadrangle, Central Oregon. U.S. Geological Survey, Geologic Investigations Series I-2683.

Sisson TW, Grove TL (1993) Experimental investigations of the role of H_2O in calc-alkaline differentiation and subduction zone magmatism. Contributions to Mineralogy and Petrology 113: 142-166.

Sisson TW, Layne GD (1993) H_2O in basalt and basaltic andesite glass inclusions from four subduction-related volcanoes. Earth and Planetary Science Letters 117: 619-635.

Taylor EM (1981) Central High Cascade Roadside Geology, Bend, Sisters, McKenzie Pass, and Santiam Pass, Oregon. US Geological Survey Circular 838: 55-58.

Taylor EM (1989) Volcanic History and Tectonic Development of the Central High Cascade Range, Oregon. In: Muffler LK, Weaver CS, Blackwell DD (Eds.) Workshop XLIV, Geological, Geophysicalm and Tectonic Settings of the Casacde Range. US Geological Survey Open-File Report 89-178. 369-394.

Taylor EM (1990) Volcanic history and tectonic development of the Central High Cascade Range, Oregon. Journal of Geophysical Research 95(B12): 19611-19622.

Toplis MJ (2005) The thermodynamics of iron and magnesium partitioning between olivine and liquid: criteria for assessing and predicting equilibrium in natural and experimental systems. Contributions to Mineralogy and Petrology 149: 22-39.

Walker JA, Roggensack K, Patino LC, Cameron BI, Matias O (2003) The water and trace element contents of melt inclusions across an active subduction zone. Contributions to Mineralogy and Petrology 146: 62-77.

Wallace PJ (2005) Volatiles in subduction zone magmas: concentrations and fluxes based on melt inclusion and volcanic gas data. Journal of Volcanology and Geothermal Research 140(1-3): 217-240.

Walowski KJ, Wallace PJ, Cashman KV, Clynne MA (2011) Inferring the magmatic plumbing system and melt evolution from olivine-hosted melt inclusions at Cinder Cone, Lasen Volcanic National Park, California. AGU Abstract.

Weaver CS, Grant WC, Malone, SD, Endo ET (1981) Post-May 18 Seismicity: Volcanic and tectonic implications. USGS Professional Paper 1250: 109-121.

Weaver CS, Baker GE (1988) Geometry of the Juan de Fuca Plate beneath Washington and northern Oregon from seismicity. Bulletin of the Seismological Society of America 78: 264-275.

Weaver JS, Langmuir CH (1990) Calculation of phase equilibrium in mineral-melt systems. Computer Geosciences 16: 1-19.

Webster JD, Kinzler RJ, Mathez EA (1999) Chloride and water solubility in basalt and andesite melts and implications for magmatic degassing. Geochimica et Cosmochimica Acta 63(5): 729-738.

Wells RE (1990) Paleomagnetic rotations and the Cenozoic tectonics of the Cascade arc, Washington, Oregon, and California. Journal of Geophysical Research 95: 19409-19417.

Wells RE, Weaver CW, Blakely RJ (1998) Fore-arc migration in Cascadia and its Neotectonic significance. Geology 26: 759-762.

Williams H (1976) The Ancient Volcanoes of Oregon. Condon Lectures Oregon State System of Higher Education. 34-36.

Wilson DS (2002) The Juan de Fuca plate and slab: isochron structure and Cenozoic plate motions. In: Kirby S, Wang K, Dunlop S (Eds.) The Cascade Subduction Zone and Related Subduction Systems. US Geological Survey Open-File Report 02-328. 9-12.

Winter JD (2001) An Introduction to Igneous and Metamorphic Petrology. Prentice Hall. 297.

Wood CA, Kienle J, Contribution by Smith JG (1990) Volcanoes of North America: United States and Canada. Cambridge University Press.

Wysoczanski R, Tani K (2006) Spectroscopic FTIR imaging of water species in silicic volcanic glasses and melt inclusions: An example from the Izu-Bonin arc. Journal of Volcanology and Geothermal Research 156: 302-314.